

ABSTRACT

LEE, ERICA SHENGKAI. Design and In Vitro Evaluation of Five Epiphyseal Plate Fracture Stabilization Methods in Canines. (Under the direction of Denis J. Marcellin-Little and Ola L.A. Harrysson)

Epiphyseal growth plate fractures of the distal femur are commonly seen in young canines that have not completed full ossification of the growth plate. Current treatment techniques involve the use of crossed Kirschner wires and commercial stainless steel plates. This raises concerns of either providing not enough stability or providing too much to the point where stress shielding is observed in the surrounding tissues or the full growth potential of the bone cannot be realized. To prevent this, a second surgery must be performed to remove these stabilization implants after proper healing of the fracture. Currently, resorbable polymers have been used to treat fractures, primarily in the cranio-maxillofacial area. This study aimed to mechanically evaluate the effectiveness of custom designed polycaprolactone (PCL) resorbable bilateral bone plates and lateral titanium plates to the current epiphyseal plate fracture repair techniques of crossed Kirschner wires and lateral commercial stainless steel bone plates. Forty identical models of the distal femur with pre-designed epiphyseal plate fractures were produced for the fixation of these five repair methods. The model constructs underwent nondestructive cranio-caudal bending, medio-lateral bending and torsional loading tests as well as destructive cranio-caudal bending and torsional loading failure tests. The study showed no statistically significant differences among the constructs for the destructive tests, suggesting the models failed prior to reaching the yield and ultimate strengths and torques of the actual constructs. However, from nondestructive tests, the constructs repaired with custom designed titanium plates displayed comparable mechanical properties to the commercial stainless steel plates. Structural stiffnesses of the titanium plate repaired constructs were not statistically significant from the commercial plate repaired constructs for nondestructive cranio-caudal bending medio-lateral bending and torsional loading tests.

The study also displayed excellent mechanical properties of the two thicknesses (4mm and 2mm) of custom designed resorbable PCL plates. Results showed both 4mm and 2mm resorbable plates were statistically more structurally stiff when responding to cranial forces compared to Kirschner wire repaired fractures. Both 4mm and 2mm resorbable plates were also more structurally stiff when responding to medial forces compared to Kirschner wire repaired

fractures and due to their bilateral attachment, also provided a marginally greater stability than the laterally attached metal plates. The resorbable 4mm and 2mm plate constructs were also marginally better in structural stiffness in response to torsional loading than the Kirschner wire constructs. Additionally, results indicated that the 2mm resorbable plate was statistically comparable to the thicker 4mm plate, in cranial bending, medial bending, and torsional bending. Custom designed titanium plates could be an effective alternative to commercial stainless steel plates for fractures observed by more mature canines, and both resorbable 4mm and 2mm PCL plates could be a more effective alternative to Kirschner wire epiphysis plate fracture repair techniques in young canines.

Design and In Vitro Evaluation of Five Epiphyseal Plate Fracture Stabilization Methods
in Canines

by
Erica Shengkai Lee

A thesis submitted to the Graduate Faculty of
North Carolina State University
In partial fulfillment of the
Requirements for the degree of
Master of Science

Biomedical Engineering

Raleigh, North Carolina
2008

APPROVED BY:

Dr. Ola L.A. Harrysson
Committee Chair

Dr. Denis J. Marcellin-Little
Committee Co-Chair

Dr. Peter L. Mente

DEDICATION

*To my parents, whose unconditional love, support, and belief in me
have provided me with everything I have ever needed to succeed in the past twenty-four years.*

BIOGRAPHY

Erica S. Lee was raised in Raleigh, NC and attended the University of North Carolina at Chapel Hill as an undergraduate. There, she began pursuing her engineering career and received her B.S. degree in Applied Sciences – Biomedical Engineering in 2006. She entered into the joint Biomedical Engineering graduate program at NCSU/UNC to pursue a Master's degree in the fall of 2006. After attaining her graduate degree, she hopes to use her knowledge to help others, either through engineering or further studies in law.

ACKNOWLEDGEMENTS

I would like to thank to Dr. Denis Marcellin-Little, for a refreshing outlook in the veterinary medicine field, being an invaluable source of information for this study, and performing 15+ hours of surgeries, pro bono. I would like to express gratitude to Dr. Ola Harrysson, for his support, understanding, and wealth of information in the industrial engineering field. I would like to thank Dr. Peter Mente for his guidance in the field of biomechanics and his help in learning equipment and concepts.

I also express appreciation to Dr. Simon Roe for his time and advice during mechanical testing, Dr. Omer Cansizoglu for all of his assistance and advice throughout the study, Brian Sutherland who helped me get the ball rolling, Paul Belcher for his assistance in providing facilities for the surgeries, and all others who contributed their time and knowledge to this study.

I am grateful to my friends, who have always been understanding when I have been MIA, my little brother Brian who is not so little anymore, and above all I am grateful to my parents who have always been proud of me and whom I hope to continue to make proud in all of my future endeavors.

TABLE OF CONTENTS

	Page
LIST OF TABLES	viii
LIST OF FIGURES	xii
TABLE OF ABBREVIATIONS	xv
1. INTRODUCTION	1
2. LITERATURE REVIEW	4
2.1. Fracture Treatment	4
2.2. Bioresorbable Materials	8
2.3. Polycaprolactone	10
2.4. Material Properties of Bioresorbable Polymers	11
2.5. Rapid Prototyping	14
2.5.1 Advantages to Rapid Prototyping	14
2.5.2 Specific Rapid Prototyping Technologies	15
2.6. Artificial Bone Models	19
2.7. Biomechanical Testing	20
3. METHODOLOGY	22
3.1. Design Process	22
3.1.1 Modeling of Femur	22
3.1.2 Design of Distal Femoral Plates	29
3.2. Fabrication Process	31
3.2.1 Fabrication of Artificial Femurs	31
3.2.2 Fabrication of Molds for Bioresorbable Plates	35
3.2.3 Fabrication of Bioresorbable Plates	37

3.2.4	Fabrication of Titanium Plates	38
3.2.5	Stainless Steel Commercial Plates	39
3.3	Plate Dimension Measurements	40
3.4	Surgical Technique	41
3.4.2	Stainless Steel Commercial Plates	44
3.4.3	Kirschner Wires	44
3.5	Biomechanical Testing	45
3.4.1	Testing Procedure Trial Runs	48
3.4.2	Coating of the Proximal Femur Sections	49
3.4.3	External Torsional Loading (nondestructive)	50
3.4.4	Cranial Bending (nondestructive)	50
3.4.5	Medial Bending (nondestructive)	51
3.4.6	External Torsional and Cranial Bending Failure Tests	52
3.5	Processing Results	53
3.6	Statistical Analysis	54
4.	RESULTS	55
4.1	Nondestructive Tests	55
4.1.1	Structural Stiffness	62
4.1.2	Displacement/Torque	66
4.2	Destructive Tests	72
4.2.1	Cranial Bending Destructive Tests	83
4.2.2	Torsional Loading Destructive Tests	85
4.3	Plate Dimensions	87
4.4	Screw Lengths	88

4.5	Duration of Surgery.....	90
5.	DISCUSSION.....	92
6.	CONCLUSION.....	99
7.	FUTURE RESEARCH.....	101
8.	REFERENCES.....	102
	APPENDICES.....	110
	Appendix A.....	111
	Appendix B.....	116

LIST OF TABLES

	Page
Table 1: Abbreviations used in this paper.	xv
Table 3.1: Randomization order of femur model production.....	34
Table 3.2: Randomization of surgery order.....	42
Table 3.3: Randomization of mechanical testing order.....	46
Table 4.1: Shapiro-Wilk normality test for cranial, medial and torsional structural stiffness variables for cycles 1, 2, 3.....	56
Table 4.2: ANOVA comparison of cycles 1,2, and 3 for all constructs during nondestructive cranial, medial and torsional testing.	57
Table 4.3: Shapiro-Wilk normality test for nondestructive test variables for all constructs.	57
Table 4.4: t-test p-values for structural stiffness from cranial bending, nondestructive tests.	62
Table 4.5: Structural stiffness for cranial bending.....	62
Table 4.6: t-test power for structural stiffness from cranial bending, nondestructive tests.....	63
Table 4.7: t-test p-values for structural stiffness from medial bending, nondestructive tests.	63
Table 4.8: Structural stiffness for medial bending.....	64
Table 4.9: t-test power for structural stiffness from medial bending, nondestructive tests.....	64
Table 4.10: t-test p-values for structural stiffness from torsional loading, nondestructive tests...	65
Table 4.11: Structural stiffness for torsional loading.	65
Table 4.12: t-test power for structural stiffness from torsional loading, nondestructive tests.	65
Table 4.13: Mann-Whitney-Wilcoxon p-values for displacement at 10N cranial bending force, nondestructive tests	66
Table 4.14: Displacement at 10N cranial bending force	66
Table 4.15: Mann-Whitney-Wilcoxon power for displacement at 10N cranial bending force, nondestructive tests	67

Table 4.16: Mann-Whitney-Wilcoxon p-values for displacement at 10N medial bending force, nondestructive tests	67
Table 4.17: Displacement at 10N medial bending force.....	68
Table 4.18: Mann-Whitney-Wilcoxon power for displacement at 10N medial bending force, nondestructive tests	68
Table 4.19: Mann-Whitney-Wilcoxon p-values for torque at 2 degrees torsional loading force, nondestructive tests.	69
Table 4.20: Torque at 2 degree torsional loading force.....	69
Table 4.21: Mann-Whitney-Wilcoxon power for torque at 2 degrees torsional loading force, nondestructive tests	69
Table 4.22: Failure testing summary.....	73
Table 4.23: Results of the destructive cranial bending tests.	81
Table 4.24: Results of the destructive torsional loading tests.....	82
Table 4.25: Mann-Whitney-Wilcoxon p-values for yield strength from cranial bending, destructive tests.	83
Table 4.26: Mann-Whitney-Wilcoxon power for yield strength from cranial bending, destructive tests.....	83
Table 4.27: Mann-Whitney-Wilcoxon p-values for ultimate strength from cranial bending, destructive tests.....	84
Table 4.28: Mann-Whitney-Wilcoxon power for ultimate strength from cranial bending, destructive tests.	84
Table 4.29: Mann-Whitney-Wilcoxon p-values for yield torque from torsional loading, destructive tests.	85
Table 4.30: Mann-Whitney-Wilcoxon power for yield torque from torsional loading, destructive tests.....	85
Table 4.31: Mann-Whitney-Wilcoxon p-values for ultimate torque from torsional loading, destructive tests.	86
Table 4.32: Mann-Whitney-Wilcoxon power for ultimate torque from torsional loading, destructive tests.	86

Table 4.33: Surface area and thickness measurements for bone plates.....	87
Table 4.34: Average screw lengths for each type of plate construct.	88
Table 4.35: Shapiro-Wilk normality test for screw lengths of all constructs.....	88
Table 4.36: t-test p-values for screw lengths.....	89
Table 4.37: t-test power for screw lengths.	89
Table 4.38: Total duration of surgery for each type of construct	90
Table 4.39: Shapiro-Wilk normality test for duration of surgery for all constructs	90
Table 4.40: Mann-Whitney-Wilcoxon p-values for duration of surgery.....	91
Table 4.41: Mann-Whitney-Wilcoxon power for duration of surgery..	91
Table A.1: Comparison of cycles 1,2, and 3 for the commercial plate specimens during non-destructive cranial, medial and torsional testing.....	111
Table A.2: Comparison of cycles 1,2, and 3 for the titanium plate specimens during non-destructive cranial, medial and torsional testing.....	112
Table A.3: Comparison of cycles 1,2, and 3 for the resorbable (4mm) plate specimens during non-destructive cranial, medial and torsional testing.....	113
Table A.4: Comparison of cycles 1,2, and 3 for the resorbable (2mm) plate specimens during non-destructive cranial, medial and torsional testing.....	114
Table A.5: Comparison of cycles 1,2, and 3 for the Kirschner wire specimens during non-destructive cranial, medial and torsional testing.....	115
Table B.1: Structural stiffness mean values of three cycles of cranial bending for all constructs.	116
Table B.2: Structural stiffness mean values of three cycles of medial bending for all constructs.	117
Table B.3: Structural stiffness mean values of three cycles of torsional loading for all constructs.	118
Table B.4: Displacement mean values of three cycles of cranial bending for all constructs at a 10N applied force.....	119

Table B.5: Displacement mean values of three cycles of medial bending for all constructs at a 10N applied force..... 120

Table B.6: Torque mean values of three cycles of torsional loading for all constructs at a 2 degree rotation..... 121

LIST OF FIGURES

	Page
Figure 2.1: Salter-Harris classification for physeal fractures.....	4
Figure 3.1: Screenshot of CT scan imported into Mimics	22
Figure 3.2: Screenshot of profile line during thresholding	24
Figure 3.3: 3D model of a skeletally immature canine femur separated into four sections	25
Figure 3.4: Stl-file of the proximal cortical femur pre-smoothing (a) and post-smoothing (b) in ClayTools.....	26
Figure 3.5: Side and frontal views of the cortical femur model	27
Figure 3.6: Top view of three locating pins positioned at the medial and lateral condyles and the anterior articular capsule of the distal femur for cortical and cancellous bone alignment during model production.....	28
Figure 3.7: Transparent view of the cancellous bone sections in relation to the cortical bone sections, aligned using the locating pins (a). View of the distal and proximal cancellous femur sections and their respective locating pins (b)	28
Figure 3.8: Lateral view of the femoral condyles after merging and cleaning of the distal and proximal cortical femur in preparation for designing the distal femoral plates.....	29
Figure 3.9: Method of designing distal femoral plates.....	30
Figure 3.10: FDM-created ABS plastic models of the femur used to make silicon molds for mass bone model production.....	31
Figure 3.11: Room temperature vulcanized silicon molds of the cortical sections of the femur..	32
Figure 3.12: Positioning of the foam inserts into the cortical silicon molds via locating pins	32
Figure 3.13: Completed replicas of the proximal and distal sections of the femur.....	35
Figure 3.14: Designed molds for the creation of the polycaprolactone bioresorbable plates created in Magics.....	36
Figure 3.15: SLA-created resin mold for bioresorbable plate production (a) and completed mold after steel liquid epoxy treatment (b).....	36

Figure 3.16: Eight 2mm medial, 2mm lateral, 4mm medial and 4mm lateral polycaprolactone bioresorbable plates (left-right).....	37
Figure 3.17: Build platform of the titanium plates	38
Figure 3.18: Completed custom designed lateral 2mm titanium plates.....	39
Figure 3.19: Stainless Steel Commercial Plate.....	39
Figure 3.20: Cut commercial plates	40
Figure 3.21: Measurements for the commercial plates.	40
Figure 3.22: Measurements for the titanium plate, and lateral 4mm and 2mm resorbable plates.	41
Figure 3.23: Measurements for the medial 4mm and 2mm resorbable plates	41
Figure 3.24: Application of the epoxy and fiberglass coating to the proximal femur section	49
Figure 3.25: Testing setup for external torsional loading.....	50
Figure 3.26: Testing setup for cranial loading.....	51
Figure 3.27: Testing setup for medial loading.....	52
Figure 4.1: Graphs of nondestructive cranial bending tests.	59
Figure 4.2: Graphs of nondestructive medial bending tests.	60
Figure 4.3: Graphs of nondestructive torsional loading tests.....	61
Figure 4.4: Graphs of overall curves for each of the eight constructs for the three nondestructive tests.....	71
Figure 4.5: Commercial plate failure specimens.	74
Figure 4.6: Titanium plate failure specimens	74
Figure 4.7: Resorbable 4mm plate failure specimens.....	75
Figure 4.8: Resorbable 2mm plate failure specimens.....	75
Figure 4.9: Kirschner wire failure specimens	76
Figure 4.10: Determination of yield and ultimate strength from a force vs. displacement graph of a resorbable 4mm plate construct in cranial destructive bending.....	76

Figure 4.11: Graphs of destructive cranial bending tests	78
Figure 4.12: Graphs of destructive torsional loading tests.....	79
Figure 5.1: Depiction of polymer flow during injection molding.....	93

TABLE OF ABBREVIATIONS

Table 1: Abbreviations used in this paper.

PCL	Polycaprolactone
PLLA	Poly-L-lactide
PGA	Polyglycolic acid
Commercial plate (C)	Commercial stainless steel plate
Titanium plate (E)	Custom designed titanium plate
Resorbable 4mm plate (K)	Custom designed polycaprolactone resorbable 4mm plate
Resorbable 2mm plate (N)	Custom designed polycaprolactone resorbable 2mm plate
Kirschner wire (W)	Kirschner wire
RP	Rapid prototyping
CT	Computed Tomography
SLA	Stereolithography
FDM	Fused Deposition Modeling
EBM	Electron Beam Melting
DRT	Direct Rapid Tooling
MTS	Materials Testing System (MTS 858 Mini Bionix II, Eden Prairie, MN)
Structural Stiffness	Stiffness of entire repaired constructs as obtained from a linear regression of the Force v Displacement or Torque v Rotation angle curves
Yield strength/torque	The maximum force/torque of the linear portion of the Force v Displacement or Torque v Rotation angle curves before a decreased change in structural stiffness
Ultimate strength/torque	The maximum force/torque of the Force v Displacement or Torque v Rotation angle curves before failure, determined as a 75% drop of collected force or torque from the maximum value

1. INTRODUCTION

Epiphyseal growth plate fractures are an injury commonly seen in young animals that are still in the growth process. The epiphyseal plates are areas of cartilage that separate the epiphysis and the shaft of the bone, and are responsible for longitudinal bone growth [1]. Young animals are prone to epiphyseal plate injuries because their plates have not ossified and are still cartilaginous. Once the animal has reached maturity its epiphyseal plates will ossify and become bone. Because the epiphyseal plates are responsible for bone growth, injury to the plates can have adverse effects such as growth arrest and angular deformities [2-4]. It is therefore essential that epiphyseal fractures be treated in a way such that the growth plate is able to properly heal and continue to promote bone growth. The scope of this research was to develop a new bioresorbable bone plate that can be used to treat distal femoral epiphyseal fractures (also known as Salter-Harris fractures) specifically in the young canine population, though this research can also be applied to children and other young animals.

There are a variety of techniques that have been used to treat Salter-Harris fractures in the canine and human populations with varying degrees of success [2, 4-7]. Methods include internal and external fixation as well as immobilization by splint or cast. One of the more common techniques used in canines utilizes Kirschner wires that are fed through holes that are drilled up through the femoral condyle to a spot on the lower shaft of the femur [5]. The goal of the Kirschner wires is to hold the condyle in place while the epiphyseal plate heals. The downside to the use of Kirschner wires is that they remain in the bone and do not allow for growth. The use of metallic bone plates and/or screws is another popular method that is used to treat epiphyseal fractures [2, 8-11]. In this case titanium or surgical grade stainless steel plates or screws are used to fixate the fracture laterally. The plates or screws hold the fracture in place while it is healing. The use of metal bone plates can however have adverse effects [11, 12]. Metal implants will remain in the body unless they are removed, meaning that they will continue to support the bone and prevent it from being stressed. This can lead to atrophy of the bone near the implant, and over time the bone will weaken and become prone to fracture. Metal bone plates or lag screws can also prevent the bone from growing because they restrict the length of the bone. Therefore, it is necessary to remove metal bone plates and lag screws in animals that have not reached maturity and are still growing.

A focus of this research was to design an implant that will help better treat epiphyseal plate fractures in young dogs. There are a few characteristics that the ideal osteosynthesis implant would have. The ideal implant would: (a) be easy to use, (b) adequately support the fracture site and hold it in place during the healing process, (c) be compatible with the body and its inner environment, (d) be a cost effective way to treat the injury, (e) gradually transfer stress to the tissue as it heals, (f) allow the bone to grow, and (g) disappear when it is no longer needed [20]. Many of the current techniques used for treating epiphyseal fractures have characteristics a-d but few possess e-g. Ideally stress would gradually be transferred to the healing bone and it has been shown that exposing healing bone to small amounts of stress can help to stimulate bone growth [5]. Studies have shown that epiphyseal fractures heal within 4-6 weeks [2, 6]. Resorbable materials currently used for fracture repair and healing show material property degradation rates ranging from one month to two years [13-17]. It is hoped that by making the bone plates out of a resorbable material, it may be possible to gradually introduce the healing bone tissue to stress as the plates degrade, but provide enough stability to the fracture site prior to sufficient healing. Also using plates made of resorbable materials would eliminate the need to perform a second operation to remove the implants after the fracture has healed. Using a resorbable bone plate that works on the same principle as a metal bone plate may therefore be a good way to treat epiphyseal fractures if it provides the same amount of stability but can degrade away after the fracture healing process is complete.

The purpose of this research is to design and compare mechanical properties of two thicknesses of custom designed polycaprolactone resorbable plates (2mm and 4mm) attached bilaterally to the distal femur to Kirschner wires and commercial stainless steel bone plates attached laterally when used for fixation of distal femoral epiphyseal fractures. Additionally, lateral custom designed titanium plates modeled to be identical to that of the 2mm resorbable plate will also be mechanically compared through cranio-caudal and medio-lateral bending tests as well as torsional loading tests. All five repair techniques will be fixated to forty identical femur models. Variables sought out from these tests include structural stiffness, displacement at a 10N applied force, torque generated from a 2 degree applied rotation angle, yield and ultimate strength, and yield and ultimate torque. It is hypothesized that the epiphyseal fractures repaired with the 4mm resorbable plates will be mechanically superior to the 2mm resorbable plates and

both will be superior to the Kirschner wire repaired fractures in all aspects of the torsional and bending tests. The titanium plate constructs will be mechanically comparable to the commercial plate constructs and both will be superior to the resorbable and Kirschner wires in all tests.

2. LITERATURE REVIEW

Treatment of epiphyseal fractures have traditionally been dominated by a few select methods though there are still many questions about the ideal treatment technique for long term success. A review of the pertinent literature has been made to address the current trends and techniques in treating epiphyseal fractures, the benefits of the rapid prototyping manufacturing process, advantageous properties of resorbable properties as well as important considerations for the long term success of femoral plates in epiphyseal fracture repair.

2.1. Fracture Treatment

Femoral fractures are the most common long bone fractures occurring in dogs, and the distal femur is the most frequently involved site for physeal fractures [18]. Salter and Harris developed the classification system that is currently used for epiphyseal fractures [19]. The Salter-Harris classification system separates epiphyseal fractures into five groups, with group I being fractures that only involve the physis without fracture to the epiphysis or metaphysis, groups II – IV are fractures that involve the epiphysis and/or the metaphysis, and group V are compressive injuries to the physis alone (Figure 2.1). The prognosis of Salter-Harris fractures in general, gets worse as the classification group increases. The majority of distal femur physeal fractures are Salter-Harris types I and II [18].

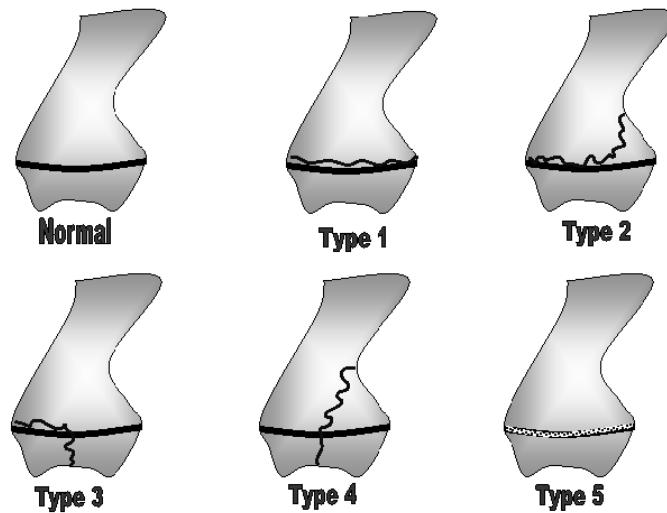


Figure 2.1: Salter-Harris classification for physeal fractures. Reprinted with permission [20].

There are a variety of methods that have been used to treat Salter-Harris fractures of the distal femur. Most methods include fracture reduction followed by either immobilization of the leg with a cast or immobilization of the fracture with rigid fixation. Studies that have been done suggest that immobilization with internal fixation may be necessary to maintain reduction in displaced fractures (Salter-Harris type II, III, and IV fractures) [2, 4, 17]. Thomson *et al.* performed a retrospective analysis looking at the outcomes of 30 Salter-Harris fractures in children [4]. They found that displaced fractures were more likely to lose reduction if external casting was used instead of internal fixation. In their study, three out of the seven patients who had a leg cast instead of internal fixation lost reduction, while none of the sixteen patients that had internal fixation experienced a loss of reduction. Riseborough *et al.* also found that internal fixation improved the outcome of displaced fractures in their retrospective study of growth disturbance following physeal fractures in children [17]. It has also been suggested by Gomes *et al.* that internal fixation is necessary to keep displaced fractures in compression in order to prevent osseous bridging [2].

There are a variety of internal fixation methods that have been used to maintain the reduction of epiphyseal fractures. The use of Kirschner wires is a technique that is widely used by surgeons [2, 19]. This technique involves wires being fed up through two holes that are drilled across the physis. The wires help to maintain the reduction of the fracture as it heals. There is however suggestion that the use of Kirschner wires may contribute to growth arrest or angular deformities because they do not allow the bone to grow [2, 21]. Additionally, Saikku-Backstrom *et al.* paired Kirschner wires with biodegradable nails to repair femoral fractures on sheep and discovered that these Kirschner wires were not strong enough and broke as early as three weeks post surgery [22].

The use of different types of screws, bone plates, and rods are other methods that have been used. Gomes *et al.* did a study to look at the treatment of physeal fractures with lag screws [2]. In their study experimental physeal fractures were created in sixty-four rabbits. Half of the rabbits had their fracture internally fixated with a single cortical screw, while the other half didn't have any type of fixation. At the end of the six week study Gomes *et al.* concluded that internal fixation with a lag screw enabled the epiphyseal to heal properly without angular deformity or

osseous bridging. Their study did not however look at the long-term effects of having screws in the epiphysis.

Stone *et al.* performed a study with young dogs where they looked at the effects of leaving pins in the epiphyseal plate [3]. In their study they placed rush pins in the left distal femurs of fifteen young dogs while leaving their right femur as a control. Stone *et al.* found that leaving the pins in the distal femur longer than one month caused the growth plate to prematurely close and led to a leg length discrepancy in the dogs. However in dogs where the rush pins were removed one-month post operation, the growth plates did not close and there was minimal effect on growth. The results of the study by Stone *et al.* suggests that interference with the growth plate in dogs should be limited to no more than one month in order to prevent growth plate closure. This suggests that it is important to limit the time for which an implant acts on the epiphyseal plates.

Hara *et al.* performed an experiment where they used biodegradable poly-L-lactide (PLLA) screws to secure Salter-Harris type IV fractures in dogs [6]. In this study experimental Salter-Harris type IV fractures were created in eight dogs and internally fixated with two PLLA screws in a lag fashion. The screws were inserted in a way such that they did not interfere with the epiphyseal plate. Hara *et al.* found that fixation with the biodegradable PLLA screws maintained their strength long enough for the fracture to heal and that the screws had not caused any significant growth arrest. Hara *et al.* suggested that PLLA screws could be used to fixate Salter-Harris type III and IV fractures as long as the epiphysis is not interfered with.

The use of biodegradable rods is a method that has been used to treat some epiphyseal fractures. Axelson *et al.* did a few studies on the use of biodegradable, polyglycolic acid (PGA) rods to fixate epiphyseal fractures in cats and dogs [9, 10]. In the first study Axelson *et al.* looked at the results from fourteen clinical cases and four experimental cases where PGA biorods (Biofix[®]) were used to fixate epiphyseal fractures of the distal femur [9]. The fractures were fixated by drilling two holes up through the condyles and driving biorods into the holes. After the operation all of the animals were able to walk on their operated leg within a week. Axelson *et al.* found that the biorods did not interfere with the growth plate significantly and that within a month after surgery, the growth plate was strong enough to break the biorods. The

result of the growth plate being able to break the rods was that the fractures healed correctly and growth was not altered significantly.

Axelsson *et al.* did a second study where they compared the use of metal rods, biodegradable polyglycolic rods, and external fixation for fixating epiphyseal and cancellous bone fractures [10]. Results showed that animals treated with biodegradable rods were able walk on their injured limb earlier than the animals treated with the metal devices or external fixation. This group also healed clinically earlier than the other groups, showing no lameness on the operated limbs. Coupled with the fact that radiographs showed no statistical differences between groups, Axelsson *et al.* concluded that fixation using biodegradable devices was as suitable for the fixation of cancellous bone and physeal fractures of dogs and cats as metallic devices or external fixation.

While metal implants can be used to fixate epiphyseal fractures, they are not ideal. Metal implants do not allow the bone to grow and therefore must be removed within three to four weeks after they are put in [8, 11]. Doing a second surgery to remove metal implants causes the financial cost, healing time, and the chance of infection all to be increased. If metal plates are left in the body they also tend to cause atrophy in the bone around them because the plate shields the bone from stress [11, 12]. A study by Breburda *et al.* suggests that small amounts of stress can help to stimulate bone growth and aid the healing process [5].

2.2 Bioresorbable Materials

An in-depth review of current uses for resorbable materials indicates that a design for a bioresorbable bone plate for the treatment of distal femoral fractures has not yet been developed. However, literature reveals the use of resorbable plates in other areas of the body such as the mandible and cranium as a solution to the concern of growth restriction that metal implants create [12, 23]. Additional advantages of bioresorbable materials are that it does not cause scattering in the neighboring structures during radiotherapy or disturb postoperative imaging. The success of the use of resorbable implants in other parts of the body gives hope for their success in the distal femur. Several concerns however, have been raised over the mechanical strengths of the material as well as the long-term adverse reactions during resorption due in part to the high crystallinity of some polymers [24].

One type of bioresorbable polymer is poly-L-lactide (PLLA), which has shown good results in the repair of mandibular condyle fractures. PLLA miniplates and screws offered efficient fracture fixation and healing in fourteen patients that underwent this surgery [25]. Suuronen *et al.* used self-reinforced poly-L-lactic acid plates and screws in the fixation of mandibular osteotomies in sheep. Degradation studies were also carried out *in vivo* and *in vitro* in rabbits and results indicated that the resorbable plates and screws retained their strength long enough for the osteotomy to consolidate. When bilateral sagittal osteotomies of the mandible were fixed with positional screws in sheep, mechanical testing showed that they turned out to be stronger than that of the unoperated control mandibles [26-31]. The degradation time of the poly-L-lactic acid homopolymer with the associated crystallinity however, is very long and crystalline remnants were still be detected in the sheep mandible five years post-operation [29]. This slow degradation of the crystalline phase of PLLA can cause complications such as a risk of inducing cancerous tissue [32]. Fortunately, it is possible to change the strength and degradation rate of PLLA by mixing it with different amounts of other bioresorbable materials such as polycaprolactone (PCL), polyglycolic acid (PGA), and poly-D-lactide (PDLA) [33]. By changing the composition of PLLA mixtures it is possible to set the rate at which the material will break down under normal conditions in the body. Suuronen *et al.* addressed this issue by using a copolymer of L- and DL-lactic acid (70/30) which reduced the crystallinity of the material [34].

Suuronen *et al.* used poly-L/DL-lactide 70/30 miniplates and screws to fix both mandibular and maxillary osteotomies producing reliable results with very few minor complications of postoperative infections [34]. The long term relapse or material related failures were reported to be similar to where titanium devices had been used. This suggests that bioresorbable materials can withstand the mechanical failure stresses as effectively as other repair techniques.

An EU multicenter study was carried out using another copolymer called self-reinforced polylactic-co-glycolide (SR-PLGA) 80/20 plates and screws in the fixation of osteotomies in cranio-maxillofacial surgery for 161 children and 4 adults [35]. The devices were reported to be easy to handle and apply intraoperatively, providing stable fixation. Postoperative complications occurred in 7.8% of the cases, indicating that this bioresorbable material could be used safely and with favorable outcome in corrective cranioplasties especially in infants and young children.

Kurpad *et al.* also used PLGA 82/18 plates to correct congenital pediatric craniofacial malformations for 51 patients of mean age of 3 years [36]. The malformations were osteotomized and reconstructed with bone graft secured by the bone plates. Radiographic and photographic examinations after 2 years follow-up showed no evidence of infection, erythema, extrusion, instability of the bony fragments or relapse. After one year of follow-up, the PLGA plates were universally impalpable, having resorbed completely between 6 months and 1 year. These results indicate that resorbable polymers are effective with the healing of fractures and advantageous in the long-term with full resorption into the body.

Gosain *et al.* conducted a study to biomechanically compare resorbable fixation systems as an alternative to metal plates and screws using bone segments from sheep [37]. Titanium miniplates, midface plates and microplates fixated with titanium screws were compared to PLGA 82/18 plates either glued directly to the bone segments or fixated with resorbable screws. Distraction and compression testing of the specimens revealed that the titanium-fixed miniplate system was significantly stronger than any other method of fixation, but resorbable plate and screw fixation was as strong as standard titanium midface and microplating systems in distraction and stronger in compression. When tested to failure, the titanium miniplate system tested in distraction was the only group to withstand a mean force of failure of greater than 350N. This could be problematic considering reported forces of the facial skeleton can reach up

to a molar bite force of 4346N. In Gosain *et al.*'s study however, all bone segments were secured with one plate spanning across each pair. Segments secured with two resorbable plates could strengthen the system in distraction and compression tests to make more comparable to or even surpass the strengths of the single-plated miniplate system.

Vaananen *et al.* examined the effect of cyclic loading of a flexible, biodegradable Inion OTPS™ copolymer ankle plate fixated with screws of the same material during twelve weeks of hydrolytic degradation [38]. One group of the study gradually increased the cyclic loading in four phases to represent gradual increases in walking distance and speed during the healing period. The second group was biomechanically tested after the twelve weeks of degradation, and the third group was used as a control for inherent viscosity measurements. Cyclic loaded specimens were axially compressed with a maximum 100N force and a minimum 10N force with a 2 degree rotation around the long axis of the plate. The study reported no significant differences between the loaded groups for any of the measured parameters with no specimens failing during the cyclic loading. No significant differences were observed in inherent viscosities at the conclusion of the study period. Vaananen *et al.* reported that the initial fixation stability provided by the ankle plate remained unchanged over the 12 weeks. The study concluded that cyclic loading did not have any clinically relevant effect on the fixation stability or the degradation properties. These promising results could also be observed in studies involving fixation of distal femur fractures considering that the femur would also undergo cyclic loading during the healing period.

2.3 Polycaprolactone

Polycaprolactone is one of the most potential candidates as a biodegradable polymer due to its availability, biodegradability, non-toxicity and biocompatibility to many drugs [39]. This FDA-approved material degrades at a rate that may support epiphyseal fractures during their 4-6 week healing period [2, 6, 15]. Additionally, PCL is highly biocompatible with osteoblasts. It is most commonly used as bone substitute material for maxiofacial reconstructive surgery [40, 41].

Fujihara *et al.* used PCL in combination with calcium to fabricate nano-structure guided-bone-regeneration membranes (GBR) to encourage bone growth and repair in mandibular or alveolar defects, and prevent the invasion of non-functional scar tissue [42]. In this case PCL

was used as the mechanical support layer due to its high tensile strength and the presence of calcium accelerated ossification.

Rohner *et al.* used PCL to fabricate scaffolds for bone regeneration in cranio-facial and orbital defects in pigs. The PCL filaments were made from PCL pellets put in a fiber-spinning machine [43]. The scaffolds had 65% porosity and had a honeycomb structure. The scaffolds were then coated with bone marrow stem cells to promote bone ingrowth. The results showed that PCL scaffolds are a very promising method to heal orbital bone defects.

Sun *et al.* examined the *in vivo* long-term degradation of PCL capsules in rats [44]. Results showed that there was a linear relationship between the molecular weight of PCL and time, and at 24 months the capsules were still intact but at 30 months the implants were fragile and completely lost their mechanical strength. At 36 months, only remnants of the capsules were left at the implantation site. Results also indicated that the PCL pieces did not accumulate in any body organs but were metabolized and ultimately excreted from the body. These results indicate that PCL's degradation life is long-term enough to provide stabilization for an ossifying bone, yet biodegradable enough to disappear from the body when no longer needed.

2.4 Material Properties of Bioresorbable Polymers

The use of bioresorbable materials in fracture healing is very common. The tensile strength, degradation rate, and physical properties of a bioresorbable implant depend on the polymer quality, composition, processing conditions, implant site, and dimensions of the implant [45]. It is interesting to look at the properties of each material and compare them with polymers that are made of a combination of two polymers.

Polycaprolactone is a polymer with high crystallinity and a low melting point. It can be injection molded and is easy to blend with other polymers. It is a good candidate for this application because it is biocompatible with the internal environment of mammalian organisms and it is biodegradable. PCL has a Young's Modulus and tensile strength of 386 MPa and 41 MPa (specifically, Tone Polymer P-787), melting point of 60°C, and a glass transition temperature of -60°C [46, 47]. The degradation rates for PCL are said to be very slow with a linear relationship to molecular weight loss and the elastomeric properties of the material can easily be modified by blending it with PLLA or PGA [45, 48]. Lam *et al.* conducted an *in vitro* degradation study on PCL and an *in vivo* study on PCL-based composite scaffolds in rabbits. A

sixth month evaluation showed virtually no molecular weight loss [15]. Preliminary studies conducted by Lam *et al.* on medical-grade PCL scaffolds implanted for two years in a rabbit evidenced gradual and late molecular weight decreases combined with excellent long term compatibility and bone regeneration. Compared to other polymers used in successful degradable implants however, PCL does not have a very high tensile strength.

Poly (L-lactic) acid is a form of polylactide (PLA) that is used in orthopedic devices because of its high mechanical strength and toughness [48]. PLLA has a Young's modulus of ~ 3.4 GPa, tensile strength ranging between (69-103 MPa), a melting point of 175°C, and a glass transition temperature of 65°C [48, 49]. Its tensile strength is much higher than PCL's. PLLA is a semi-crystalline polymer and decomposes slowly in the body by hydrolysis. Brady calculated that a 50 to 90 mg implant took 1.5 years to completely dissolve in the abdominal wall of rats [14]. In another study, the *in situ* presence of crystals were clinically observed up to 5.7 years after implantation [13].

A third polymer considered for this study is polyglycolic acid. It has a young's modulus of 6.9 GPa, a melting point of 225°C and a glass transition temperature of $\sim 35^\circ\text{C}$ [49]. It has a tensile strength comparable to that of PLLA (69-128 MPa); nevertheless, it has a much higher decomposition rate. Due to its greater hydrolytic inclination, its strength disappears within one month [16, 17].

An important issue to note about biodegradable polymers is that studies have shown that poly(α -hydroxy acids) such as PGA and PLA undergo bulk degradation where its mass loss is accompanied by a release gradient of acidic by-products that *in vivo*, results in inflammatory reactions [13, 50]. These reactions may be more severe if the implants' surrounding tissue has poor vascularization or low metabolic activity. Polycaprolactone on the other hand, degrades much more slowly than poly(α -hydroxy acids) *in vivo* to yield ϵ -hydroxycaproic acid. This slow degradation rate exposes less amounts of acid to the body than poly(α -hydroxy acids) over the same amount of time which suggests better reaction *in vivo*. Its breakdown is initiated by non-enzymatic ester hydrolysis in the extracellular matrix, and the final stage of degradation involves phagocytosis of polymer fragments by macrophages and giant cells, indicating a much more biocompatible reaction of the body [48].

Various copolymers have also been developed as potential resorbable implant materials. Poly(lactic-co-glycolide) polymers are easily synthesized today with specific compositions to obtain a certain degradation rate. A copolymer composed of 65 % PLA and 35% PGA loses most of its tensile strength after 4 weeks, and about 80% of its weight after 12 weeks [45]. Therefore, a copolymer may be the best option for the resorbable bone plates. The exact degradation rate as well as polymer composition need to be empirically determined, so that the plates will stabilize the fracture yet gradually transfer loads back to the bone, and enable the bone to keep growing.

Yasin *et al.* tested blends of polyhydroxybutyrate-polyhydroxyvalerate (PHB-PHV) with different percentages of PCL [51]. Their results showed that copolymers that contained 20% PCL were more compatible than blends with higher percentages. Varying the composition of blends also affects the degradation rate. For instance, increasing the PCL composition of a material makes that material more hydrophobic, because PCL is highly crystalline; therefore, hydrolytic degradation takes longer.

Fiber reinforcement of polymers is also a method to attain the mechanical properties desirable for resorbable implants. Lewis *et al.* produced PLLA bone plates reinforced with alumina-boria-silica fibers and were able to increase the flexural modulus of PLLA to 9.0 GPa [52]. Another study showed that calcium meta-phosphate fibers increased the flexural modulus of PLLA to 15.9 GPa [53]. This proves that there is a wide range of options for designing plates with exact material properties.

2.5 Rapid Prototyping

Rapid prototyping (RP) is becoming a very popular technology in surgical medicine. It eliminates drawbacks that have caused a lot of grief to patients in the past, and allows for surgery planning and simulation like never before. Once the surgeon can hold the physical model of the bone with a deformity for example, they can better plan the surgery and therefore reduce the time of the surgery, limiting the risk of infection, and have the option of explaining the procedure to the patient by showing them the model [54].

2.5.1 Advantages to Rapid Prototyping

An article by Liska *et al.* reported the procedure used in a custom total knee replacement to manage a medial femoral condylar nonunion in a dog using RP and its advantages [55]. In this study, a computed tomographic scan was used to build a stereolithography RP model of the distal portion of the femur. This model was then used to create a custom augment to replace the missing medial femoral condyle and a custom stem for intramedullary condylar cemented fixation. The model was then used to rehearse the surgery before the custom prosthesis was implanted. This article shows the various advantages RP can be used for to help create a surgical procedure with minimal complications.

A study by Harrysson *et al.* also showed the beneficial impact of RP and models on the accuracy of surgery [56]. Computed tomography (CT) scans were used to create a stereolithography RP model of a bilateral multifocal pelvic limb deformity in a dog. This model was then used to construct room temperature vulcanized (RTV) silicone molds which were then used to cast polyurethane patterns for pre-surgical planning and rehearsal. These physical models enabled surgeon to have a clear understanding of the surgical procedure which positively influenced the clinical outcome.

RP facilitates the creation of implants or models from imaging scans, making them very similar to the original organ or bone. RP models have enabled surgeons to carry out surgeries that were once thought impossible [56, 57]. In addition, RP implants can be custom made for each patient, thereby eliminating the amount of time required to contour commercially standard implants during surgery. Liu Yaxiong explains that standard mandibular implants were traditionally made out of metal and would not adequately fit to the patients jaw. The simple

shapes of the bone substitutes improve the patient's appearance and helps to reduce their physical pain [58]. This suggests that rapid prototyping is not only a more effective technique for developing custom mandibular implants but it also improves the quality of life of patients.

Heissler *et al.* demonstrated the useful advantages of RP techniques in his article presenting custom-made cast titanium implants produced with computer aided design and manufacturing for the reconstruction of cranium defects [59]. Casting methods make it possible to form very thinly tapered structures and to obtain more complex geometrical structures with smaller diameters that would otherwise be impossible with milling techniques.

Johnson conducted a study of using customized titanium plates for internal fixation of six patients with femoral fractures [60]. These patients all had complex problems surpassing treatment possibilities of using intramedullary nailing or standard plate fixation. Instead, custom plates were individually designed using computed axial tomographic scans while altering plate dimensions to increase strength, height, length, and placement of screw holes to enhance stability of the repaired system. Johnson reported successful results of fracture ossification with the implants being well tolerated. This study further demonstrates the advantages of RP techniques, especially in creating plates for fixation of difficult fracture problems.

2.5.2 Specific Rapid Prototyping Technologies

Potamianos *et al.* highlights several rapid prototyping methods currently utilized for surgery such as stereolithography (SLA) and fused deposition modeling (FDM) [61]. Stereolithography creates 3D models out of acrylate photopolymer or epoxy resin, by tracing a UV laser across a vat of resin. The resin is cured by the laser to create a solid thin slice and the build platform is lowered so that the solid layer is just below the surface of the resin. The next slice is formed on top of the previous and the build platform lowers step by step until the object is complete. The object is then removed from the vat, cleaned of its support structures and then post-cured in an ultraviolet (UV) oven. SLA however, does pose a risk of warping and shrinkage of parts for large models. Fused deposition modeling is a process that creates 3D models out of heated thermoplastic material that is extruded through a nozzle as it moves across the build platform. Build materials such as polycarbonate, polypropylene and other various polymers are used to create the object layer by layer in the positive z-axis. Both of these RP techniques can generate physical models of 3D computer designed models or medical imaged anatomical

objects scanned into a computer system. Potamianos *et al.* also adds that medical applications of rapid prototyping include production of anatomical prototypes from x-ray, CT or MRI data and direct production of casting molds for custom surgical implants, designed with CAD software to fit patient data [61].

Electron beam melting (EBM) is a rapid prototyping technique where an electron beam melts individual layers of metal powders to create full density metal parts in a high vacuum chamber. The melted material uses pure alloy in powder form of the final material to be fabricated and therefore does not require additional thermal treatment to obtain the full mechanical properties of the metal part. Marcellin-Little *et al.* utilized this RP process for the fabrication of custom titanium bone plates in their *in vitro* evaluation of a custom cutting jig and custom plate for canine tibial plateau leveling [62]. Other uses of the EBM process have included direct fabrication of orthopedic implants [63].

Kling-Petersen *et al.* explains a relatively new haptic modeling tool developed by SensAble Technologies Inc. used during the design of 3D computer models before rapid prototyping into physical models [64]. This modeling tool enables an imported model or a user-defined block of “clay” to be manipulated similar to traditional techniques used by clay artists with the help of a SensAble Technologies PHANTOM haptic arm. The model can be manipulated with instantaneous haptic feedback as well as visual feedback, enabling precise and intuitive changes. Strengths of this modeling tool can be applied to medical uses, where one of the main concerns with 3D scanning of medical specimens is that the technique leaves holes or gaps in the dataset corresponding to areas in shadows such as orifices and deep grooves. Traditional 3D reconstruction often shows unnatural ridges or uneven areas as a result of triangulation and/or tessellation processes. With this haptic device, defects can be easily corrected, gaps can be filled, and uneven ridges can be smoothed, essentially “cleaning” the non-geometric 3D object and readying it for further 3D graphic manipulation [64].

Direct rapid tooling (DRT) is a process that allows the manufacture of production tools, offering a faster response to market needs for custom parts. DRT is not the manufacture of final parts, but is the manufacture of molds, dies, and other mass production tools to create the final parts. A review by Karpatis *et al.* elaborates on some methods of direct rapid tooling, one of which is the use of SLA technology [65]. Stereolithography can be used to create patterns

for preparation of silicon RTV molds, for investment casting, or as a prototype epoxy mold for injection molding (DirectAIM) or for the manufacturing of the mold cavity and core (Keltool). If molds are created for plastic injection, cooling channels should be efficiently placed in thermally strategic areas within the mold to reduce production time.

Injection molding is a mass reproduction technology, where melted material is injected into a mold at a very high pressure. Currently this technology is the most popular method for creating plastic parts, and can be used with molds created through machining or direct rapid tooling. During the manufacturing of thermoplastics such as PCL, the molecules within the polymers become oriented by the deformation of the polymer melt during processing. The flexible molecular chains are stretched and because of their entanglement, are not able to relax fast enough before the injection molded part cools and solidifies. This phenomena can be multiplied at lower processing temperatures, leading to higher degrees of molecular orientation which affects the stiffness and strength properties of the polymer component [66]. Early studies have shown that a molecular orientation distribution exists especially across the thickness of thin injection molded parts [67]. In addition to the melting of thermoplastics inducing the orientation of the polymer molecules, a mechanism called the fountain flow effect can also be responsible. The fountain flow effect is caused by the no-slip condition on the mold walls, which forces material from the center of the part to flow outward to the mold surfaces. The melt flows inside the mold cavity freeze upon contact with the cooler mold walls, and subsequent melts flow between the frozen layers, forcing the melt skin at the front to stretch and unroll onto the cool wall where it instantly freezes. This causes the molecules that move past the free flow front to be oriented in the flow direction [66]. Flow down the center of the melt path becomes increasingly difficult because the melt cools during the flow and the distance moved by the melt front decreases with time. This can make filling of the impression difficult if long flow paths are involved, especially if there are obstructions such as core pins or the necessary filling of irregular corners. Stresses in the part result from this mechanism, which will be greatest at points furthest from the gate [68]. The melt processing of the polymers and the fountain flow effect may raise some concerns over the mechanical properties of the bioresorbable plates if core pins are in place in the mold, especially for thinner designs.

A study conducted by Tay created an injection mold based on electroless nickel plating and epoxy resin [69]. Results showed that the epoxy resin improved compressive strength and the nickel enhanced the hardness, conductivity, ductility, lubricity, wear, and abrasion resistance without affecting dimensional accuracy. This suggests that a combination of epoxy and metal would greatly benefit the creation of direct rapid tooling injection molds.

Pistner *et al.* conducted a long-term degradation study evaluating the injection molded PLLA versus machined PLLA blocks and rods implanted into the dorsal muscle of rats [70]. Due to the melting and re-solidifying process, the injection molded PLLA developed a rough surface within weeks, deep resorptive lacunae after a year, and became totally or nearly totally degraded after two years. Machined PLLA on the other hand remained stable in form and structure throughout the entire observation period. This suggests that injection molded polymers are better suited for exhibiting desired degradable characteristics.

A study conducted by Altpeter *et al.* examined the material effects of polycaprolactone and poly(lactide) when injection molded to investigate the effect of processing parameters on the physical properties of the moldings [71]. Results showed that PLLA had a high sensitivity to melt temperature with the molecular weight and ductility reducing substantially at high temperatures. Crystallinity was also enhanced in PLLA, compromising its mechanical properties. Alternatively, PCL was shown to be less sensitive to temperature than PLLA. Altpeter *et al.* also noted that processing temperature in combination with the grade of PCL used was influential for the mechanical properties of resulting moldings. In the study, they used two grades of PCL, and discovered that the higher grade was less sensitive to higher melt temperatures than the lower grade.

2.6 Artificial Bone Models

When conducting studies involving the repeatability of a procedure, there are a few options for the method of approach. When involving bones, the study can either use multiple cadavers or artificial bones. There are several disadvantages to both methods. When using cadavers, though it will be clinically realistic, there will be some variation between the different sources of the tissue that must be taken into account. With artificial bones, the variability between different cadaveric bone sources will be eliminated but the exact characteristics of the bone (cortical and cancellous) will be hard to mimic. Several studies have utilized a two-step process to create a more realistic model comparable to real bone and to provide realistic tactile feedback especially during cutting and drilling of the bone.

Hildreth *et al.* created twenty seven tibial replicas using rapid prototyping and indirect rapid tooling methods for an *in vitro* evaluation of five canine tibial plateau leveling methods [72]. The silicone mold casted models consisted of a cortical bone region reproduced with a mixture of 2-component epoxy, bone powder and glass fibers and a cancellous bone region reproduced with polyamine foam within the cortical region. This bone composite was devised by testing combinations of materials and comparing the composite's mechanical properties with that of cadaveric tibiae. In addition to creating models with comparable flexural modulus to canine tibia, these models had the advantages of being identical in size, shape and texture to the cadaveric tibiae. In the study, the tibial plateau leveling osteotomy (TPLO) method involved the tightening of six cortical screws. These screws were tightened with a factory-calibrated torque wrench to 1.13 Nm. This value may be a good torque measurement for other cortical screws tightened into these composites.

Another study by Marcellin-Little *et al.* created ten tibial replicas with a cortical and cancellous region for the *in vitro* evaluation of a custom cutting jig and custom plate for canine tibial plateau leveling[62]. In this study the cortical and cancellous bone regions of a tibia extracted via CT scans were rapid prototyped into stereolithography models. These SLA models were then used to create silicone rubber molds of cortical and cancellous regions. The cancellous core was cast using polyurethane foam and then inserted into the larger cortical mold where a mixture of epoxy, bone powder and shredded fiberglass was cast around the core.

2.7 Biomechanical Testing

Biomechanical strength testing is a widely accepted and useful means of evaluating the effectiveness of orthopedic fixation devices [73-76]. *Ex vivo* biomechanical testing should attempt to mimic physiological loading conditions. Often, only the primarily acting loads can be applied because bone is subjected to complex intrinsic and extrinsic forces *in vivo* [73]. Salter-Harris type I fractures are typically produced by shearing and avulsion forces [77] and in the distal femoral physis, bending forces may also be important [78].

Sukhiani *et al.* biomechanically compared different pin fixation techniques for canine distal femoral physal fractures [79]. The study used torsional testing on a servohydraulic Bionics 858 Materials Testing Machine as a means of mimicking shear loads at the distal femoral physis and also because torsional instability has shown to be the most common cause of failure with pin fixation techniques [73, 80]. Results showed that of all the fixation techniques, the crossed-pin technique sustained the greatest load to failure.

In another study, Snow *et al.* mechanically compared locking compression plates (LCP) to low-contact dynamic compression plates (DCP) on a synthetic model of osteoporotic bone [81]. Four-point bending tests of a maximum 3.5 N-m moment were conducted on the synthetic bone after the different plates were used to bridge separate bone sections. Torsional testing was also conducted with a maximum load of 3.5 N-m. This study suggests possible methods of fracture repair mechanical tests and appropriate testing values.

The bending strengths of biodegradable nails tested with Kirschner wires were determined using a 4-point bending test using a Lloyd 6000R Materials Testing Machine [22]. In this study the bending strength of solid SR-PLA96 nails was determined to be 28.6 Nm, by calculating the moment required to produce a permanent deflection of 0.13mm. In one study, a torsion loading facility was developed especially for polymeric implant rods to evaluate shear performance and failure [82]. This was achieved by modifying an MTS universal testing machine. The sample was placed into clamp style holders, and then a piece of high-toughness nylon rope was moved up vertically through the loading of the machine to cause a drum to rotate around the shaft and apply torque to the sample. The study found that the testing apparatus was effective in measuring the shear deformation behavior of polymeric and metal

implant materials. In the case of biodegradable implants, it is also important to know how the mechanical properties change over time after implantation.

In a study of *in vitro* degradation of PLLA composites, a 3-point bending test was used to measure the bending strength as the material degraded over a period of 20 days [83]. It was found that the bending strength as well as other mechanical properties decreased rapidly over the 20 days for all the types of PLLA composites in the study as they degraded *in vitro*. For this reason it is important to match the degradation rate of the implanted material to the healing rate of the fracture, so as to optimize required support and promote healing. Much more research needs to be completed before it can be determined if a biodegradable polymer implant is feasible for the repair of distal femoral fractures. It must be determined if the implant would have enough strength to prevent displacement and would maintain its mechanical properties long enough to successfully repair distal femoral fractures.

3. METHODOLOGY

3.1 Design Process

The design process of this research involved taking an imaging scan of a femur to create anatomical artificial femur models and custom designed plates specifically contoured to match the medial and lateral surface of the distal aspect of the femur. Various software modeling programs were used in this process and are described below.

3.1.1 Modeling of Femur

A CT scan of a three month old skeletally immature femur from a large female dog was imported into Mimics (Materialise, Leuven, Belgium), a software package used for editing of medical images and to recreate 3-dimensional structures (Figure 3.1).

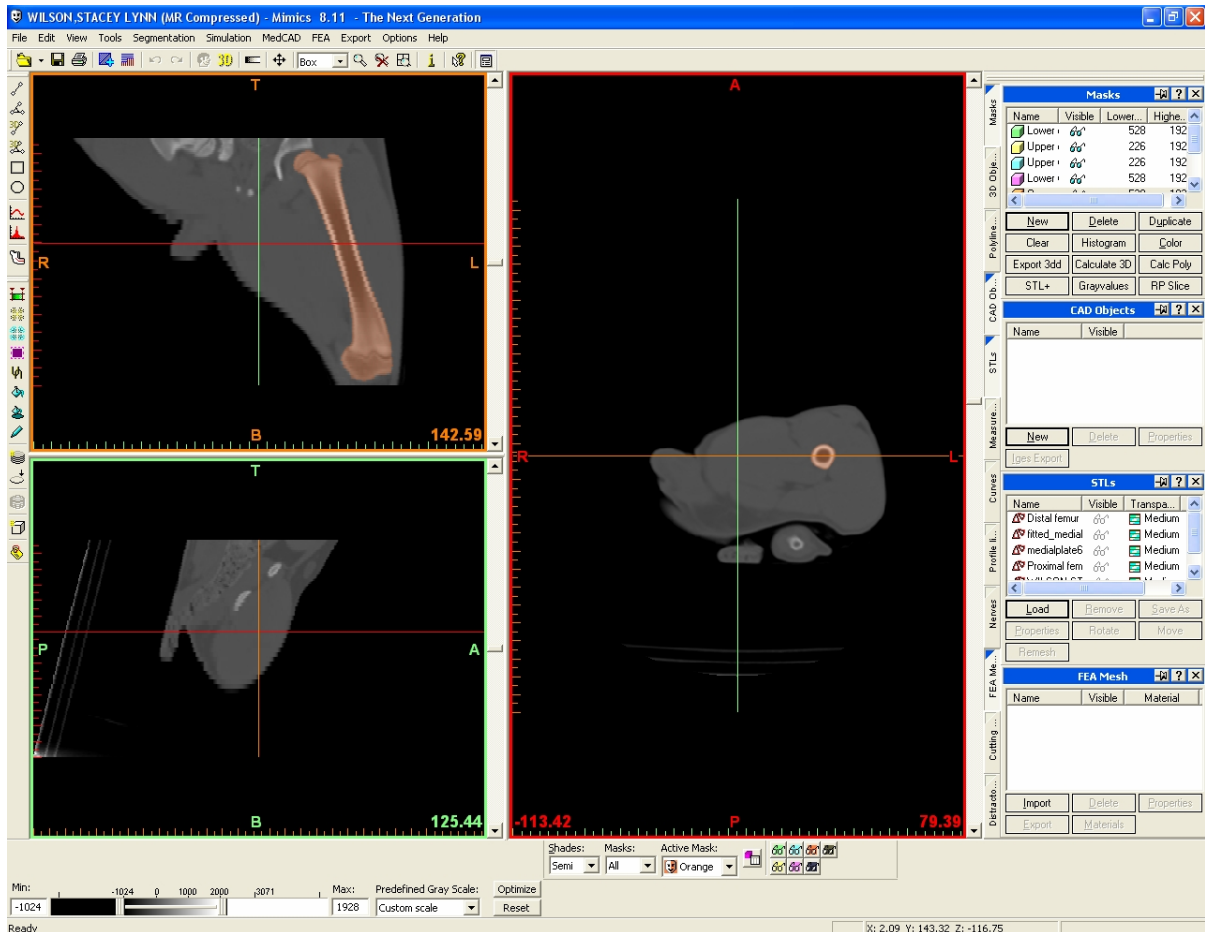


Figure 3.1: Screenshot of CT scan imported into Mimics

Contrast and threshold features of the program were applied to the CT images to optimize bone capture and 3D reconstruction. Adjusting contrast settings of the images displayed in the different views resulted in a slight separation between soft and hard tissues. After contrast enhancement, the profile function was utilized to obtain optimal thresholding values of the bone intensity by viewing the resulting selections on the 3-directional viewing windows. Using the “*profile line*”, the bone intensity was determined and the threshold value was set to the bone intensity value. After defining the location of the line on the image, an intensity profile is generated based on the line. The straight line value is the current threshold value. For a good visualization model, the threshold value was selected slightly above the intensity plateau (Figure 3.2). It was ensured that the profile line was checked on other images to ensure an average threshold value was determined. The primary reason for thresholding is to obtain an optimal value of intensity that will enable the bone to appear more clearly with minimum soft tissue attached to it. Thresholding was also used to separate the hard cortical tissue and the softer cancellous tissue of the femur to reproduce a physical anatomically correct model later on during artificial femur production.

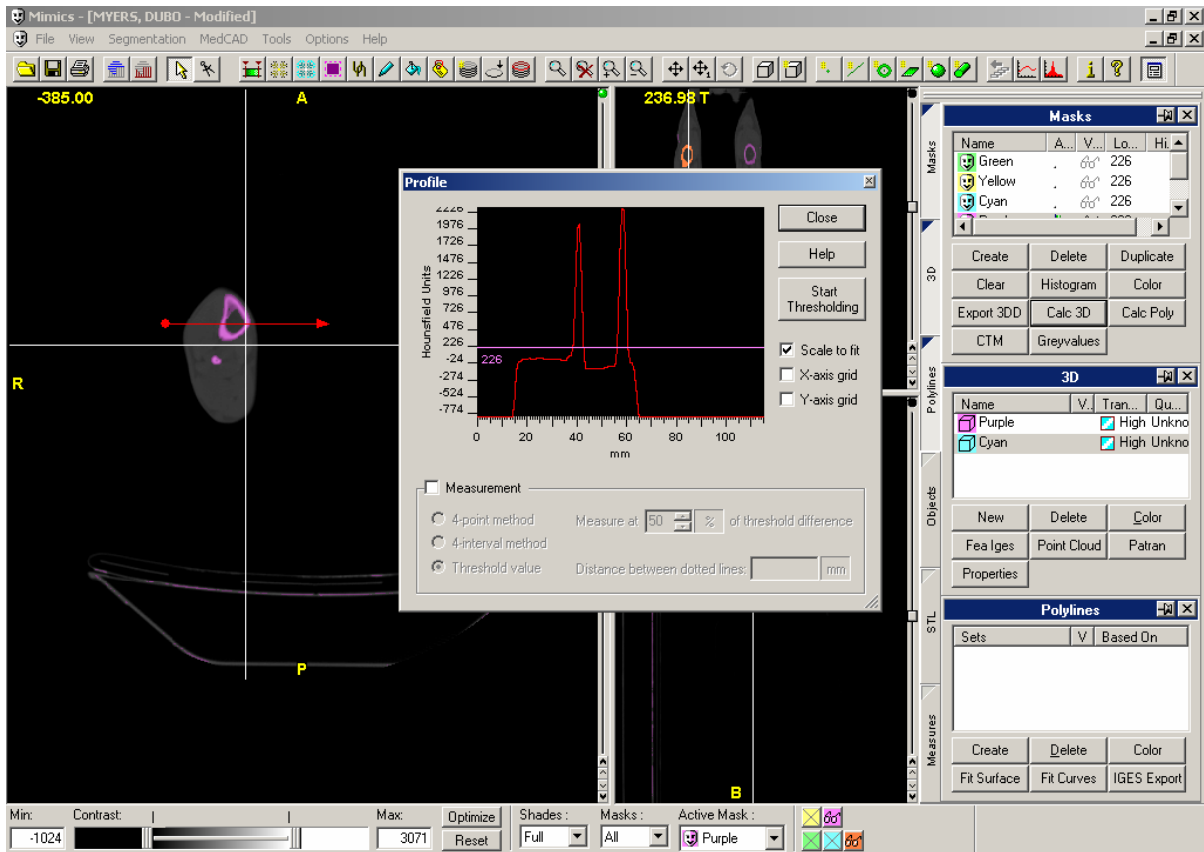


Figure 3.2: Screenshot of profile line during thresholding

The *region growing* function in Mimics was used to separate the femur from the rest of the anatomy of the dog and also to separate the femoral diaphysis and the epiphysis. Region growing is a feature where the program user only needs to select the desired tissue area on one CT slice and the respective areas on all other CT slices are automatically selected for the creation of a new “mask” with specific data. These masks are ultimately used to create a 3D model from the CT scans. After selecting the point of interest on the source mask, a new mask with all points connected to the point of interest can be created. Complete isolation of the femur in the source mask was necessary to create the new mask of just the femur data, as well as separating the distal and proximal sections. This was achieved with image editing of the CT slices using the draw and erase tools while progressing through all of the image slices and rotating through the different views in Mimics.

After using image editing and region growing to create new masks of the separated cortical and cancellous tissues of just the femur, image editing was then used again to separate

the proximal and distal regions of both types of tissues. The separation of the femur at the epiphyseal plate simulates the fracture that would occur at that location. Once CT data manipulation was complete, four different stl-files were created: the cortical distal femur, cancellous distal femur, cortical proximal femur and the cancellous proximal femur (Figure 3.3).

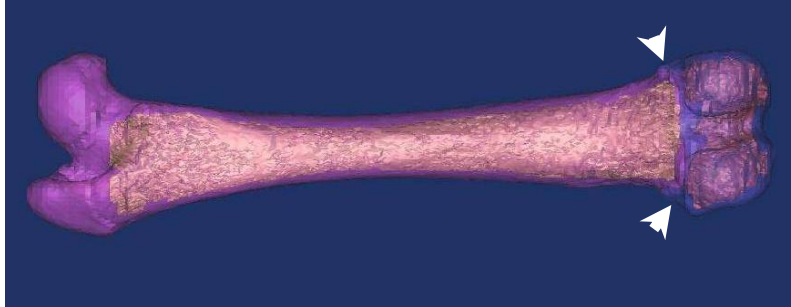


Figure 3.3: 3D model of a skeletally immature canine femur separated into four sections: a proximal and distal cortical section (purple) and a proximal and distal cancellous section (yellow). The arrowheads point at the separation (distal femoral physis)

A drawback with Mimics is that when the 3D models of the bones are isolated through image editing of the CT slices, some surrounding tissues can be inadvertently selected during the process. This was also the case during the creation of the epiphyseal fracture. Therefore, the stl-files of the cortical femur were imported into ClayTools (SensAble Technologies, Woburn, MA) and were smoothed using the PHANTOM Omni haptic device and the smoothing tool (Figure 3.4). The epiphyseal fracture region was adjusted to create a better fit between the proximal and distal sections, and the distal surface was also smoothed of erroneous surrounding tissues. Care was taken not to alter the medial and lateral surfaces of the femur. The cleaned files were then imported into Magics (Materialise, Leuven, Belgium) for designing of the femur models and both the polycaprolactone and titanium custom plates.

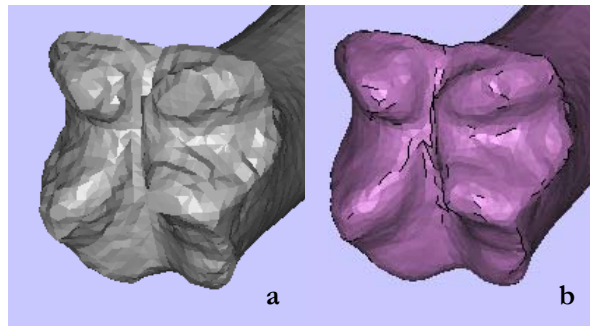


Figure 3.4: Stl-file of the proximal cortical femur pre-smoothing (a) and post-smoothing (b) in ClayTools

In preparation for the biomechanical testing, a cylinder measuring 50.7mm (2in) in diameter and 40mm in height was attached to the distal portion of the cortical femur in alignment with the long axis of the bone using a secondary cylinder as a guide for positioning. The distal cylinder dimensions were determined based on an existing testing jig used with the MTS servo-hydraulic loading machines for biomechanical testing. A 9.8mm (0.4in) diameter hole was created through the anterior-posterior axis of the proximal bone at a distance of 145mm from the cylinder-distal bone interface to allow a method for rotational testing (Figure 3.5). Additionally, the proximal bone was truncated of its femoral head at approximately 160mm from the cylinder-distal bone interface.

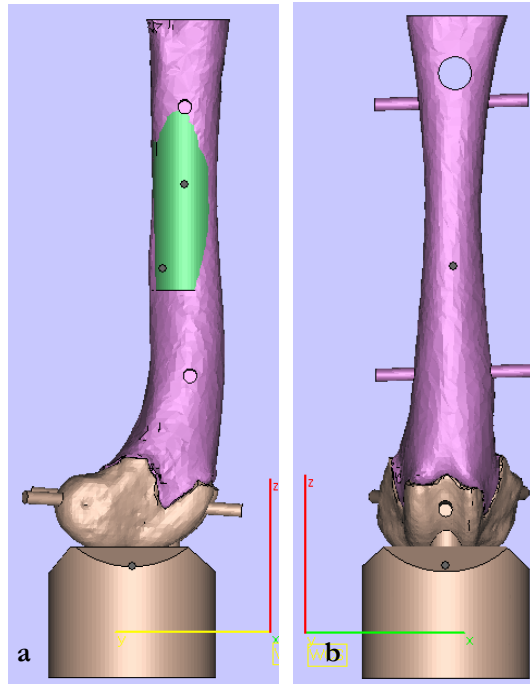


Figure 3.5: Side and frontal views of the cortical femur model. The shaft of the femur was aligned with a cylinder guide (green) shown in (a). A 50.7mm (2in) diameter cylinder was attached to the distal portion of the femur to fit into a testing jig. The 9.8mm (0.4in) diameter hole through the anterior-posterior axis of the proximal bone was created for torsional testing shown in (b).

Four locating pins of diameter 4mm were attached to the medial and lateral aspects of the proximal cortical femur distanced 82mm apart with the distal pin distanced 52mm from the cylinder-distal bone interface. Three locating pins of 4mm were attached in the anterior and posterior aspects of the distal cortical femur, one each at the posterior medial and lateral condyles and the third at the anterior articular capsule (Figure 3.6).

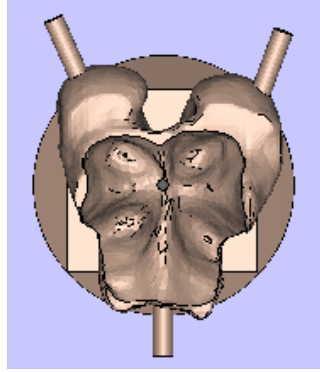


Figure 3.6: Top view of three locating pins positioned at the medial and lateral condyles and the anterior articular capsule of the distal femur for cortical and cancellous bone alignment during model production

These locating pins served as a reference to align the cancellous portions of the femur in relation to the cortical femur when creating the bone replicas. The distal and proximal cancellous femur were aligned within the distal and proximal cortical femur and pins were also attached in the respective areas of the existing pins (Figure 3.7).

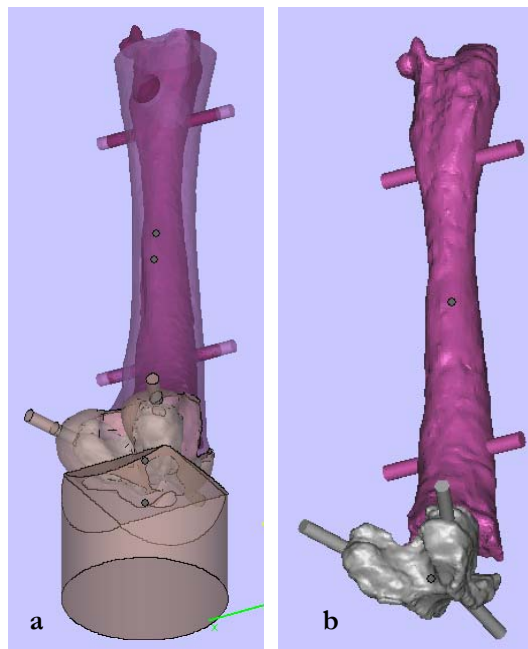


Figure 3.7: Transparent view of the cancellous bone sections in relation to the cortical bone sections, aligned using the locating pins (a). View of the distal and proximal cancellous femur sections and their respective locating pins (b)

3.1.2 Design of Distal Femoral Plates

The custom plate design ultimately used for the fabrication of the bioresorbable and titanium plates was created using Magics and ClayTools. The distal and proximal cortical sections of the femur were first merged at the epiphyseal plate in Magics for the plate design (Figure 3.8).

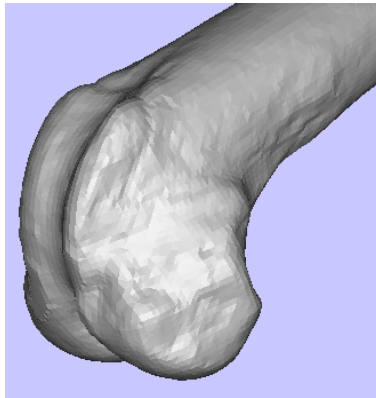


Figure 3.8: Lateral view of the femoral condyles after merging and cleaning of the distal and proximal cortical femur in preparation for designing the distal femoral plates.

Orienting the distal end of the femur to a medial-lateral view, a rough shape of the plate at the desired location was extracted from the bone using the *cut* function. To create plates that would be exactly contoured to the surface of the femur, The medial and lateral surfaces were each selected and offset at both 2mm and 4mm thicknesses. These stl-files were then opened in ClayTools for cleaning, smoothing and more refined shapening. The *boolean subtract* function in Magics was used to position and create six beveled screw holes using prescribed location instructions from a board certified veterinarian surgeon (Figure 3.9).

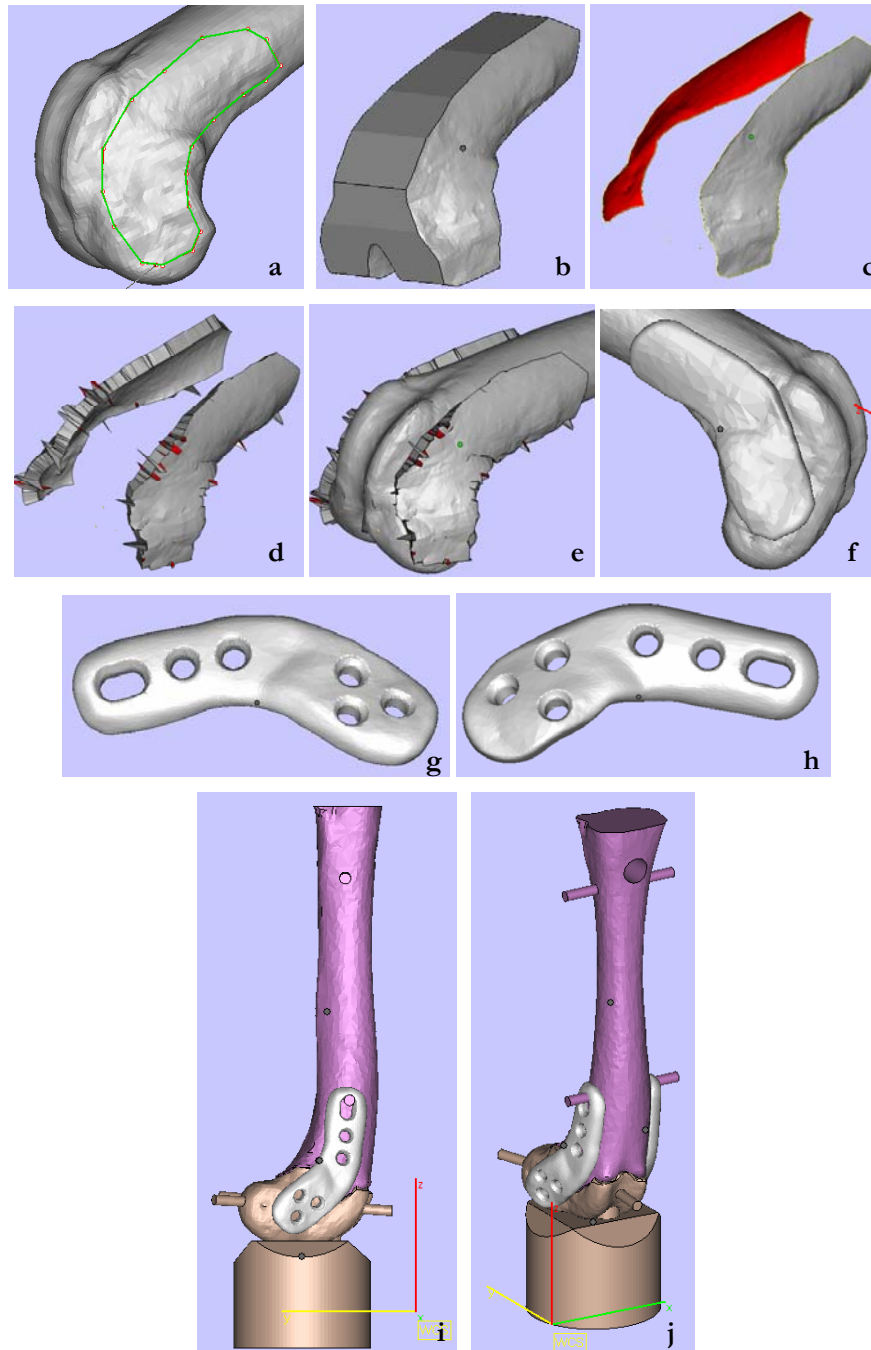


Figure 3.9: Method of designing distal femoral plates. Isolating area of distal femur for the location of the custom plate (a), extracting the desired location and deleting unnecessary surfaces (b-c), offsetting the surfaces to either 2mm or 4mm (d-e), refined and smoothed custom plates post-ClayTools application (f), 3D rendering of completed medial and lateral custom plates with positioned holes (g-h), placement of custom plates in relation to femur segments (i-j).

3.2 Fabrication Process

Fabrication of the artificial femurs, resorbable plates, and titanium plates utilized several rapid prototyping processes. FDM models and RTV silicon molds were created to mass produce identical anatomical artificial femur models. SLA and injection molding were processes used to create the resorbable plates and EBM technology was the rapid prototyping technique to create the titanium plates. The stainless steel commercial plates were also modified by truncating them to match the appearance of the custom designed plates for testing purposes.

3.2.1 Fabrication of Artificial Femurs

The completed designs of the four femur sections were then sent to a Dimension SST fused deposition modeling rapid prototyping machine (Dimension, Eden Prairie, MN) to create the parts using ABS plastic (Figure 3.10). These prototypes were used to make four RTV silicon molds (Mold Max 30, Smooth-On Inc., Easton, PA) which would be used to create the artificial femurs (Figure 3.11).



Figure 3.10: FDM-created ABS plastic models of the femur used to make silicon molds for mass bone model production



Figure 3.11: Room temperature vulcanized silicon molds of the cortical sections of the femur.

The femurs were created as a 2-piece foam and bone powder mixture with the foam representing the softer and inner cancellous portion of the distal and proximal femur and the bone powder mixture representing the harder and outer cortical portion of the distal and proximal femur. First, the two cancellous molds were filled with TC-300 rigid polyurethane foam (Burman Industries, Van Nuys, CA) with a 1:1 ratio and allowed to harden for 24 hours. Once hardened, these foam inserts were removed making sure to keep the locator pins intact, and then placed into molds for their respective cortical portions using the locator pin imprints as guides (Figure 3.12).

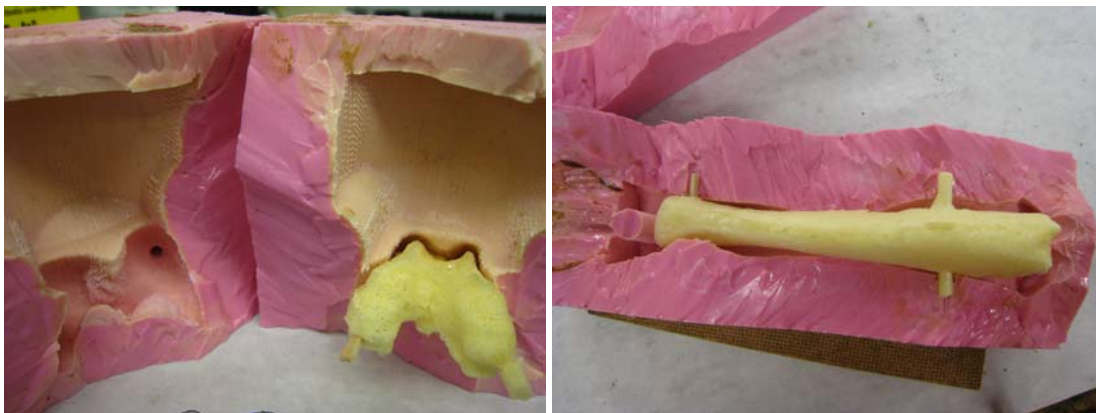


Figure 3.12: Positioning of the foam inserts into the cortical silicon molds via locating pins. Distal section (left) and proximal section (right).

Prior to placement of the inserts, the molds were treated with mold release spray (Smooth-On). The proximal foam insert was truncated just above the proximal two pins to allow the creation of the designed 9.8mm (0.4in) diameter hole at the anterior-posterior axis. These molds were then filled with a bone meal (Scotts Miracle Gro, Marysville, OH)/ EP5340 epoxy resin (Eager Polymers, Illinois) mixture at a ratio of 30% by weight with the resin mixture at a 4:1 ratio of part A and part B. The molds were clamped and allowed to set for approximately 24 hours before removal. Creation of the forty replicas (Figure 3.13) was randomized according to Table 3.1.

Table 3.1: Randomization order of femur model production

Production Order	Proximal Bone #	Distal Bone #
1	37	26
2	16	21
3	10	4
4	20	20
5	29	33
6	12	37
7	38	7
8	1	18
9	14	27
10	6	3
11	25	13
12	32	24
13	18	1
14	17	16
15	39	30
16	5	14
17	8	5
18	27	22
19	3	36
20	9	11
21	28	32
22	36	10
23	24	35
24	40	34
25	13	39
26	22	31
27	30	19
28	35	15
29	33	28
30	26	9
31	11	6
32	15	29
33	7	38
34	31	23
35	19	25
36	23	17
37	2	2
38	34	40
39	4	8
40	21	12



Figure 3.13: Completed replicas of the proximal and distal sections of the femur.

3.2.2 Fabrication of Molds for Bioresorbable Plates

The polycaprolactone bioresorbable plates were manufactured through an injection molding process using custom resin/steel epoxy molds. To create the plate molds, the stl-files of the 2mm and 4mm custom plates were opened in Magics and reoriented to the x-y plane with the screw holes oriented as closely in the z-axis direction as possible. This was performed to ensure the parting line of the mold would slice the mold for the easiest extraction of the plate and the mold material for the screw holes would come out cleanly when the mold was pulled apart. Using the *generate mold* tooling function in Magics, upper and lower cavities of the mold were designed to slice roughly in the middle of the plate and a runner from the sprue and a gate between the runner and cavity were placed into the mold (Figure 3.14). The undersides of the molds were hollowed in preparation for a steel liquid epoxy material to reinforce the molds' strength during use.

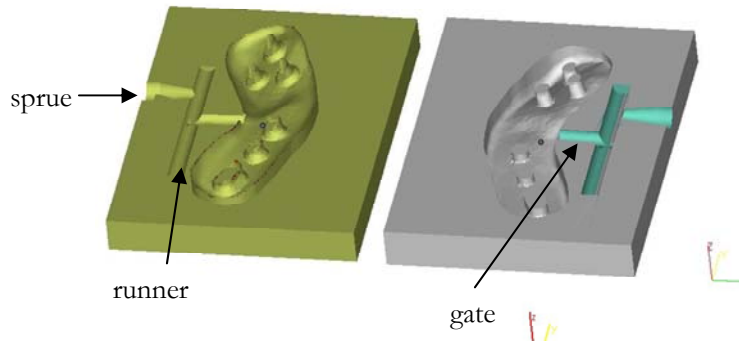


Figure 3.14: Designed molds for the creation of the polycaprolactone bioresorbable plates created in Magics

The stl-files of these molds were imported into the 3D Lightyear (3D Systems, Rock Hill, South Carolina) software for verification, cleaning and to prepare the platform for building the parts on a SLA-190 stereolithography machine (3D Systems) using Somos 11110 WaterShed resin (DSM Somos, Elgin Illinois). Once the parts were completed, they were cleaned of their support structure and placed into a UV oven for further curing. The inner surfaces of the mold were sanded to provide a smoother finish and to insure a tight seal during the injection molding. A steel liquid epoxy mixture (Loctite Fixmaster, Fel-Pro, Commerce city, CO) was poured into the hollowed portion of the molds and was allowed to set for 24 hours (Figure 3.15).



Figure 3.15: SLA-created resin mold for bioresorbable plate production (a) and completed mold after steel liquid epoxy treatment (b)

3.2.3 Fabrication of Bioresorbable Plates

The medial and lateral 2mm and 4mm bioresorbable plates were made out of polycaprolactone (Tone Polymer P-787, Union Carbide Corporation, Danbury, Connecticut) using the resin/steel epoxy molds. The polycaprolactone beads were first placed in an oven at 30 C for 10 minutes to dry out the material before adding into the barrel of the injection molding machine. Temperature and pressure of the injection molding machine was set to ~150°C and 400psi. Once the polycaprolactone beads were sufficiently melted, it was injected into the resin/steel epoxy molds and they were clamped shut and cooled for 5-10 minutes. Once the plates were hardened, the edges were cleaned with a knife and the screw holes were redefined using a drill press rotating at 620 rpm. Eight 2mm medial, 2mm lateral, 4mm medial, and 4mm lateral bioresorbable plates were created using this process (Figure 3.16).

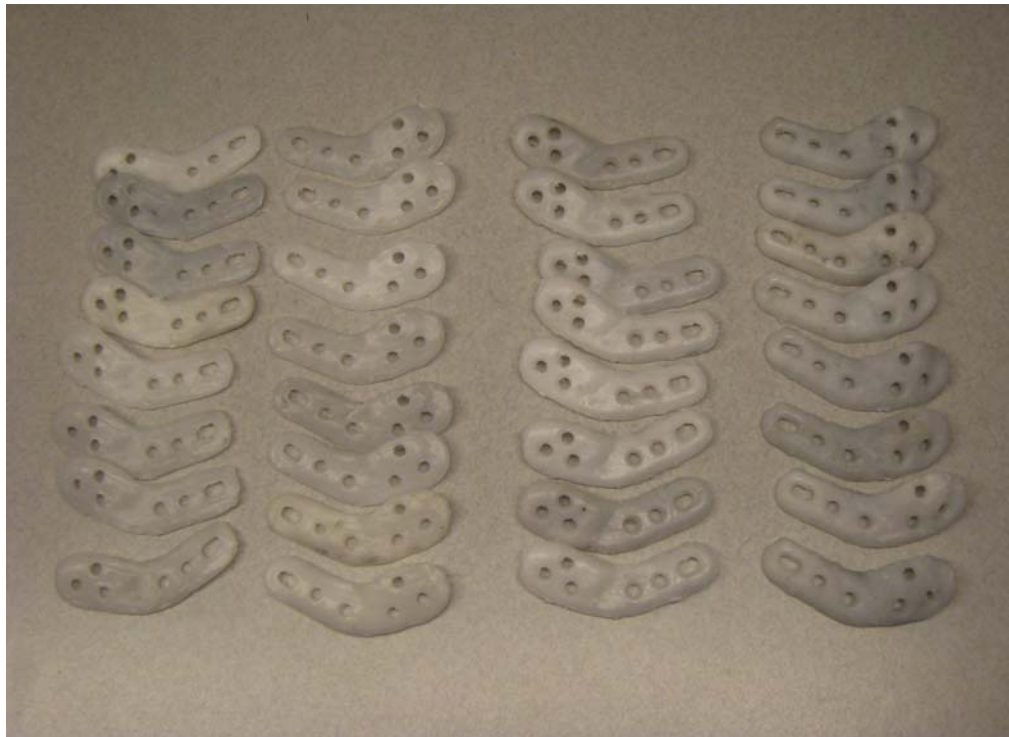


Figure 3.16: Eight 2mm medial, 2mm lateral, 4mm medial and 4mm lateral polycaprolactone bioresorbable plates (left-right)

3.2.4 Fabrication of Titanium Plates

The lateral titanium (Arcam Ti6Al4V powder) plates were created on an A2 Electron Beam Melting (EBM) machine (Arcam, Mölndal, Sweden) using the lateral 2mm custom plate stl-file. Using Magics, the stl-file was replicated and placed on a 210mm x 210mm x 10mm build platform with its necessary support structures. The saved mgx-file was sliced, prepared, and sent to the EBM machine for building (Figure 3.17).

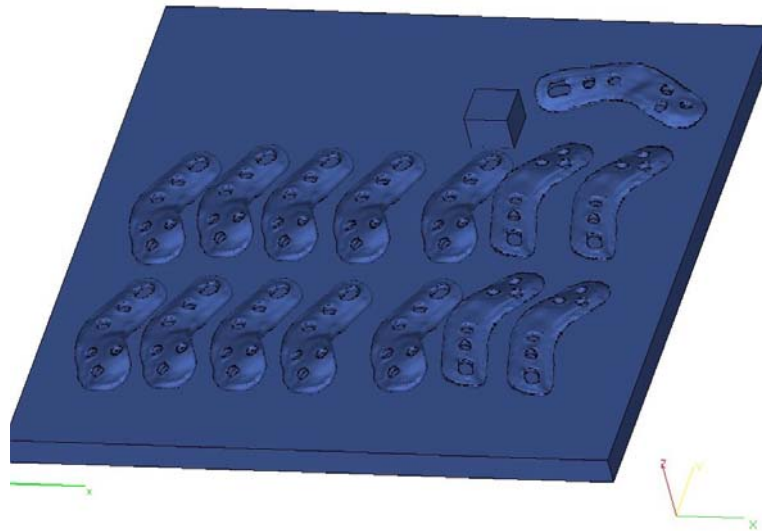


Figure 3.17: Build platform of the titanium plates. Ten lateral plates and five medial plates were built using the stl-file of the 2mm plates

Once cooled in the build chamber, the plates were removed and finished using a high-speed dremel to remove the burrs and to polish the surface. The edges of the holes were redefined using the dremel and beveled using a manufacturing drill press rotating at 620 rpm (Figure 3.18).

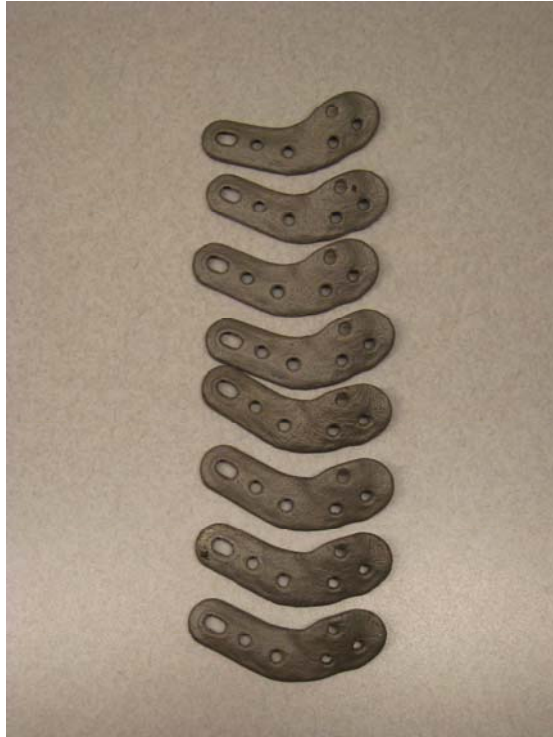


Figure 3.18: Completed custom designed lateral 2mm titanium plates

3.2.5 Stainless Steel Commercial Plates

Eight stainless steel 3.5mm left distal femur plates (J-428U) were obtained from Jorgensen Laboratories Inc (Loveland, CO) (Figure 3.19).

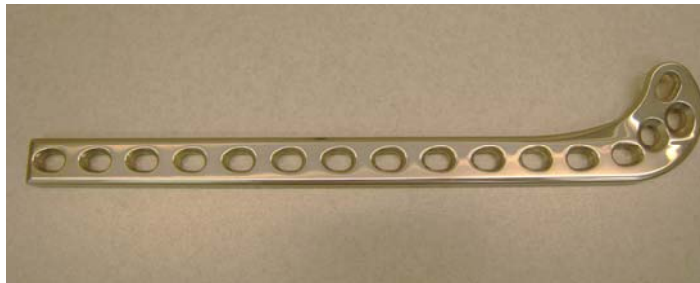


Figure 3.19: Stainless Steel Commercial Plate

The plates were truncated at the middle of the eighth hole from the distal end to (9th hole from the proximal end) with an aluminum oxide wheel on a water cooled abrasive cut-off saw (Mark V 600, East Granby, CT), to make the plates conform to the appearance of the custom plates (Figure 3.20). Seven holes remained on the distal plate for screw attachment.



Figure 3.20: Cut commercial plates

3.3 Plate Dimension Measurements

Approximate surface area and thickness of the four types of plates were measured to determine differences between the plate fixation techniques, in addition to the extra screw hole for the commercial plate. Using calipers, five measurements were made on each of the different types of plates; two widths, two lengths and one thickness measurement (Figure 3.21, Figure 3.22, Figure 3.23). An approximate surface area was calculated using the width and length measurements.

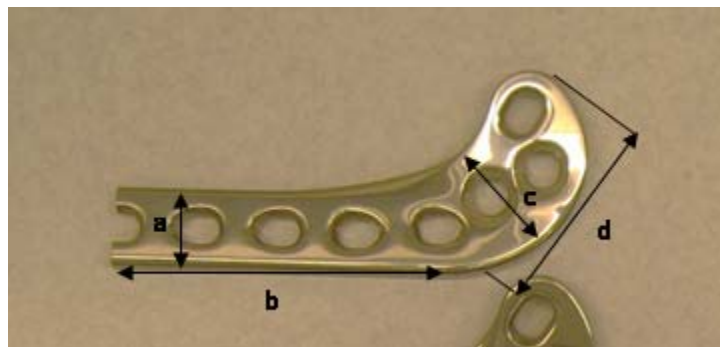


Figure 3.21: Measurements for the commercial plates. Width, length of the proximal end of plate (a,b) and width, length of the distal end of plate (c,d).

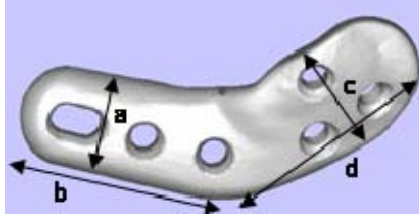


Figure 3.22: Measurements for the titanium plate, and lateral 4mm and 2mm resorbable plates. Width, length of the proximal plate (a,b) and width, length of the distal plate (c,d).

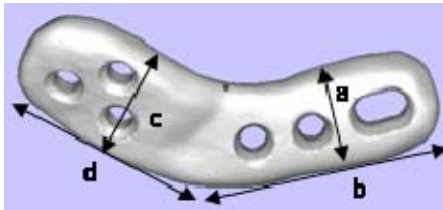


Figure 3.23: Measurements for the medial 4mm and 2mm resorbable plates. Width, length of the proximal plate (a,b) and width, length of the distal plate (c,d).

3.4 Surgical Technique

Surgeries to fixate the distal and proximal sections of the femur using the five different techniques were performed by a board certified veterinarian in a randomized order according to Table 3.2. Rehearsal surgeries were performed on spare femur models for the Kirschner wire, commercial plate, and 2mm resorbable plate surgical technique to plan the procedure approach. Screws for all plates were placed after drilling a pilot hole slightly smaller than the screw diameter.

Table 3.2: Randomization of surgery order.

Surgery Order Proximal/Distal #	Surgery Type/Number*
1	K3
2	E1
3	K6
4	K2
5	C8
6	E8
7	C7
8	C6
9	N6
10	E6
11	K8
12	K7
13	N8
14	E3
15	W1
16	N7
17	N5
18	E4
19	C2
20	W6
21	W2
22	N3
23	C4
24	C5
25	N4
26	N2
27	C3
28	N1
29	W5
30	E2
31	E5
32	W4
33	E7
34	K5
35	W7
36	K4
37	K1
38	W8
39	W3
40	C1

Table 3.2 continued.

*Eight specimens per construct type; commercial plate (C), titanium plate (E), resorbable 4mm plate (K), resorbable 2mm plate (N), and Kirschner wires (W)

3.4.1 Bioresorbable and Titanium Plates

Surgeries for the custom-designed bioresorbable and titanium plates were performed by first securing the lateral plate with six 3.5mm titanium screws (Synthes, Monument, CO) of lengths 12mm, 14mm, 28mm, 30mm 32mm, 38mm or 40mm. For the titanium plates, screw lengths were chosen so that the lateral inserted screw threads would protrude from the medial side as much as possible to ensure complete utilization of the screw as a fixation device. For the resorbable plates, screw lengths were chosen so that lateral inserted screws would not protrude under the medial plate but medial inserted screws would protrude from the lateral side as much as possible. The distal section of the femur was held by a table vice while the proximal section was compressed against the epiphyseal plate fracture until the two sections were sufficiently secured. After fixation of the lateral plate, femurs designated to be secured with 2mm or 4mm bioresorbable plates were also secured with their respective medial plate using the same process with care not to harm the lateral plate. The time to fixate the lateral and medial plates was noted for all surgeries.

3.4.2 Stainless Steel Commercial Plates

Surgeries for the commercial plate were conducted by first compressing the distal and proximal femur sections against the epiphyseal plate fracture and contouring the plate to the lateral side of the femur with a plate press. The plates were secured with seven 316L stainless-steel screws (Synthes, Monument, CO) of lengths 20mm, 28mm, 30mm, 34mm and 40mm. Screw lengths were chosen so that the lateral inserted screw threads would protrude from the medial side as much as possible. Using the table vice to grip the distal section of the femur, the proximal femur was compressed against the distal femur until the two sections were sufficiently secured. The time to perform the entire procedure was noted.

3.4.3 Kirschner Wires

Surgeries with the Kirschner wires were conducted using 285mm long 316L stainless-steel 2.0mm wires with trocar points (Synthes, Monument, CO). Using the table vice to grip the distal section of the femur, the proximal femur section was compressed against the distal section

as two wires were each inserted through the lateral and then medial condyles to create a crossed orientation. The time to perform the procedure was noted for all surgeries.

3.5 Biomechanical Testing

Mechanical testing of the bone models was performed on an MTS 858 Mini Bionix II - Servo-Hydraulic Axial Load Frame and a MTS 858 Mini Bionix II - Servo-Hydraulic Axial Torsion Load Frame (MTS, Eden Prairie, MN) for bending and torsional tests, respectively. All screws were torqued with a Cedar digital torque tester/screwdriver (Model DSD-4, Imada, Inc., Northbrook, IL) to 1.13Nm for the commercial and titanium plates, and 0.283Nm (25% of screw torque used for metal plates) for the resorbable plates for consistency prior to testing [72]. Torquing of the screws was immediately halted if there was a sudden decrease in torque suggesting stripping of threads, or if the screw began to penetrate through the resorbable plates. All femur models underwent three different nondestructive testing configurations of external torsional loading, cranial bending and medial bending, and one of two destructive tests of either torsional loading or cranio-caudal bending to failure. Each of the three nondestructive tests were cycled four times, with the first cycle acting as a preconditioning run and excluded from data analysis. Tests were conducted in a randomized order according to Table 3.3.

Table 3.3: Randomization of mechanical testing order

Testing Order	Construct Type*	First Test ^a	Second Test ^a	Third Test ^a	Failure Test ^b
1	W4	CB	MB	ET	ET
2	N1	ET	MB	CB	CB
3	C7	MB	CB	ET	ET
4	W6	MB	CB	ET	ET
5	C4	MB	ET	CB	CB
6	K4	CB	MB	ET	ET
7	W3	MB	CB	ET	ET
8	E3	MB	CB	ET	ET
9	E8	CB	ET	MB	ET
10	E7	CB	ET	MB	CB
11	C3	CB	MB	ET	ET
12	C8	CB	MB	ET	ET
13	E4	CB	ET	MB	ET
14	K2	MB	CB	ET	ET
15	N7	MB	CB	ET	ET
16	K5	ET	MB	CB	CB
17	W1	CB	MB	ET	ET
18	W7	ET	CB	MB	CB
19	C1	MB	ET	CB	CB
20	K7	CB	MB	ET	ET
21	K1	CB	ET	MB	CB
22	N5	ET	CB	MB	CB
23	N6	MB	CB	ET	ET
24	C2	ET	MB	CB	CB
25	N2	CB	MB	ET	ET
26	N4	ET	CB	MB	ET
27	K6	ET	CB	MB	CB
28	K8	MB	ET	CB	ET
29	E5	MB	ET	CB	CB
30	N8	MB	ET	CB	CB
31	C5	ET	MB	CB	CB
32	E1	MB	ET	CB	CB
33	N3	CB	ET	MB	CB
34	K3	ET	MB	CB	CB
35	E2	MB	ET	CB	CB
36	W5	MB	CB	ET	CB
37	W8	CB	MB	ET	CB
38	C6	CB	ET	MB	ET
39	E6	CB	MB	ET	ET
40	W2	MB	CB	ET	CB

Table 3.3 continued.

* commercial plate (C), titanium plate (E), resorbable 4mm plate (K), resorbable 2mm plate (N), and Kirschner wires (W)

^a nondestructive biomechanical testing order of cranial bending (CB), medial bending (MB) and external torsion (ET)

^b one failure test of either cranial bending or external torsion

3.4.1 Testing Procedure Trial Runs

Prior to the testing of any of the femur models, the nondestructive torsional MTS procedure was determined by conducting tests on a trial specimen that had been used for Kirschner wire surgery rehearsal. The trial specimen was progressively rotated at a rate of 10 deg/min to a rotation of 1 degree, 1.5 degrees and 2 degrees until it was determined that 2 degrees of rotation was sufficient to measure the torque generated for all types of constructs without causing destructive harm to any type of construct. The trial specimen was then torsionally loaded to failure to ensure proper operation of the testing machine. Determination of the nondestructive cranial and medial bending MTS procedures was determined by conducting tests on the 2mm resorbable surgery rehearsal specimen. Tested as a cantilever beam, it was determined that a 10N load placed on the trial specimen 100mm away from the epiphyseal plate fracture site at a rate of 0.5 mm/s would be sufficient to measure the crosshead displacement of each type of construct without displaying any destructive results. The trial specimen was then cranially loaded to failure to ensure proper operation of the testing machine.

3.4.2 Coating of the Proximal Femur Sections

After the testing procedure was determined with the trial runs, all of the femur models were then applied with an EP5340 epoxy resin and fiberglass coating along the shaft of the proximal section and any thin cortical areas where signs of the cancellous bone were prominent. The femurs were first hand-coated with a thin layer of epoxy before application of individual strands of fiberglass in a crisscross fashion and then another thin application of epoxy to ensure fiberglass epoxy-saturation to the surface of the models (Figure 3.24). The models were allowed to cure for 24 hours before any mechanical testing was performed.



Figure 3.24: Application of the epoxy and fiberglass coating to the proximal femur section

3.4.3 External Torsional Loading (nondestructive)

Nondestructive external torsional loading of the proximal section in relation to the distal section of the femur was performed in four consecutive cycles at a crosshead rotation rate of 10 deg/min to a maximum 2 degree angle rotation for each of the models in a randomized order, with the first cycle acting as a preconditioning run [81]. The distal femur section was placed in the rotational testing jig fixed rigidly to the MTS table and a 9.8mm (0.4in) diameter rod was inserted through the hole in the proximal femur section (Figure 3.25). This rod would enable application of the 2 degrees of rotation by the MTS machine crosshead. Care was given to reduce the slack in the system as much as possible as the crosshead was rotated to where it was just in contact with both sides of the rod before zeroing the angle of rotation.



Figure 3.25: Testing setup for external torsional loading

3.4.4 Cranial Bending (nondestructive)

Nondestructive cranial bending of the femur was performed in four consecutive cycles at a crosshead displacement rate of 0.5mm/s with a 10N load applied at a moment arm of 100mm from the epiphyseal plate fracture site, generating 1N-m [81]. The first of the four cycles acted as a preconditioning run and was excluded from analysis. The femur was cranially positioned

with the distal section placed in the bend testing jig fixed rigidly to the MTS table so that it would act like a cantilever beam during testing (Figure 3.26). Care was given to reduce the slack in the system as much as possible and the crosshead was lowered to where it was just in contact with the femur before zeroing the displacement.



Figure 3.26: Testing setup for cranial loading

3.4.5 Medial Bending (nondestructive)

Nondestructive medial bending of the femur was performed in four consecutive cycles at a crosshead displacement rate of 0.5mm/s with a 10N load applied 100mm from the epiphyseal plate fracture site, generating 1N-m [81]. The first of the four cycles acted as a preconditioning run and was excluded from analysis. The femur was medially positioned with the distal section placed in the bend testing jig fixed rigidly to the MTS table so that it would act like a cantilever beam during testing (Figure 3.27). Care was given to reduce the slack in the system as much as possible and the crosshead was lowered to where it was just in contact with the femur before zeroing the displacement.



Figure 3.27: Testing setup for medial loading

3.4.6 External Torsional and Cranial Bending Failure Tests

The destructive external torsional loading of the proximal section in relation to the distal section of the femur was conducted on four of each type of repair method. The setup for this test was exactly the same as that of the nondestructive external torsional loading where the distal section was secured to the MTS table with a rod inserted through the proximal section with both sides touching the crosshead and minimizing slack of the system. The crosshead externally rotated the proximal femur at 10 deg/min until failure, determined as a 75% drop of collected torque from the maximum value.

The destructive cranial bending of the femur was conducted on four of each type of repair method. The setup for this test was exactly the same as that of the nondestructive cranial bending where the distal section was secured to the MTS table with the femur oriented cranially as a cantilever beam. The crosshead loaded the femur at 100mm proximal of the epiphyseal plate fracture site at a rate of 0.5mm/s until failure, determined as a 75% drop of collected force from the maximum value.

3.5 Processing Results

Force and displacement values were recorded for the destructive and nondestructive cranial and medial bending tests. Torque and rotation values were recorded for the destructive and nondestructive external torsion tests. These files were imported into Excel for post processing.

A spreadsheet was set up for each nondestructive trial to determine structural stiffness of each construct. Graphs of the force versus displacement were plotted for the bending tests for each of the three cycles from 0 to 10N of force. Graphs were also generated for torque versus rotation for the torsion tests for each of the three cycles from 0 to 2 degrees of rotation. A linear regression line was generated for each of the curves to determine the structural stiffness using the following relationship.

$$k = \frac{P}{\delta}$$

Where k = structural stiffness, P = force applied, and δ = displacement produced by the force. Structural stiffness was chosen as an adequate variable because the overall stiffness of the constructs was of interest to this study, rather than the material stiffness of the each type of bone plate and crossed Kirschner wires. The displacement for the 10N applied force was also recorded for the bending tests as well as the torque generated from the 2 degrees of rotation for the torsion test. These values were examined to determine if there was a significant difference between the different constructs in response to a smaller, nondestructive load.

A spreadsheet was also set up for each destructive trial to determine the yield and ultimate strength or yield and ultimate torque for the cranial bending or external torsion tests, respectively. The yield strength and yield torque are defined as the maximum force and torque of the linear portion of the cranial bending tests and torsional loading tests before a decreased change in structural stiffness. Ultimate strength and torque are defined as the maximum force and torque of the cranial bending and torsional loading tests before failure, determined as a 75% drop of collected force or torque from the maximum value. Graphs of the force versus displacement were plotted for the load to failure for the bending tests and graphs were also generated for the torque versus rotation load to failure for the torsion tests.

Overall force versus displacement and torque versus rotation curves were also generated for nondestructive tests by taking the third cycle of each specimen and averaging them together for each type of construct. These curves were all plotted on one caudal bending, medial bending, and external torsion graph for visual comparison of structural stiffness values.

3.6 Statistical Analysis

Prior to testing for significance, variables were evaluated with a Shapiro-Wilk test for normality, because of its good power properties as compared to a wide range of alternative tests [84, 85]. If the test showed no evidence of non-normality, the variables analyzed for significance were the structural stiffness and the displacement or torque for a respective 10N load or 2 degree rotation for the nondestructive tests, and the yield and ultimate strength or the yield and ultimate torque for the destructive tests. An unpaired two-tailed t-test was performed on these values to test for variability between the different types of constructs, with a 0.05 p-value to determine significance. If the Shapiro-Wilk test showed evidence of non-normality, a two-tailed Mann-Whitney-Wilcoxon two-sample test was used to determine whether their probability distributions were equal, with a 0.05 p-value to determine significance.

A Bonferroni correction was conducted to avoid spurious positives. An alpha of 6.25E-03 was used to determine significance for the structural stiffness, displacement at 10N and torque from 2 degrees of rotation nondestructive variables. An alpha of 1.25E-02 was used to determine significance for the yield and ultimate strength or torque destructive variables.

Structural stiffness for the nondestructive tests was also evaluated using an ANOVA test to capture any significant difference between the three cycles after a Shapiro-Wilk test for normality. A p-value of 0.05 was used to determine significance. If there were no significant differences, the variables obtained from the nondestructive three cycles were averaged to a single value per specimen before variable comparison between constructs.

All statistical analyses were conducted using Excel Analysis ToolPak, an Excel Toolkit compiled by Syracuse Research Corporation (Syracuse, NY), and Power and Precision (Biostat, Englewood, NJ).

4. RESULTS

Forty femur specimens were tested, 8 commercial plate constructs, 8 titanium plate constructs, 8 resorbable 4mm plate constructs, 8 resorbable 2mm plate constructs, and 8 Kirschner wire constructs. Each specimen underwent three nondestructive tests of caudal bending, medial bending and torsional loading with three cycles per test and an extra preconditioning cycle. Each specimen then underwent one of two destructive tests of either caudal bending or torsional loading.

4.1 Nondestructive Tests

A total of 118 nondestructive tests were performed on the 40 specimens. Torsional loading data was not collected on two Kirschner wire specimens due to fracture during setup (W1) and software collection difficulties (W4).

The nondestructive tests generated several variables for each specimen, one of which was the structural stiffness. The three cycles of the three tests each produced three structural stiffness values (Appendix A). A Shapiro-Wilk test was conducted to test for normality of the data, with test statistic values greater than the $W_{0.05}(=0.82)$ representing no evidence of non-normality (Table 4.1).

Table 4.1: Shapiro-Wilk normality test for cranial, medial and torsional structural stiffness variables for cycles 1, 2, 3. A test statistic less than $W_{0.05}=0.82$ is significant.

<i>Shapiro-Wilk Test for Normality</i>			
<i>Structural Stiffness</i>			
<i>W test statistic</i>			
Cranial Structural Stiffness			
Construct Type	Cycle1	Cycle2	Cycle3
Comm.	0.91	0.91	0.91
Tit.	0.92	0.92	0.92
Res. 4mm	0.93	0.93	0.93
Res. 2mm	0.97	0.97	0.97
K. Wires	0.83	0.83	0.83
Medial Structural Stiffness			
Construct Type	Cycle1	Cycle2	Cycle3
Comm.	0.91	0.91	0.91
Tit.	0.89	0.89	0.89
Res. 4mm	0.96	0.96	0.96
Res. 2mm	0.94	0.94	0.94
K. Wires	0.86	0.86	0.86
Torsional Structural Stiffness			
Construct Type	Cycle1	Cycle2	Cycle3
Comm.	0.85	0.85	0.85
Tit.	0.99	0.99	0.99
Res. 4mm	0.99	0.99	0.99
Res. 2mm	0.85	0.85	0.85
K. Wires	0.90	0.90	0.90

As evidenced in Table 4.1, all test statistic values were greater than $W_{0.05}$ indicating no evidence of non-normality and allowing the use of an ANOVA f-test to make certain these repeated tests were not destructive to the specimens. The statistical analysis used a type I error rate of 0.05 in all cases, therefore a p-value of less than 0.05 indicates evidence of a statistically significant difference between the compared values (Table 4.2).

Table 4.2: ANOVA comparison of cycles 1,2, and 3 for all constructs during nondestructive cranial, medial and torsional testing. A p-value less than 0.05 is significant.

ANOVA <i>Structural stiffness between cycles 1, 2, 3</i> <i>p-values</i>			
Construct Type	Cranial Bending (N/m)	Medial Bending (N/m)	Torsional Loading (N-m/rad)
Comm.	0.99	0.98	1.00
Tit.	0.99	1.00	0.99
Res. 4mm	1.00	1.00	1.00
Res. 2mm	0.99	1.00	1.00
K. Wires	1.00	1.00	1.00

All structural stiffness values for all constructs were found to be non-significant between the three nondestructive cycles, with a power of 0.05. With all specimens having shown non-variability between cycles for all three types of tests, the structural stiffness and maximum displacements for a 10N load or maximum torques for a two degree rotation values for the cycles were averaged into one value for each specimen for statistical comparison of differences (Appendix B). A Shapiro-Wilk test was conducted on the six variables for each of the construct types to test for normality, with test statistic values greater than the $W_{0.05}(=0.82)$ representing no evidence of non-normality (Table 4.3).

Table 4.3: Shapiro-Wilk normality test for nondestructive test variables for all constructs. A test statistic less than $W_{0.05}=0.82$ is significant.

Shapiro-Wilk Test for Normality <i>Nondestructive variables</i> <i>W test statistic</i>						
Construct Type	Cranial Structural Stiffness	Medial Structural Stiffness	Torsional Structural Stiffness	Cranial Displacement at 10N	Medial Displacement at 10N	Torque at 2 degrees
Comm.	0.91	0.91	0.85	0.96	0.89	0.79
Tit.	0.92	0.89	0.99	0.92	0.91	0.98
Res. 4mm	0.93	0.96	0.99	0.88	0.87	0.98
Res. 2mm	0.97	0.94	0.85	0.95	0.91	0.92
K. Wires	0.83	0.86	0.9	0.74	0.79	0.98

Non-normality of data was evidenced for the Kirschner wires for cranial and medial displacement at 10N and also for the commercial plate constructs for torque generated at 2 degrees of rotation. A two-tailed Mann-Whitney-Wilcoxon test was used for the statistical comparisons between constructs for the cranial and medial displacement at 10N and torque generated at 2 degrees of rotation, with a $6.25E-03$ alpha to determine significance. An unpaired two-tailed t-test was performed on the structural stiffness values to test for variability between the constructs, with a $6.25E-03$ alpha to determine significance. The statistical analysis used a type I error rate of 0.05 in all cases, and with a Bonferroni correction a p-value less than $6.25E-03$ indicates evidence of a statistically significant difference between the compared values.

Having shown non-variability between cycles for all three types of tests from the ANOVA analysis (Table 4.2), the third cycle was graphed for each of the various constructs (Figure 4.1, Figure 4.2, Figure 4.3). Commercial, titanium plate, and Kirschner wire constructs exhibited similar responses to the 10N load across all specimens for cranial bending. Both resorbable 4mm and 2mm plate constructs displayed some variability among different specimens during nondestructive bending. During medial bending, titanium plate and Kirschner wire constructs displayed some variability whereas the other fracture repair techniques did not show as much differentiation among specimens. Nondestructive torsional loading tests did not show much variability among specimens for all constructs except the titanium plate repaired models. Torsional loading tests did however reveal signs of construct settling through the tests for all fixation techniques.

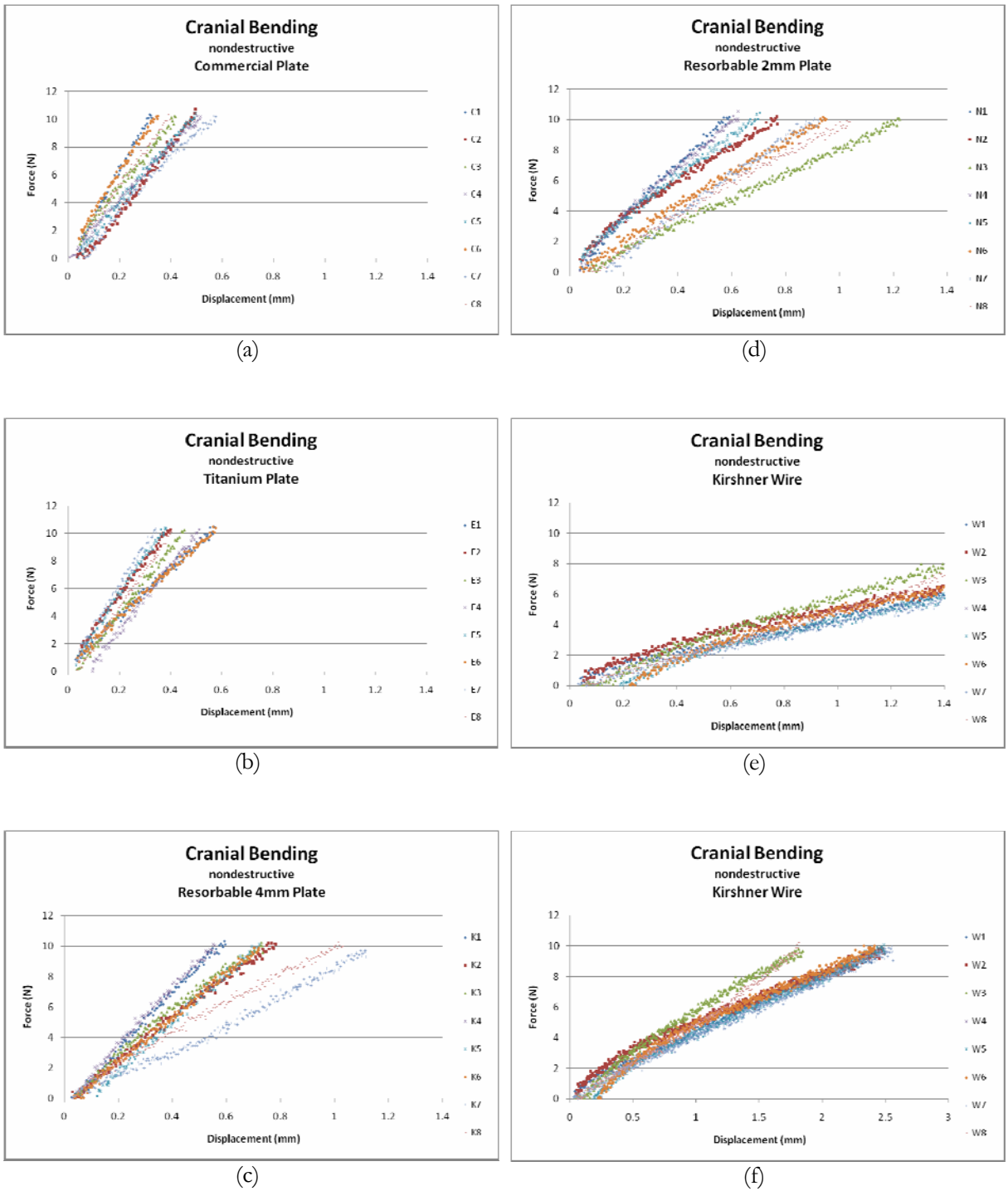
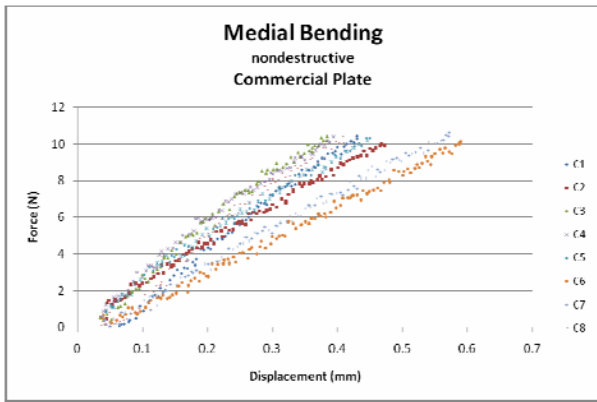
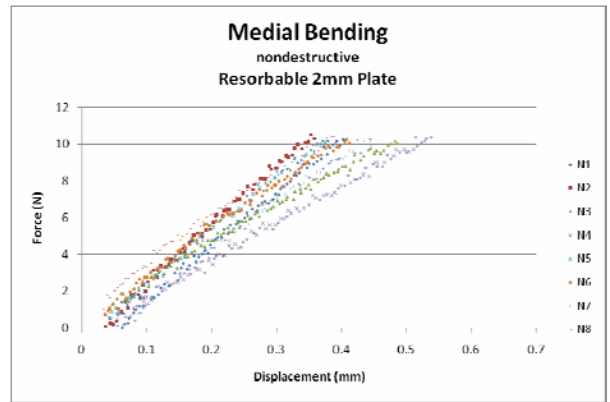


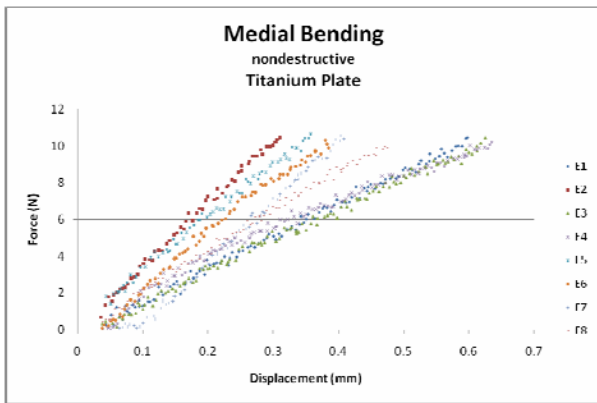
Figure 4.1: Graphs of nondestructive cranial bending tests. Commercial plate (a), titanium plate (b), resorbable 4mm plate (c), resorbable 2mm plate (d) and Kirshner wire (e) constructs. (f) is an x-axis autoscaled graph of the Kirshner wire constructs.



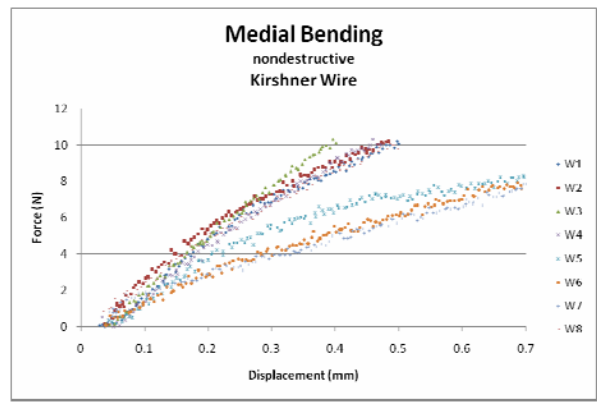
(a)



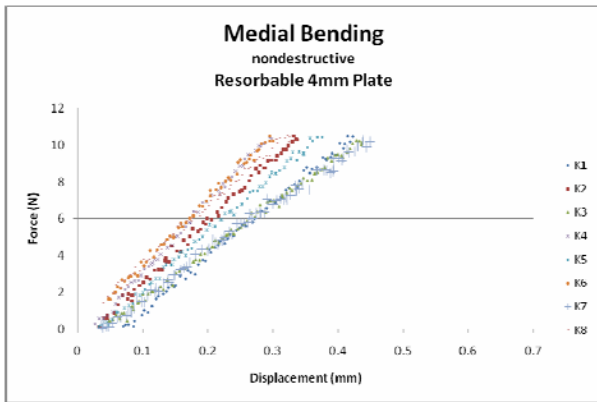
(d)



(b)

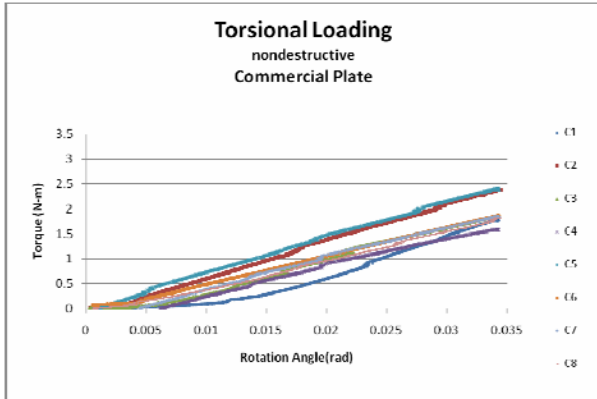


(e)

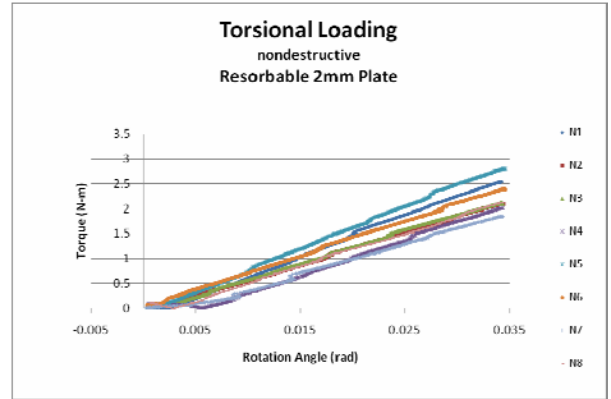


(c)

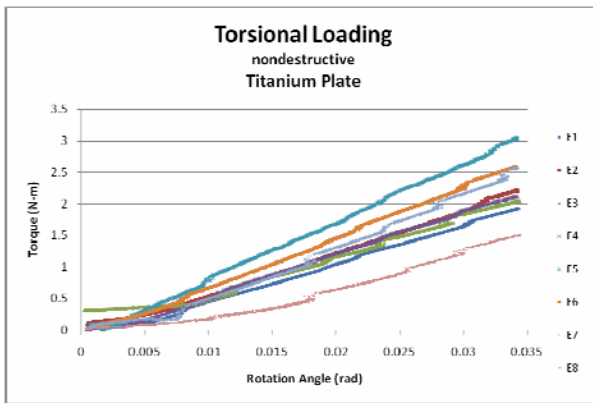
Figure 4.2: Graphs of nondestructive medial bending tests. Commercial plate (a), titanium plate (b), resorbable 4mm plate (c), resorbable 2mm plate (d) and Kirshner wire (e) constructs.



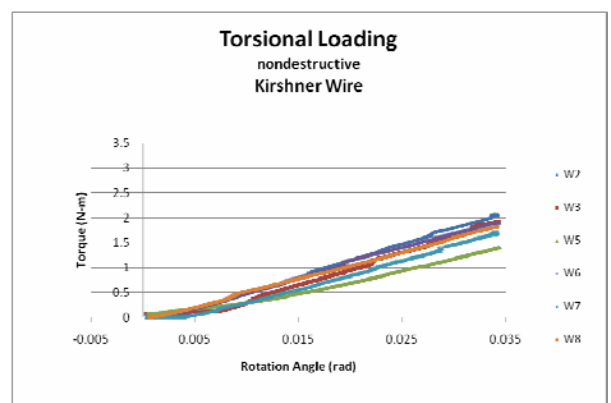
(a)



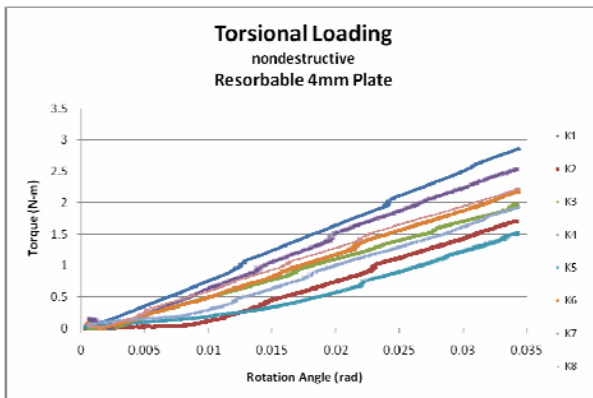
(d)



(b)



(e)



(c)

Figure 4.3: Graphs of nondestructive torsional loading tests. Commercial plate (a), titanium plate (b), resorbable 4mm plate (c), resorbable 2mm plate (d) and Kirschner wire (e) constructs.

4.1.1 Structural Stiffness

Structural stiffness values obtained from cranial bending tests showed no significant differences between the commercial plate constructs (24.66 ± 4.71 kN/m) and the titanium plate constructs (24.07 ± 4.67 kN/m) with a p-value of 0.80, and no significant differences between the resorbable 4mm plate constructs (14.41 ± 3.73 kN/m) and the resorbable 2mm plate constructs (12.86 ± 3.23 kN/m) with a p-value of 0.39. Commercial plates showed a significantly higher structural stiffness compared to the resorbable 4mm plate constructs, resorbable 2mm constructs, and Kirschner wires. Analysis showed significantly higher structural stiffness values for the titanium plate constructs when compared to both the resorbable 4mm and the resorbable 2mm constructs, as well as the Kirschner wire constructs. Resorbable 4mm plate constructs showed significantly higher structural stiffness compared to the Kirschner wires. Resorbable 2mm plate constructs also showed a significantly higher structural stiffness with the Kirschner wire constructs (Table 4.4, Table 4.5). Respective powers for the conducted t-tests are reported in Table 4.6.

Table 4.4: t-test p-values for structural stiffness from cranial bending, nondestructive tests. A p-value less than 6.25E-03 is significant.

<i>t-test</i> <i>Structural Stiffness - Cranial Bending</i> <i>p-values</i>					
Construct	Comm.	Tit.	Res. 4mm	Res. 2mm	K.Wires
Comm.	1	0.80	3.29E-04	7.83E-05	3.02E-06
Tit.		1	5.21E-04	1.18E-04	3.57E-06
Res. 4mm			1	0.39	7.25E-05
Res. 2mm				1	6.63E-05
K. Wires					1

Table 4.5: Structural stiffness for cranial bending. Overall mean and standard deviation (SD) values provided for each construct.

<i>Structural Stiffness (kN/m)</i> <i>Cranial Bending</i>					
Construct	Comm.	Tit.	Res. 4mm	Res. 2mm	K. Wires
mean	24.66	24.07	14.41	12.86	4.69
SD	4.71	4.67	3.73	3.23	1.45

Table 4.6: t-test power for structural stiffness from cranial bending, nondestructive tests. Values indicate the percentage of constructs that would be expected to yield a significant effect.

<i>t-test</i> Structural Stiffness - Cranial Bending <i>power</i>					
Construct	Comm.	Tit.	Res. 4mm	Res. 2mm	K. Wires
Comm.	1	0.01	0.92	0.99	1.00
Tit.		1	0.89	0.98	1.00
Res. 4mm			1	0.03	1.00
Res. 2mm				1	1.00
K. Wires					1

Structural stiffness values obtained from medial bending tests showed no significant differences between the commercial plate constructs (24.71 ± 4.48 kN/m), the titanium plate constructs (24.83 ± 7.56 kN/m), the resorbable 4mm plate constructs (31.51 ± 4.72 kN/m), the resorbable 2mm plate constructs (25.93 ± 4.17 kN/m), and Kirschner wire constructs (18.35 ± 7.50 kN/m) for any of the comparisons except a marginally higher structural stiffness for the resorbable 2mm plate constructs when compared to the Kirschner wire (p -value $1.23E-03$) (Table 4.7, Table 4.8). Respective powers for the conducted t-tests are reported in Table 4.9.

Table 4.7: t-test p -values for structural stiffness from medial bending, nondestructive tests. A p -value less than $6.25E-03$ is significant.

<i>t-test</i> Structural Stiffness - Medial Bending <i>p-values</i>					
Construct	Comm.	Tit.	Res. 4mm	Res. 2mm	K. Wires
Comm.	1	0.97	0.01	0.58	0.06
Tit.		1	0.06	0.73	0.11
Res. 4mm			1	0.03	$1.23E-03$
Res. 2mm				1	0.03
K. Wires					1

Table 4.8: Structural stiffness for medial bending. Overall mean and standard deviation (SD) values provided for each construct.

Structural Stiffness (kN/m)					
Medial Bending					
Construct	Comm.	Tit.	Res. 4mm	Res. 2mm	K. Wires
mean	24.71	24.83	31.51	25.93	18.35
SD	4.48	7.56	4.72	4.17	7.50

Table 4.9: t-test power for structural stiffness from medial bending, nondestructive tests. Values indicate the percentage of constructs that would be expected to yield a significant effect.

t-test					
Structural Stiffness - Medial Bending					
power					
Construct	Comm.	Tit.	Res. 4mm	Res. 2mm	K. Wires
Comm.	1	0.01	0.43	0.01	0.17
Tit.		1	0.19	0.01	0.11
Res. 4mm			1	0.29	0.82
Res. 2mm				1	0.29
K. Wires					1

Structural stiffness values obtained from torsional loading tests showed no significant differences between the commercial plate constructs (60.85 ± 7.78 N-m/rad), the titanium plate constructs (65.96 ± 14.77 N-m/rad), resorbable 4mm plate constructs (63.17 ± 13.33 N-m/rad), resorbable 2mm plate constructs (67.91 ± 9.69 N-m/rad), and the Kirschner wire constructs (54.25 ± 8.20 N-m/rad) for any of the comparisons (Table 4.10, Table 4.11). Respective powers for the conducted t-tests are reported in Table 4.12.

Table 4.10: t-test p-values for structural stiffness from torsional loading, nondestructive tests. A p-value less than 6.25E-03 is significant.

<i>t-test</i> <i>Structural Stiffness - Torsional Loading</i> <i>p-values</i>					
Construct	Comm.	Tit.	Res. 4mm	Res. 2mm	K. Wires
Comm.	1	0.41	0.68	0.13	0.16
Tit.		1	0.70	0.76	0.09
Res. 4mm			1	0.43	0.15
Res. 2mm				1	0.02
K. Wires					1

Table 4.11: Structural stiffness for torsional loading. Overall mean and standard deviation (SD) values provided for each construct.

<i>Structural Stiffness (N-m/rad)</i> <i>Torsional Loading</i>					
Construct	Comm.	Tit.	Res. 4mm	Res. 2mm	K. Wires
mean	60.85	65.96	63.17	67.91	54.25
SD	7.78	14.77	13.33	9.69	8.20

Table 4.12: t-test power for structural stiffness from torsional loading, nondestructive tests. Values indicate the percentage of constructs that would be expected to yield a significant effect.

<i>t-test</i> <i>Structural Stiffness - Torsional Loading</i> <i>power</i>					
Construct	Comm.	Tit.	Res. 4mm	Res. 2mm	K. Wires
Comm.	1	0.02	0.01	0.09	0.10
Tit.		1	0.01	0.01	0.15
Res. 4mm			1	0.02	0.09
Res. 2mm				1	0.46
K. Wires					1

4.1.2 Displacement/Torque

With a 10N cranial load, displacement responses of the constructs showed significantly lower values for the commercial plate constructs (0.46 ± 0.11 mm) and titanium plate constructs (0.46 ± 0.09 mm) when compared to both resorbable 4mm (0.79 ± 0.20 mm) and resorbable 2mm (0.86 ± 0.23 mm) plate constructs as well as the Kirschner wire constructs (2.22 ± 0.41 mm). Both resorbable plate constructs also exhibited less displacement than the Kirschner wire constructs. Comparisons that showed no significant differences were the commercial and titanium plate constructs (p-value 0.96) and the resorbable 4mm and 2mm plate constructs with a p-value of 0.56 (Table 4.13, Table 4.14). Respective powers for the conducted Mann-Whitney-Wilcoxon tests are reported in Table 4.15.

Table 4.13: Mann-Whitney-Wilcoxon p-values for displacement at 10N cranial bending force, nondestructive tests. A p-value less than 6.25E-03 is significant.

<i>Mann-Whitney-Wilcoxon Test</i>					
<i>Displacement at 10N - Cranial Bending</i>					
<i>p-values</i>					
Construct	Comm.	Tit.	Res. 4mm	Res. 2mm	K. Wires
Comm.	1	0.96	1.95E-03	1.63E-03	7.78E-04
Tit.		1	9.39E-04	7.78E-04	7.78E-04
Res. 4mm			1	0.56	7.78E-04
Res. 2mm				1	7.78E-04
K. Wires					1

Table 4.14: Displacement at 10N cranial bending force. Overall mean and standard deviation (SD) values provided for each construct.

<i>Displacement at 10N (mm)</i>					
<i>Cranial Bending</i>					
Construct	Comm.	Tit.	Res. 4mm	Res. 2mm	K. Wires
mean	0.46	0.46	0.79	0.86	2.22
SD	0.11	0.09	0.20	0.23	0.41

Table 4.15: Mann-Whitney-Wilcoxon power for displacement at 10N cranial bending force, nondestructive tests. Values indicate the percentage of constructs that would be expected to yield a significant effect.

<i>Mann-Whitney-Wilcoxon Test Displacement at 10N - Cranial Bending power</i>					
Construct	Comm.	Tit.	Res. 4mm	Res. 2mm	K. Wires
Comm.	1	0.01	0.96	0.96	1.00
Tit.		1	1.00	1.00	1.00
Res. 4mm			1	0.03	1.00
Res. 2mm				1	1.00
K. Wires					1

All displacement values when applied a 10N medial bending load showed no significant differences between the commercial plate constructs (0.46 ± 0.07 mm), titanium plate constructs (0.48 ± 0.13 mm), resorbable 4mm plate constructs (0.37 ± 0.06 mm), resorbable 2mm plate constructs (0.43 ± 0.06 mm), and the Kirschner wire constructs (0.76 ± 0.30 mm) except the comparison between the resorbable 4mm plate when compared to the Kirschner wire constructs, with a p-value of 2.32E-03 (Table 4.16, Table 4.17). Respective powers for the conducted Mann-Whitney-Wilcoxon tests are reported in Table 4.18.

Table 4.16: Mann-Whitney-Wilcoxon p-values for displacement at 10N medial bending force, nondestructive tests. A p-value less than 6.25E-03 is significant.

<i>Mann-Whitney-Wilcoxon Test Displacement at 10N - Medial Bending p-values</i>					
Construct	Comm.	Tit.	Res. 4mm	Res. 2mm	K. Wires
Comm.	1	0.96	0.05	0.29	0.07
Tit.		1	0.09	0.60	0.16
Res. 4mm			1	0.10	2.32E-03
Res. 2mm				1	0.03
K. Wires					1

Table 4.17: Displacement at 10N medial bending force. Overall mean and standard deviation (SD) values provided for each construct.

<i>Displacement at 10N (mm)</i> <i>Medial Bending</i>					
Construct	Comm.	Tit.	Res. 4mm	Res. 2mm	K. Wires
mean	0.46	0.48	0.37	0.43	0.76
SD	0.07	0.13	0.06	0.06	0.30

Table 4.18: Mann-Whitney-Wilcoxon power for displacement at 10N medial bending force, nondestructive tests. Values indicate the percentage of constructs that would be expected to yield a significant effect.

<i>Mann-Whitney-Wilcoxon Test</i> <i>Displacement at 10N - Medial Bending</i> <i>power</i>					
Construct	Comm.	Tit.	Res. 4mm	Res. 2mm	K. Wires
Comm.	1	0.01	0.44	0.07	0.26
Tit.		1	0.26	0.03	0.14
Res. 4mm			1	0.26	0.96
Res. 2mm				1	0.64
K. Wires					1

Torque values generated when applied a 2 degree rotation angle during torsional loading showed no significant differences between the commercial plate constructs (1.93 ± 0.29 N-m), the titanium plate constructs (2.24 ± 0.46 N-m), the resorbable 4mm plate constructs (2.11 ± 0.43 N-m), the resorbable 2mm plate constructs (2.12 ± 0.51 N-m), and the Kirschner wire constructs (1.76 ± 0.23 N-m) for all types of comparisons (Table 4.19, Table 4.20). Respective powers for the conducted Mann-Whitney-Wilcoxon tests are reported in Table 4.21.

Table 4.19: Mann-Whitney-Wilcoxon p-values for torque at 2 degrees torsional loading force, nondestructive tests. A p-value less than 6.25E-03 is significant.

<i>Mann-Whitney-Wilcoxon Test</i>					
<i>Torque at 2 deg - Cranial Bending</i>					
<i>p-values</i>					
Construct	Comm.	Tit.	Res. 4mm	Res. 2mm	K. Wires
Comm.	1	0.09	0.34	0.10	0.33
Tit.		1	0.56	0.56	0.03
Res. 4mm			1	0.83	0.11
Res. 2mm				1	0.04
K. Wires					1

Table 4.20: Torque at 2 degree torsional loading force. Overall mean and standard deviation (SD) values provided for each construct.

<i>Torque at 2 deg (N-m)</i>					
<i>Torsional Loading</i>					
Construct	Comm.	Tit.	Res. 4mm	Res. 2mm	K. Wires
mean	1.93	2.24	2.11	2.12	1.76
SD	0.29	0.46	0.43	0.51	0.23

Table 4.21: Mann-Whitney-Wilcoxon power for torque at 2 degrees torsional loading force, nondestructive tests. Values indicate the percentage of constructs that would be expected to yield a significant effect.

<i>Mann-Whitney-Wilcoxon Test</i>					
<i>Torque at 2 deg - Cranial Bending</i>					
<i>power</i>					
Construct	Comm.	Tit.	Res. 4mm	Res. 2mm	K. Wires
Comm.	1	0.26	0.07	0.26	0.06
Tit.		1	0.03	0.03	0.57
Res. 4mm			1	0.01	0.22
Res. 2mm				1	0.57
K. Wires					1

Overall curves of each construct were generated by averaging the data of the third cycle of all the specimens together by matching the respective forces of all the specimens for the cranial and medial bending, and by matching the respective rotation angles of all the specimens for the torsional loading before averaging (Figure 4.4). Commercial and titanium plate

constructs exhibited very similar structural stiffnesses and resorbable plates exhibited similar structural stiffnesses as well during cranial bending tests. All bone plate constructs were structurally stiffer than Kirschner wire repaired fractures, with the metal bone plates being the most structurally stiff. Medial bending tests showed that all plate constructs appeared to be similar to each other in structural stiffness and were all much more structurally stiff than Kirschner wire constructs. Torsional loading did not display any significant differences between fracture repair techniques.

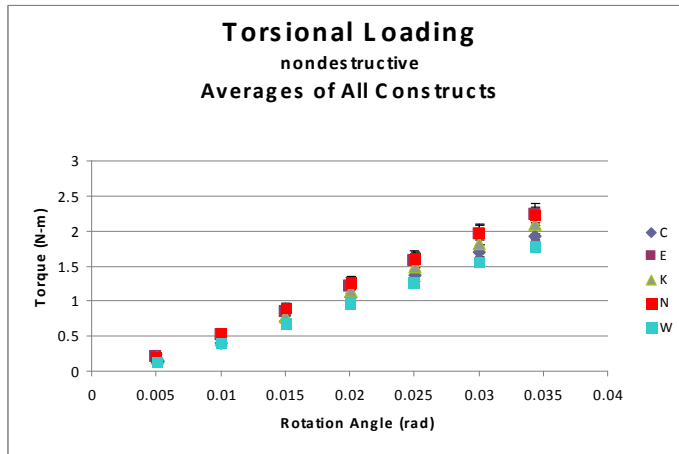
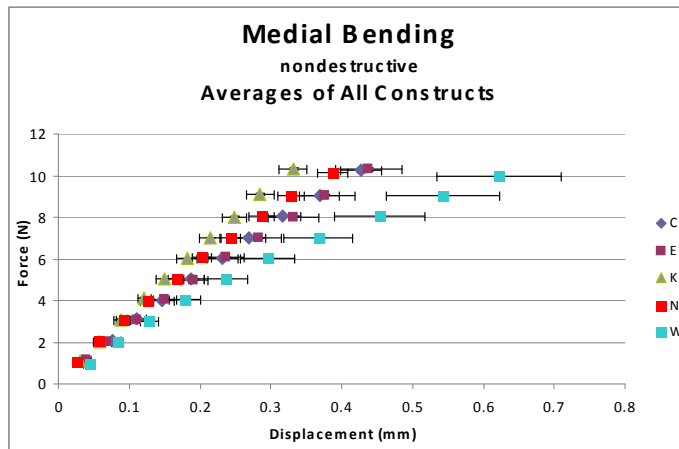
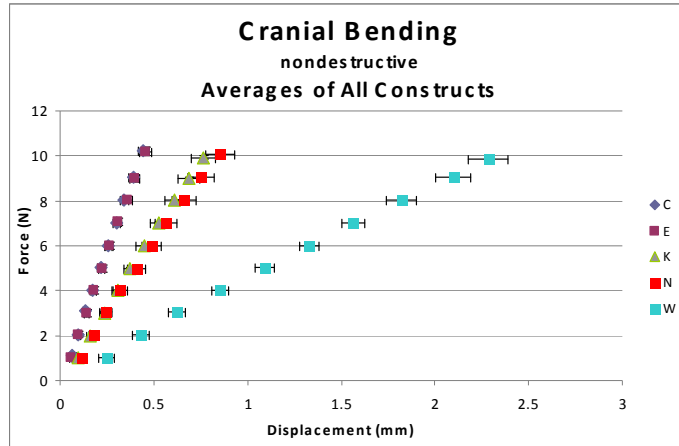


Figure 4.4: Graphs of overall curves for each of the eight constructs for the three nondestructive tests. The overall curves were generated by averaging the specimens of each construct. Commercial plate (C), titanium plate (E), resorbable 4mm plate (K), resorbable 2mm plate (N), and Kirschner wires (W)

4.2 Destructive Tests

The cranial bending and external torsion destructive tests generated 38 data files. One Kirschner wire specimen (W1) fractured during setup and resorbable 2mm plate specimen (N1) had software collection difficulties. Cranial bending tests resulted in various types of failures (Table 4.22). Constructs resulted in either internal cracking with no exterior signs of failure, fracture at the medial or lateral condyles of the distal section of the femur (Figure 4.5, Figure 4.6), fracture under the plate (Figure 4.7), or permanent widening of the epiphyseal fracture site. Two resorbable 2mm constructs displayed plastic deformation of the plate at screw holes (Figure 4.8). Kirschner wire constructs undergoing destructive cranial bending tests resulted in fracture of the bone at wire insertion points or internal cracking (Figure 4.9). External torsional loading tests most often resulted in shaft fracture of the proximal section of the femur, but also displayed internal fracture with no visible exterior signs, and two Kirschner wire constructs resulted in a fracture of the distal section of the femur (Figure 4.9, Table 4.22).

Table 4.22: Failure testing summary. The table lists the type of failure test and the failure mode for each specimen. Commercial plate (C), titanium plate (E), resorbable 4mm plate (K), resorbable 2mm plate (N), and Kirschner wires (W). Cranial bending (CB) and torsional loading (ET).

Sample	Failure Test	Result
C1	CB	No visible exterior signs
C2	CB	Fracture at the lateral condyle
C4	CB	No visible exterior signs
C5	CB	No visible exterior signs
E1	CB	No visible exterior signs
E2	CB	Widened gap at epiphyseal fracture site
E5	CB	No visible exterior signs
E7	CB	Fracture at lateral side
K1	CB	No visible exterior signs
K3	CB	Caudal fracture at third proximal screw insertion pt on medial side
K5	CB	Fracture at lateral condyle
K6	CB	Fracture at medial condyle
N1	CB	--- (software collection difficulties)
N3	CB	Fracture at lateral distal section, plastic deform of plate
N5	CB	Fracture at lateral condyle
N8	CB	Widened gap of epiphyseal fracture, plastic deform of plate
W2	CB	Fracture at wire insertion point on medial side
W5	CB	No visible external signs
W7	CB	Fracture at wire insertion point on medial side
W8	CB	Fracture at wire insertion points on medial side
C3	ET	Fracture at shaft
C6	ET	No visible exterior signs
C7	ET	Fracture at shaft
C8	ET	Fracture at shaft
E3	ET	Fracture at shaft
E4	ET	Fracture at shaft
E6	ET	Fracture at shaft
E8	ET	Fracture at shaft
K2	ET	Fracture at shaft
K4	ET	Fracture at shaft
K7	ET	Fracture at shaft
K8	ET	Fracture under lateral plate
N2	ET	Fracture at shaft
N4	ET	No visible external signs
N6	ET	Fracture at shaft
N7	ET	Fracture at shaft
W1	ET	--- (broken during setup)
W3	ET	Fracture at shaft
W4	ET	Fracture of distal section on lateral side, loosening of testing jig
W6	ET	Fracture of distal section on lateral side

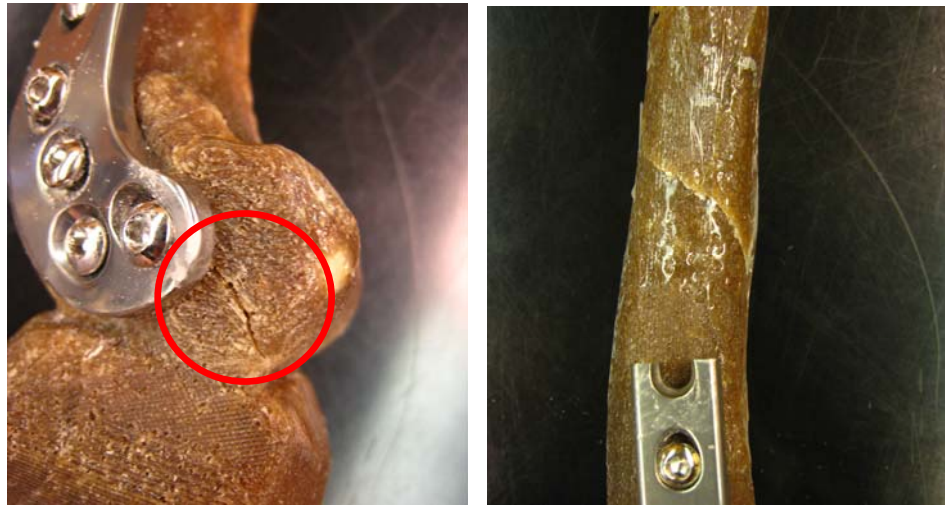


Figure 4.5: Commercial plate failure specimens. The image on the left underwent cranial bending and resulted in a lateral condyle fracture. The image on the right underwent torsional loading and fractured at the proximal shaft.



Figure 4.6: Titanium plate failure specimens. Cranial bending resulted in a lateral fracture of the distal section (left). Torsional loading resulted in a fracture at the proximal shaft.



Figure 4.7: Resorbable 4mm plate failure specimens. The image on the left displays a fracture under the lateral plate from cranial testing. The image on the right displays a fracture at the shaft of the proximal section from torsional loading.



Figure 4.8: Resorbable 2mm plate failure specimens. The left image exhibits a widened gap at the epiphyseal plate fracture site as well as plastic deformation of the plate at the distal screws from destructive cranial bending. The image on the right displays a fracture of the proximal shaft from destructive torsional loading.



Figure 4.9: Kirschner wire failure specimens. The cranial bending test resulted in fracture at the wire insertion points (left) and the torsional bending test resulted in a lateral fracture of the distal section (right).

Certain variables were of interest for the destructive tests; the yield and ultimate strength for the cranial bending tests and the yield and ultimate torque for the external torsion loading tests. The yield strength and torque are defined as the maximum force and torque of the linear portion of the cranial bending tests or torsional loading tests before a decreased change in structural stiffness. Ultimate strength and torque are defined as the maximum force and torque of the cranial bending and torsional loading tests before failure, determined as a 75% drop of collected force or torque from the maximum value. Figure 4.10 depicts the route used to obtain the yield and ultimate strength values from a resorbable 4mm plate construct that underwent cranial destructive bending.

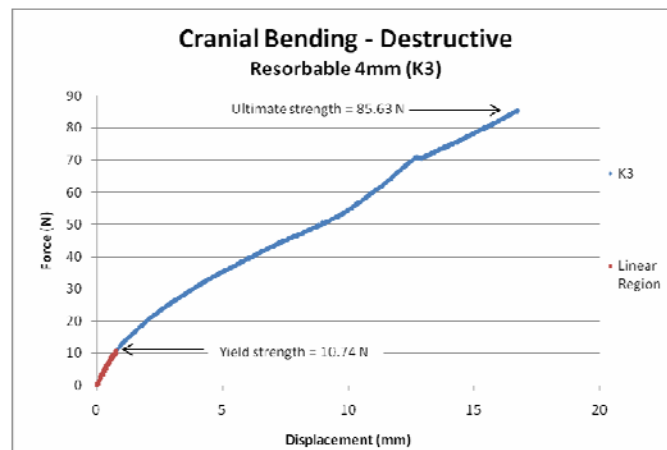
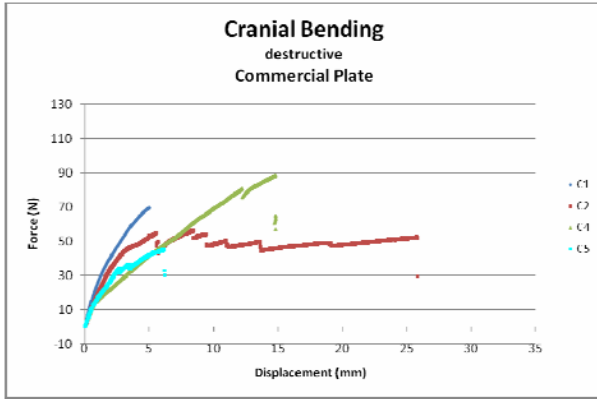


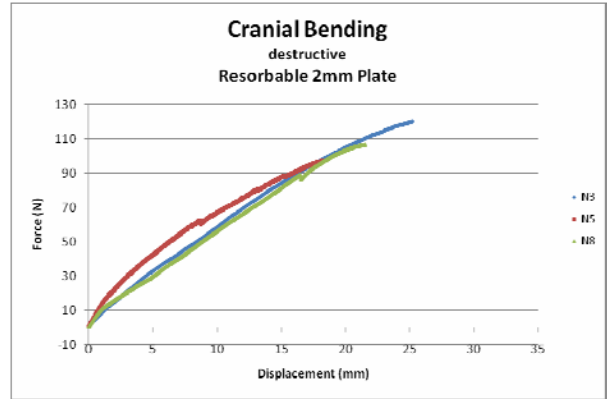
Figure 4.10: Determination of yield and ultimate strength from a force vs. displacement graph of a resorbable 4mm plate construct in cranial destructive bending.

Graphs of each construct type were generated for cranial bending and torsional loading destructive tests (Figure 4.11, Figure 4.12). For all types of constructs in cranial bending, it appears that there was a more uniform structural stiffness among each specimen before reaching the yield strengths, when the force vs. displacement curves then deviated into lesser structural stiffness values. Some constructs such as commercial plate construct 2, 4, 5 (C2, C4, C5), titanium plate construct 2 (E2), resorbable 4mm plate construct 5 (K5), resorbable 2mm plate construct 5, 8 (N5, N8), and Kirschner wire construct 5, 8 (W5, W8) experienced several minor crack failures during cranial bending before reaching ultimate strength and final failure of a 75% drop of collected force.

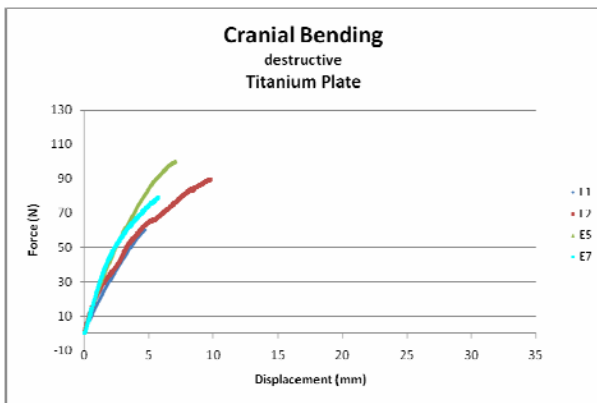
Overall, constructs failed with external torsional loading experienced a more linear torque vs. rotation angle curve through the entire destructive testing procedure, though there was also some deviation of the curves among each type of construct after the yield torque. Titanium plate construct 3 (E3) contained some slack, which required settling of the system and resulted in a greater rotation angle before torque was experienced. Kirschner wire construct 4 (W4) experienced loosening of the rotational testing jig fixated on the distal section of the femur explaining the periodic failure-like response on the torque vs. rotation angle curve. Ultimate torque for titanium plate construct 6 (E6) and resorbable 2mm plate construct 7 (N7) were much higher than all other constructs in the same group.



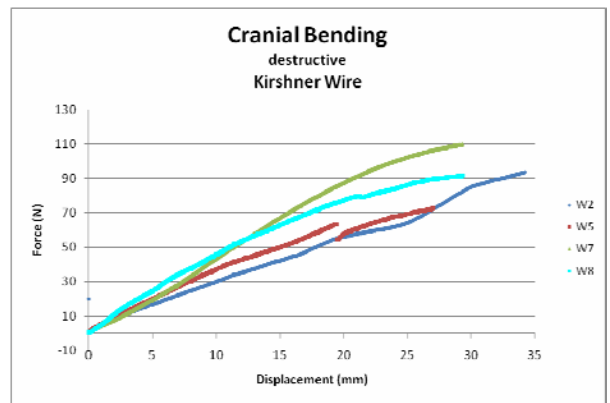
(a)



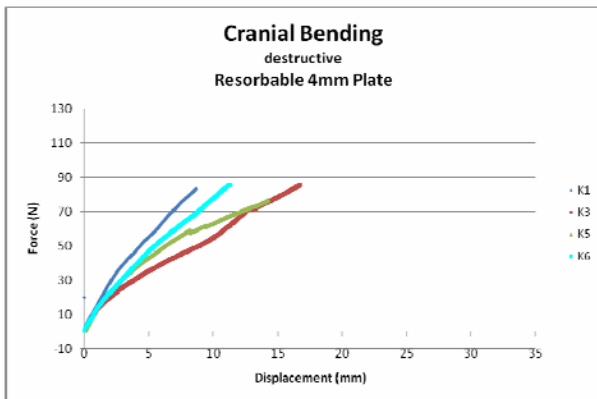
(d)



(b)

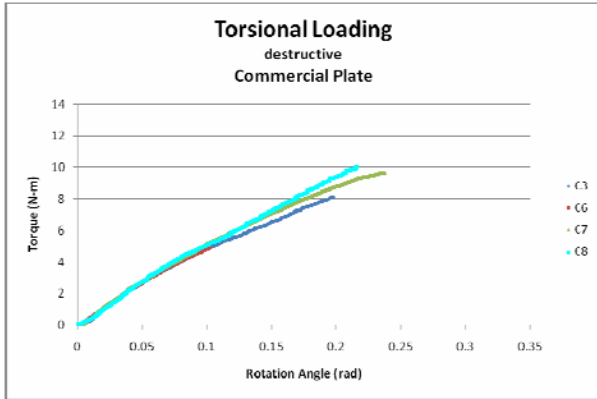


(e)

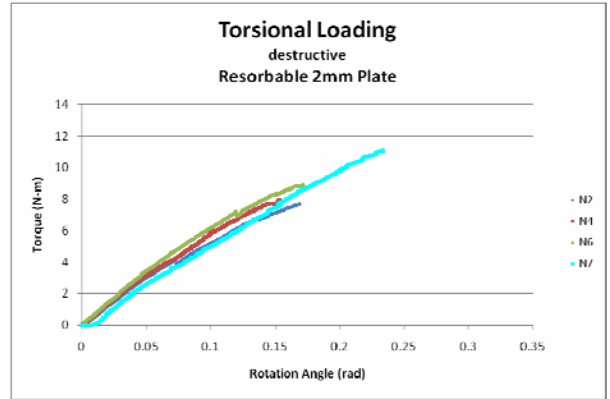


(c)

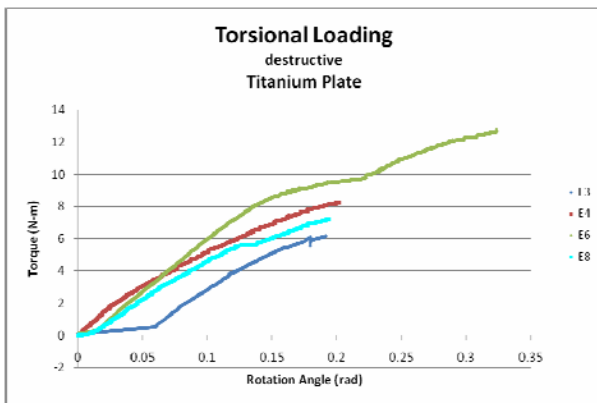
Figure 4.11: Graphs of destructive cranial bending tests. Commercial plate (a), titanium plate (b), resorbable 4mm plate (c), resorbable 2mm plate (d) and Kirshner wire (e) constructs.



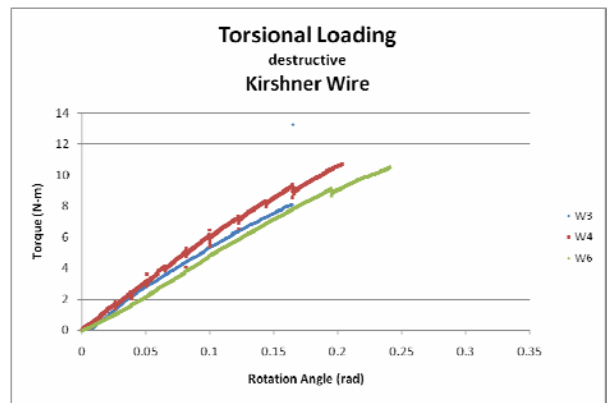
(a)



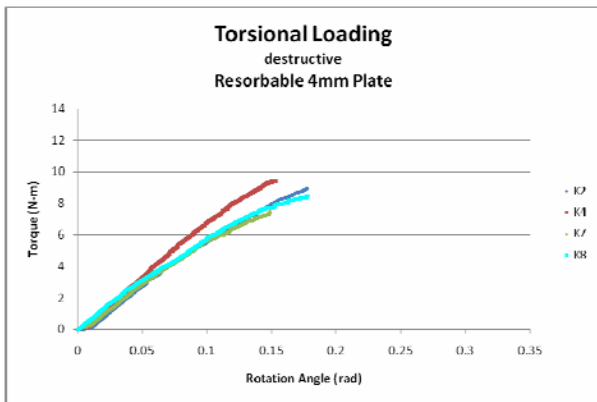
(d)



(b)



(e)



(c)

Figure 4.12: Graphs of destructive torsional loading tests. Commercial plate (a), titanium plate (b), resorbable 4mm plate (c), resorbable 2mm plate (d) and Kirshner wire (e) constructs.

Table 4.23 and Table 4.24 are the destructive testing values for the yield and ultimate strength or torque variables obtained from all constructs. A two-tailed Mann-Whitney-Wilcoxon test was performed on these values to test for variability between the constructs, with an alpha of 1.25E-02 to determine significance. The statistical analysis used a type I error rate of 0.05 in all cases, and with a Bonferroni correction a p-value less than 1.25E-02 indicates evidence of a statistically significant difference between the compared values.

Table 4.23: Results of the destructive cranial bending tests. Individual values of yield strength and ultimate strength are reported. Mean and standard deviation (SD) of each construct are also given. Commercial plate (C), titanium plate (E), resorbable 4mm plate (K), resorbable 2mm plate (N), and Kirschner wires (W)

<i>Cranial Bending Failure Test</i>	yield strength (N)	ultimate strength (N)
C1	22.10	69.74
C2	7.10	56.37
C4	14.15	88.75
C5	11.15	45.61
mean	13.63	65.12
SD	6.35	18.59
E1	10.12	60.12
E2	20.08	89.71
E5	55.83	100.35
E7	31.88	79.50
mean	29.48	82.42
SD	19.69	17.13
K1	32.40	83.62
K3	10.74	85.63
K5	9.75	76.87
K6	11.83	85.81
mean	16.18	82.98
SD	10.84	4.19
N1	---	---
N3	27.06	120.26
N5	13.04	97.10
N8	6.56	106.89
mean	15.55	108.08
SD	10.48	11.62
W2	14.56	93.99
W5	37.81	72.82
W7	15.10	110.14
W8	3.11	92.00
mean	17.65	92.24
SD	14.53	15.28

Table 4.24: Results of the destructive torsional loading tests. Individual values of yield torque and ultimate torque are reported. Mean and standard deviation (SD) of each construct are also given. Commercial plate (C), titanium plate (E), resorbable 4mm plate (K), resorbable 2mm plate (N), and Kirschner wires (W)

<i>Torsional Loading Failure Test</i>	yield torque (N-m)	ultimate torque (N-m)
C3	1.69	8.14
C6	1.79	4.90
C7	1.60	9.69
C8	4.21	10.06
mean	2.32	8.20
SD	1.26	2.35
E3	6.20	6.20
E4	1.29	8.22
E6	7.59	12.77
E8	5.45	7.20
mean	5.13	8.60
SD	2.71	2.90
K2	4.69	8.96
K4	3.00	9.46
K7	3.00	7.54
K8	3.23	8.49
mean	3.48	8.61
SD	0.82	0.82
N2	3.17	7.66
N4	2.92	7.64
N6	2.79	8.89
N7	2.25	11.07
mean	2.79	8.82
SD	0.39	1.61
W1	---	---
W3	3.44	13.22
W4	1.44	10.69
W6	5.01	10.51
mean	3.30	11.47
SD	1.79	1.52

4.2.1 Cranial Bending Destructive Tests

Yield strength values for destructive cranial bending showed no significant differences among the commercial plate constructs (13.63 ± 6.35 N), the titanium plate constructs (29.48 ± 19.69 N), the resorbable 4mm plate constructs (16.18 ± 10.84 N), the resorbable 2mm plate constructs (15.55 ± 10.48 N), and the Kirschner wire constructs (15.10 ± 3.11 N) for any comparisons (Table 4.25). Respective powers for the conducted Mann-Whitney-Wilcoxon tests are reported in Table 4.26.

Table 4.25: Mann-Whitney-Wilcoxon p-values for yield strength from cranial bending, destructive tests. A p-value less than 1.25E-02 is significant.

<i>Mann-Whitney-Wilcoxon Test Yield Strength - Cranial Bending p-values</i>					
Construct	Comm.	Tit.	Res. 4mm	Res. 2mm	K. Wires
Comm.	1	0.25	1.00	1.00	0.56
Tit.		1	0.39	0.29	0.39
Res. 4mm			1	1.00	0.56
Res. 2mm				1	0.72
K. Wires					1

Table 4.26: Mann-Whitney-Wilcoxon power for yield strength from cranial bending, destructive tests. Values indicate the percentage of constructs that would be expected to yield a significant effect.

<i>Mann-Whitney-Wilcoxon Test Yield Strength - Cranial Bending power</i>					
Construct	Comm.	Tit.	Res. 4mm	Res. 2mm	K. Wires
Comm.	1	0.15	0.01	0.01	0.03
Tit.		1	0.09	0.15	0.09
Res. 4mm			1	0.01	0.03
Res. 2mm				1	0.03
K. Wires					1

Ultimate strength values for destructive cranial bending also showed no significant differences for commercial plate constructs (65.12 ± 18.59 N), the titanium plate constructs

(82.42 ± 17.13 N), the resorbable 4mm plate constructs (82.98 ± 4.19 N), and the Kirschner wire constructs (110.14 ± 92.00 N) for all comparisons (Table 4.27). Respective powers for the conducted Mann-Whitney-Wilcoxon tests are reported in Table 4.28.

Table 4.27: Mann-Whitney-Wilcoxon p-values for ultimate strength from cranial bending, destructive tests. A p-value less than 1.25E-02 is significant.

<i>Mann-Whitney-Wilcoxon Test</i> <i>Ultimate Strength - Cranial Bending</i> <i>p-values</i>					
Construct	Comm.	Tit.	Res. 4mm	Res. 2mm	K. Wires
Comm.	1	0.15	0.25	0.03	0.04
Tit.		1	0.77	0.08	0.39
Res. 4mm			1	0.03	0.25
Res. 2mm				1	0.16
K. Wires					1

Table 4.28: Mann-Whitney-Wilcoxon power for ultimate strength from cranial bending, destructive tests. Values indicate the percentage of constructs that would be expected to yield a significant effect.

<i>Mann-Whitney-Wilcoxon Test</i> <i>Ultimate Strength - Cranial Bending</i> <i>power</i>					
Construct	Comm.	Tit.	Res. 4mm	Res. 2mm	K. Wires
Comm.	1	0.25	0.15	1.00	0.75
Tit.		1	0.02	0.48	0.09
Res. 4mm			1	1.00	0.15
Res. 2mm				1	0.33
K. Wires					1

4.2.2 Torsional Loading Destructive Tests

Yield torque values for destructive torsional loading showed no significant differences among any comparisons for the commercial plate constructs (2.32 ± 1.26 N-m), titanium plate constructs (5.13 ± 2.71 N-m), resorbable 4mm plate constructs (3.48 ± 0.82 N-m), resorbable 2mm plate constructs (2.79 ± 0.39 N-m), and Kirschner wire constructs (3.30 ± 1.79 N-m) (Table 4.29). Respective powers for the conducted Mann-Whitney-Wilcoxon tests are reported in Table 4.30.

Table 4.29: Mann-Whitney-Wilcoxon p-values for yield torque from torsional loading, destructive tests. A p-value less than 1.25E-02 is significant.

<i>Mann-Whitney-Wilcoxon Test Yield Torque - Torsional Loading p-values</i>					
Construct	Comm.	Tit.	Res. 4mm	Res. 2mm	K. Wires
Comm.	1	0.25	0.15	0.25	0.72
Tit.		1	0.25	0.25	0.29
Res. 4mm			1	0.08	0.72
Res. 2mm				1	0.48
K. Wires					1

Table 4.30: Mann-Whitney-Wilcoxon power for yield torque from torsional loading, destructive tests. Values indicate the percentage of constructs that would be expected to yield a significant effect.

<i>Mann-Whitney-Wilcoxon Test Yield Torque - Torsional Loading power</i>					
Construct	Comm.	Tit.	Res. 4mm	Res. 2mm	K. Wires
Comm.	1	0.15	0.25	0.15	0.03
Tit.		1	0.15	0.15	0.13
Res. 4mm			1	0.55	0.03
Res. 2mm				1	0.05
K. Wires					1

Similarly, ultimate torque values for destructive torsional loading showed no significant differences among any of the constructs for the commercial plate constructs (8.20 ± 2.35 N-m) compared to the titanium plate constructs (8.60 ± 2.90 N-m), resorbable 4mm plate constructs

(8.61 ± 0.82 N-m), resorbable 2mm plate constructs (8.82 ± 1.61 N-m), and Kirschner wire constructs (11.47 ± 1.52 N-m) (Table 4.31). Respective powers for the conducted Mann-Whitney-Wilcoxon tests are reported in Table 4.32.

Table 4.31: Mann-Whitney-Wilcoxon p-values for ultimate torque from torsional loading, destructive tests. A p-value less than 1.25E-02 is significant.

<i>Mann-Whitney-Wilcoxon Test</i> <i>Ultimate Torque - Torsional Loading</i> <i>p-values</i>					
Construct	Comm.	Tit.	Res. 4mm	Res. 2mm	K. Wires
Comm.	1	1.00	0.77	1.00	0.03
Tit.		1	0.39	0.56	0.16
Res. 4mm			1	1.00	0.03
Res. 2mm				1	0.16
K. Wires					1

Table 4.32: Mann-Whitney-Wilcoxon power for ultimate torque from torsional loading, destructive tests. Values indicate the percentage of constructs that would be expected to yield a significant effect.

<i>Mann-Whitney-Wilcoxon Test</i> <i>Ultimate Torque - Torsional Loading</i> <i>power</i>					
Construct	Comm.	Tit.	Res. 4mm	Res. 2mm	K. Wires
Comm.	1	0.01	0.02	0.01	1.00
Tit.		1	0.09	0.03	0.33
Res. 4mm			1	0.01	1.00
Res. 2mm				1	0.33
K. Wires					1

4.3 Plate Dimensions

Approximate surface area and thickness measurements of the different bone plates are reported below in Table 4.33. The location of each measurement is described in Figure 3.21, Figure 3.22, and Figure 3.23. Overall, the surface areas between the lateral plates for all constructs are roughly the same. The commercial plates are approximately twice as thick as the titanium plates, but have similar surface areas. The medial and lateral resorbable plates all have similar surface areas, with the resorbable 4mm plate approximately twice as thick as the resorbable 2mm plates. The titanium and lateral resorbable 2mm plates show expected similar surface area and thickness dimensions having been fabricated using the same custom lateral plate design.

Table 4.33: Surface area and thickness measurements for bone plates.

<i>Bone Plate Dimensions</i>				
Lateral Plate				
Measurement (mm)	Commercial	Titanium	Resorbable 4mm	Resorbable 2mm
Width (a)	11.96	14.61	14.81	14.55
Length (b)	47.57	30.15	32.26	32.79
Width (c)	18.59	18.42	19.94	18.49
Length (d)	27.94	30.12	31.12	31.24
Surface Area	1088.63	995.08	1098.08	1054.95
Thickness	4.47	2.41	4.47	2.18
Medial Plate				
Measurement (mm)	---	---	Resorbable 4mm	Resorbable 2mm
Width (a)	---	---	15.01	15.52
Length (b)	---	---	32.69	33.71
Width (c)	---	---	17.91	18.31
Length (d)	---	---	30.86	29.44
Surface Area	---	---	1043.35	1062.21
Thickness	---	---	4.04	2.13

4.4 Screw Lengths

Average screw lengths used for each plate construct is reported below in Table 4.34.

Table 4.34: Average screw lengths for each type of plate construct. Overall mean and standard deviation (SD) of each type of construct are also given.

<i>Screw Length (mm)</i> <i>Plate Constructs</i>				
	Lateral Plate		Lateral and Medial Plate	
Construct No.	Commercial	Titanium	Resorbable 4mm	Resorbable 2mm
1	35.14	32.33	30.33	34.33
2	30.57	28.00	31.67	33.84
3	34.86	33.67	30.75	32.34
4	32.86	32.33	33.33	32.34
5	28.00	33.00	33.17	31.34
6	30.86	28.33	29.5	30.67
7	32.29	38.00	30.50	31.50
8	30.86	30.33	30.00	29.34
Mean	31.93	32.00	31.16	31.96
SD	2.37	3.21	1.43	1.63

A Shapiro-Wilk test was conducted for each construct to test for a normal distribution prior to conducting comparison tests. All constructs did not show evidence of non-normality Table 4.35. A two-tailed t-test was performed on these values to test for variability between the commercial and titanium constructs as well as the resorbable 4mm and 2mm constructs, with an alpha of 6.25E-03 to determine significance (Table 4.36). Both tests showed no significant differences between the compared constructs, however the power of the resorbable 4mm and 2mm t-test is 0.25, meaning that 25% of the constructs would be expected to yield a significant effect (Table 4.37).

Table 4.35: Shapiro-Wilk normality test for screw lengths of all constructs. A test statistic less than $W_{0.05}=0.82$ is significant.

<i>Shapiro-Wilk Test for Normality</i> <i>Screw Length</i> <i>W test statistic</i>			
Commercial	Titanium	Res. 4mm	Res. 2mm
0.95	0.93	0.88	0.97

Table 4.36: t-test p-values for screw lengths. A p-value less than 6.25E-03 is significant.

<i>t-test</i> <i>Screw Length</i> <i>p-values</i>		
Construct Comparison	Commercial vs. Titanium	Resorbable 4mm vs. 2mm
p-value	0.96	0.31

Table 4.37: t-test power for screw lengths. Values indicate the percentage of constructs that would be expected to yield a significant effect.

<i>t-test</i> <i>Screw Length</i> <i>power</i>		
Construct Comparison	Commercial vs. Titanium	Resorbable 4mm vs. 2mm
power	0.01	0.25

4.5 Duration of Surgery

Overall surgery time for the five different techniques is reported below in Table 4.38.

Table 4.38: Total duration of surgery for each type of construct. Mean and standard deviation (SD) of each type of construct are also given.

<i>Duration of Surgery (min)</i>					
Construct No.	Commercial	Titanium	Res. 4mm	Res. 2mm	K. Wires
1	7.03	15.78	10.40	10.82	3.88
2	8.18	5.82	11.78	13.83	2.5
3	7.22	5.87	19.07	14.23	1.97
4	9.67	5.25	10.50	16.18	3.22
5	7.23	5.65	10.87	9.68	3.40
6	10.82	5.30	13.87	20.10	2.85
7	10.08	5.37	11.32	10.42	2.77
8	10.12	5.42	12.15	10.38	2.57
Mean	8.79	6.81	12.49	13.21	2.89
SD	1.54	3.63	2.88	3.62	0.60

A Shapiro-Wilk test was conducted for each construct to test for a normal distribution prior to conducting comparison tests. The titanium and resorbable 4mm plate constructs showed evidence of non-normality (Table 4.39). A two-tailed Mann-Whitney-Wilcoxon test was performed on these values to test for variability between the constructs, with an alpha of 6.25E-03 to determine significance.

Table 4.39: Shapiro-Wilk normality test for duration of surgery for all constructs. A test statistic less than $W_{0.05}=0.82$ is significant.

<i>Shapiro-Wilk Test for Normality</i>				
<i>Duration of Surgery</i>				
<i>W test statistic</i>				
Commercial	Titanium	Resorbable 4mm	Resorbable 2mm	Kirschner Wires
0.86	0.48	0.74	0.88	0.98

Surgery time for commercial plate fixation (8.79 ± 1.54 min) was not significantly different from the titanium plate fixation time (6.81 ± 3.63 min) with a p-value of 0.01, but was significantly

shorter in duration compared to the resorbable 4mm plate (12.49 ± 2.88 min), resorbable 2mm plate (13.21 ± 3.62 min) with p-values $1.63E-03$ and $5.38E-03$, respectively. Compared to the Kirschner wire (2.89 ± 0.60 min) fixation times, the commercial plate was significantly shorter (p-value $7.78E-04$). There was no significant difference for the titanium plate fixation time compared to resorbable 4mm plate time (p-value $8.65E-03$) or the resorbable 2mm plate time (p-value $6.32E-03$) but was significantly longer than the Kirschner wire fixation time (p-value $7.78E-04$). Resorbable 4mm and 2mm plate fixation times were not significantly different from each other (p-value 0.92). However, resorbable 4mm plates and resorbable 2mm plates were significantly longer in duration when compared to Kirschner wire fixation time (Table 4.40). Respective power values for each Mann-Whitney-Wilcoxon test are provided in Table 4.41.

Table 4.40: Mann-Whitney-Wilcoxon p-values for duration of surgery.
A p-value less than $6.25E-03$ is significant.

<i>Mann-Whitney-Wilcoxon Test</i>					
<i>Duration of Surgery</i>					
<i>p-values</i>					
Construct	Comm.	Tit.	Res. 4mm	Res. 2mm	K. Wires
Comm.	1	0.01	$1.63E-03$	$5.38E-03$	$7.78E-04$
Tit.		1	$8.65E-03$	$6.32E-03$	$7.78E-04$
Res. 4mm			1	0.92	$7.78E-04$
Res. 2mm				1	$7.78E-04$
K. Wires					1

Table 4.41: Mann-Whitney-Wilcoxon power for duration of surgery.
Values indicate the percentage of constructs that would be expected to yield a significant effect.

<i>Mann-Whitney-Wilcoxon Test</i>					
<i>Duration of Surgery</i>					
<i>power</i>					
Construct	Comm.	Tit.	Res. 4mm	Res. 2mm	K. Wires
Comm.	1	0.84	0.96	0.84	1.00
Tit.		1	0.84	0.84	1.00
Res. 4mm			1	0.01	1.00
Res. 2mm				1	1.00
K. Wires					1

5. DISCUSSION

The main objective of this study was to determine the suitability of bilaterally attached polycaprolactone resorbable plates as a method for stabilizing epiphyseal fractures of the distal canine femur by comparing them to current Kirschner wire and lateral commercial stainless steel plate attachment techniques as well as a custom lateral titanium plate produced from the same design as the resorbable plates. There were several hypotheses of this study: 1) The resorbable 4mm PCL plate would be mechanically superior to the thinner resorbable 2mm PCL plate. 2) These resorbable plates would be superior in structural stiffness, displacement at a 10N applied force, torque generated from a 2 degree applied rotation angle, yield and ultimate strength, and yield and ultimate torque in bending and torsional tests to the current Kirschner wire repair techniques. 3) The fractures repaired with the custom designed titanium would be mechanically comparable to the commercial stainless steel plate constructs. 4) All metal bone plates would be mechanically superior to the resorbable polymer bone plates and Kirschner wires for all tests.

Interestingly enough, the results of most tests failed to reject the first null hypothesis that the two resorbable plates were not significantly different. Although it was hypothesized that a thicker polymer plate would provide more stability to the fracture area than a polymer plate half as thick, statistical comparisons revealed no significant differences between the structural stiffness results from all nondestructive tests. Additionally, when examining the displacement at a 10N applied force, there were no significant differences between the two resorbable plates during cranial bending or medial bending, and no significant differences for the torque generated from a two degree applied rotation angle. Destructive failure tests also did not show any significant differences for yield strength, ultimate strength and yield torque or ultimate. Although test results did not reveal any statistically significant differences between the two plate thicknesses, it is interesting that the resorbable 2mm plates were more structurally stiff during torsional loading than the resorbable 4mm plates. A possible reason for this could be the screw lengths used for the fixation of the different plates. An examination of the screw lengths did not reveal statistically significant differences between the two resorbable plates (Table 4.36), but the resorbable 2mm plate average screw lengths were marginally longer than the 4mm plate screw lengths. Other dissimilarity between the two plate thicknesses was the observed plastic deformation at distal screw holes for two of the resorbable 2mm plates after destructive cranial

tests (Figure 4.8). A plausible explanation could be the mold design used in this study. The mold material used to create the screw holes could have obstructed the flow of the melted polycaprolactone during injection molding and could have created stress locations near the holes because of their relative location to the gate (Figure 5.1) [68].

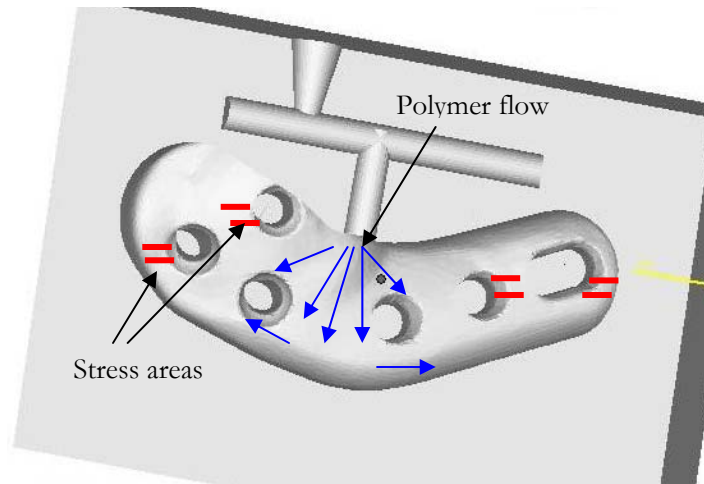


Figure 5.1: Depiction of polymer flow during injection molding

Results from the nondestructive tests indicate that thicker resorbable plates were not more effectiveness in terms of providing stability or displacement and torque response to applied force and rotation of the fracture site. This is promising because a disadvantage to using thicker resorbable plates is that the degradation time for more PCL in the body will be longer and could induce some stress shielding if the bilateral plates are still sufficiently strong after complete fracture ossification. With thinner resorbable implants, the fracture site could still experience small amounts of stress, which could help stimulate bone growth and aid the healing process [5]. In addition, although PCL has shown to be very biocompatible, from an implant biomaterial standpoint, the less amount of foreign material *in vivo*, the better response for the surrounding tissues.

The second hypothesis of the study had differing results amongst the conducted tests. Constructs repaired bilaterally with resorbable 4mm plates and 2mm plates both showed a higher structural stiffness when compared to the Kirschner wire constructs under nondestructive cranial bending, supporting the hypothesis. From medial bending tests, comparisons between the Kirschner wire constructs and resorbable 4mm constructs showed a marginally higher structural stiffness for the plate constructs, again supporting the second

hypothesis. However the resorbable 2mm constructs were not significantly more structurally stiff compared to the Kirschner wires. In fact, for medial bending tests the Kirschner wires were not statistically different in structural stiffness compared to any other type of construct except for the thicker resorbable plates. This indicates the Kirschner wire fixation type being almost as equally strong as most of the plate fixation techniques. An examination of the surface area and thickness of the resorbable 4mm plate (Table 4.33) as being one of the highest in value among the plate types coupled with the bilateral fixation technique could also be a factor for its higher structural stiffness compared to the Kirschner wires.

With nondestructive torsional loading however, the structural stiffness of the Kirschner wire constructs were not significantly different from the resorbable 4mm plates or the resorbable 2mm plates. Though not statistically different, the resorbable 4mm (63.17 ± 13.33 N-m/rad) and resorbable 2mm (67.91 ± 9.69 N-m/rad) plates were in fact slightly stiffer than the Kirschner wire constructs (54.24 ± 8.20 N-m/rad). Again, bilateral fixation technique of these resorbable plates could be responsible for its higher structural stiffness. These combined results suggest that the resorbable bone plates are a much better alternative to Kirschner wire repaired fractures due to their structurally stiffer response to cranial bending forces, in addition to being comparable if not superior to medial bending and torsional loading forces.

The cranial displacement of the constructs when applied a 10N force revealed statistically significant differences between the resorbable 4mm plates or the resorbable 2mm plates when compared to the Kirschner wire constructs, with the resorbable plates both experiencing less displacement than the Kirschner wire constructs. Medial displacement from a 10N force also showed significant differences between the resorbable 4mm plates when compared to the wire constructs with less displacement. The resorbable 2mm plates also showed less displacement than the Kirschner wire constructs during medial bending in spite of displaying marginally insignificant differences. The effectiveness of these resorbable plates could be due largely in part to their bilateral fixation to the fracture site. This increased stability allows them to better withstand cranial and medial loads to the fracture site. The torsion loading test data for torque generated from a 2 degree rotation angle, however failed to reject the null hypothesis. Both the resorbable 4mm plate constructs and the 2mm plate constructs did not generate a statistically significant amount of torque compared to the Kirschner wire constructs

(p-value 0.11, p-value 0.04). Though not statistically significant, the resorbable 4mm (2.11 ± 0.43 N-m) and resorbable 2mm plate constructs (2.12 ± 0.51 N-m) did generate slightly more torque than the Kirschner wire constructs (1.76 ± 0.23 N-m). It is also important to note that structural stiffness and torque generation values from the nondestructive torsional loading tests showed no significant differences across all compared constructs. This suggests not the inadequacy of the resorbable plate constructs providing more stability than the Kirschner wire constructs, but perhaps the angle of rotation during the nondestructive test could have been greater to reveal stronger differences between the five repair techniques, as suggested by the amount of construct settling during the 0-2 degree rotation testing for all fixation techniques indicating that true evaluation of mechanical response was not achieved (Figure 4.3). These displacement and torque results coupled with the structural stiffness results suggest the appropriateness of using the resorbable plates for distal femoral epiphyseal fracture repairs than the Kirschner wire repair technique in young dogs. Research has already shown the ineffectiveness of Kirschner wires for providing enough stabilization during the fracture ossification period and the permanent growth arrest or deformities observed in response to the repair technique [2, 21, 22]. Overall, resorbable plates avoid these concerns by providing much more adequate stabilization to the limb and yet have the ability to degrade over time. This degradation process could slowly transfer the stresses back to the tissue during the healing process. The custom designs of these resorbable plates are also attractive in such that they conform exactly to the contours of the bone to provide a good fit for the surgeon during the repair process.

The third hypothesis was supported by data from all conducted tests. Nondestructive cranial bending tests showed no significant differences in structural stiffness between the commercial stainless steel plates and the custom designed titanium plates (p-value 0.80). Medial bending tests and torsional loading tests also showed no statistically significant differences in structural stiffness (p-value 0.97, p-value 0.41). No significant differences between the commercial and titanium plates were observed for cranial displacement (p-value 0.96) or for medial displacement (p-value 0.96) in response to a 10N applied force. Torque generated from the applied 2 degree rotation also showed no statistically significant differences between the two constructs (p-value 0.09). The mechanical similarities between these two bone plates suggest

that the titanium plates could be an alternative method to commercial stainless steel plates. Advantages to the titanium plate are that it is custom designed to contour the lateral side of the distal femur thus avoiding the contouring process required with the commercial plate, the titanium plate's design process allows specific placement of screw holes to provide maximum fixation stability for each individual case, and it contains one less screw hole than the commercial plate, possibly reducing the duration time for the fixation process and material costs. Additionally, examinations of the dimensions between the two plates reveal a much higher thickness and a slightly higher surface area for the commercial plate than the titanium plate. A custom designed titanium plate could be a comparable alternative to current commercial stainless steel bone plates for fixation of epiphyseal plate fractures in more mature dogs, but stress shielding of the surrounding tissues may still be a valid concern [11, 12].

The fourth hypothesis was supported by the structural stiffness data from the cranial bending tests for both the commercial and titanium plate constructs when compared to all other fracture repair techniques. Both commercial plate and titanium plate constructs had a greater structural stiffness when compared to the resorbable and Kirschner wire constructs. The greater structural stiffnesses of the metal plates have raised some concern in the medical field over providing too much support to the fracture site and inducing stress shielding [11, 12, 37]. The lower structural stiffness of the resorbable plates could prevent this stress shielding during and after fracture ossification.

Medially however, there were no significant differences between the metal plates compared to all other repair techniques. As mentioned before, Kirschner wires were not statistically different in structural stiffness compared to any other type of construct except for the thicker resorbable plates. This indicates the crossed orientation of the Kirschner wires allow it to be almost as equally strong as most of the plate fixation techniques in response to medial loads. The structural stiffness values of the resorbable plates in medial bending tests were actually marginally higher than the metal plates and could be due to their similar surface areas and bilateral attachment compared to the laterally attached metal plates. Torsional loading tests also failed to reject the fourth null hypothesis that the metal bone plates were not significantly different from the resorbable bone plates and the Kirschner wires. Commercial and titanium plates showed no statistically significant differences between the resorbable 4mm, 2mm

plates or the wire constructs. Again, these results suggest that the forces applied during nondestructive torsional loading may not have been great enough to see a true difference of response among the different types of tested constructs.

Cranial displacement data from a 10N force supported the fourth hypothesis. Less displacement was evidenced for the commercial plate constructs when compared to the resorbable 4mm plates, 2mm plates, and the Kirschner wire constructs. Less displacement was also evidenced for the titanium plate constructs when compared the resorbable and wire constructs. This goes along with the structural stiffness comparisons of cranial bending. More stabilization is provided for the resorbable plate constructs than the Kirschner wire constructs, and even more stabilization is provided for the metal plates than the resorbable plate constructs.

Medial displacement data response for the 10N applied force on the other hand, had the opposite outcome. None of the metal plate constructs experienced significantly less displacement than the resorbable or wire constructs. These results also go along with the medial bending structural stiffness comparisons. It appears the crossed orientation of the Kirschner wires and the bilateral attachment of the resorbable plates enabled strong enough resistance to medial loads to be comparable to the metal plate repaired fractures

Similarly, torque generated from a 2 degree external rotation also failed to reject the null hypothesis for all comparisons. Commercial plate constructs showed no statistically significant differences between the resorbable 4mm plates (p-value 0.34), resorbable 2mm plates (p-value 0.10) and the Kirschner wires (p-value 0.33). Titanium plate constructs showed no significant differences between the resorbable 4mm and 2mm plates (p-value 0.56, p-value 0.56) as well as the wire constructs (p-value 0.03). Due to the lack of differing responses to torsional forces, these results again suggest that a greater angle of rotation is required of the proximal section of the femur in response to the distal section.

Destructive cranial and torsional force tests applied to these constructs did not reveal any statistically significant yield and ultimate strengths or yield and ultimate torques between the constructs. Almost all yield strengths observed during cranial bending were at 15N, and almost all yield torques were observed at 3 N-m for torsional loading. These results suggest that the femur models could have had a lower yield and ultimate strength as well as a lower yield and ultimate torque compared to the tested repair techniques, and fractured before proper torque

and strength values for the actual constructs themselves could be obtained. This lowered strength and torque values may have resulted in a deviation of the femur production process where the shredded fiberglass was applied with a thin coating of epoxy after bone production and surgery of the fracture repairs was complete instead of applying the fiberglass during the epoxy and bone power process [62, 72]. Beginnings of the first screw pullout for the bone plate constructs all could have occurred at the same yield strength and torque due to this deviation of model production. Alternatively, the failure of the models prior to adequate assessment of the construct strengths and torque could be an indication that the fracture repair methods are suitable enough for these epiphyseal repairs, and that in a clinical setting, forces strong enough to cause failure of the limb would fracture the bone first before failing the implant, especially in the torsion loading failure tests.

Statistical analysis of the length of time for different fracture repair techniques revealed that Kirschner wires had the shortest fixation time when compared to all bone plate constructs. Although comparison of commercial to titanium plates showed no statistically significant differences (p-value 0.01), the titanium plate fixation time was on average slightly faster probably due to the elimination of plate contouring and one less required screw. Both resorbable plates showed no significant difference in length of fixation time (p-value 0.92). Commercial and titanium plates were significantly shorter in fixation time compared to both resorbable 4mm plates and resorbable 2mm plates. Although it may be more attractive to have a shorter length of fixation time, the effectiveness of the type of fixation must also be taken into account. Kirschner wires are the fastest repair technique, but they are the most ineffective for epiphyseal plate fracture repairs. On the other hand, though the resorbable plate techniques have the lengthiest surgery time and could require the creation of two incisions at the repair site due to their bilateral attachment, their advantages for fracture repair could outweigh this particular disadvantage.

6. CONCLUSION

This was an *in vitro* study designed to mechanically compare the effectiveness of custom designed polycaprolactone resorbable bilateral bone plates and lateral titanium plates to current epiphyseal plate fracture repair techniques such as Kirschner wires and lateral commercial stainless steel bone plates. Forty identical models of the distal femur with pre-designed epiphyseal plate fractures were produced for the fixation of these five repair methods. The constructs underwent nondestructive cranio-caudal bending, medio-lateral bending and torsional loading tests as well as destructive cranio-caudal bending and torsional loading failure tests. The study showed no statistically significant differences among the constructs for the destructive tests, suggesting the models failed prior to reaching the yield and ultimate strengths and torques of the actual constructs. However, from nondestructive tests, the study showed comparable mechanical properties between constructs repaired by the custom designed titanium plates and the commercial stainless steel plates. Structural stiffnesses of both types of repaired constructs were not statistically significant for nondestructive cranio-caudal bending, medio-lateral bending and torsional loading tests. Other factors such as the custom contour and thinner design of the titanium plate, design potential for individual screw hole placement for each patient to provide maximum fixation, and possibly reduced surgery time and material costs indicate that the titanium plate could be a good alternative to current commercial plates.

The study also showed excellent mechanical properties of two thicknesses (4mm and 2mm) of custom designed resorbable PCL plates. Results showed that overall, both resorbable plates were statistically more structurally stiff when responding to cranial and medial forces compared to Kirschner wire repaired fractures. The resorbable plate constructs were also slightly better in structural stiffness in response to torsional loading than the Kirschner wire constructs. The material properties of the resorbable PCL plates suggest that it could not only provide better stabilization than Kirschner wire repairs, but that its degradation process could aid the fracture healing process by slowly transferring stresses from the plates back to the bone, and eliminating the stress shielding concern that long-term implantation of metal plates create for surrounding bone tissue. The resorbable plates actually provided more stability than the metal plates in response to medial loads, which could be due largely to their bilateral fixation. Additionally, results indicated that the 2mm resorbable plate was statistically comparable to the

thicker 4mm plate, in cranial bending, medial bending and torsional loading tests, suggesting that smaller amounts of resorbable material are adequate enough for fracture stabilization which could be advantageous in terms of controlling the degradation rate of the plate after fracture ossification. The study showed that bilateral attachment of PCL resorbable plates could be an excellent alternative to current Kirschner wire fixation techniques for epiphyseal plate fracture repairs in young dogs.

7. FUTURE RESEARCH

Several directions of further investigation in this research area could be taken. Nondestructive torsional loading tests with a greater applied force could be performed to establish a better mechanical response between different constructs. Yield and ultimate strength values for these constructs could be reassessed using models produced with a fiberglass, bone powder and epoxy mixture or with similar cadaveric bones. Prior to creation of further bone models, a study should be conducted to examine the exact expansion values of polyurethane foam, which could be easily done by creating a silicone RTV mold of a cylinder of known measurements and creating a polyurethane foam model to measure changes in dimensions. With these results, appropriate adjustments for the thresholding values used in the Mimics program for extraction of the cancellous bone region can be made.

Studies could be conducted to examine the degradation rate of the polycaprolactone plates and their mechanical response during epiphyseal plate fracture repair to better correlate the fracture healing period with the degradation rate. Similarly, future studies could also examine the potential of copolymers such a PCL-PGA or PCL-PLLA copolymer to either quicken or slow down the degradation rate.

The assessment of *in vivo* micromotion between the different types of constructs during the healing process is also recommended. Studies have shown that more than 150 microns of movement alters tissue ossification [86, 87]. Rather than osteoblasts at the fracture site, there has been evidence that fibrous tissue takes its place. This would drastically alter the strength of the repaired bone and could be suspect if similar fractures of the same bone occur in the future.

From a mass production standpoint, a “standard” resorbable plate could be investigated as an alternative to custom designed plates for each individual patient. The current technique for resorbable plate production requires the use of direct rapid tooling technology to create a resin and steel liquid epoxy mold for injection molding, which could be costly to the patient. Instead, standard sized plates could be devised for patients who are similar in size, and with the elastic properties of the 2mm thin plates, a slightly deviated contour from the medial and lateral sides of the distal femur could still provide a stable fit during surgery.

8. REFERENCES

1. Martini, F.H. and E.F. Bartholomew, *Essentials of Anatomy and Physiology*: 2nd Edition. 2000, New Jersey: Prentice Hall.
2. Gomes, L.S. and J.B. Volpon, Experimental physeal fracture-separations treated with rigid internal fixation. *J Bone Joint Surg Am*, 1993. 75(12): p. 1756-1764.
3. Stone, E.A., C.W. Betts, and G.N. Rowland, Effect of Rush pins on the distal femoral growth plate of young dogs. *Am J Vet Res*, 1981. 42(2): p. 261-5.
4. Thomson, J.D., S.J. Stricker, and M.M. Williams, Fractures of the distal femoral epiphyseal plate. *J Pediatr Orthop*, 1995. 15(4): p. 474-8.
5. Breburda, E., et al., The influence of intermittent external dynamic pressure and tension forces on the healing of an epiphyseal fracture. *Arch Orthop Trauma Surg*, 2001. 121(8): p. 443-9.
6. Hara, Y., et al., Application of oriented poly-L-lactide screws for experimental Salter-Harris type 4 fracture in distal femoral condyle of the dog. *J Vet Med Sci*, 1994. 56(5): p. 817-22.
7. Kregor, P.J., et al., Distal femoral fracture fixation utilizing the Less Invasive Stabilization System (L.I.S.S.): the technique and early results. *Injury*, 2001. 32 Suppl 3: p. SC32-47.
8. Axelson, A., et al., The use of a biodegradable implant in fracture fixation: a review of the literature and a report of two clinical cases. *J. Small Anim. Pract*, 1988. 29: p. 249-255.
9. Axelson, P., et al., Biodegradable implants in the fixation of physeal fractures in cats and dogs. *Acta Vet Scand*, 1988. 29(3-4): p. 477-84.
10. Axelson, P.B., Fixation of cancellous bone and physeal fractures in dogs and cats. A comparison of the use of self-reinforced biodegradable devices to the use of metallic devices and external fixations. *Acta Vet Scand*, 1989. 30(3): p. 259-65.
11. McLaughlin, R.M. and J.K. Roush, Repairing fractures with bone plate and screw fixation. *Veterinary Medicine*, 1999. 94(1): p. 64-73.

12. Mazzonetto, R., A.O. Paza, and D.B. Spagnoli, A retrospective evaluation of rigid fixation in orthognathic surgery using a biodegradable self-reinforced (70L:30DL) polyactide. *Int. J. Oral Maxillofac*, 2004. 33: p. 664-669.
13. Bergsma, J.E., et al., Late degradation tissue response to poly(-lactide) bone plates and screws. *Biomaterials*, 1995. 16(1): p. 25-31.
14. Brady, J.M., et al., Resorption rate, route of elimination, and ultrastructure of the implant site of polylactic acid in the abdominal wall of the rat. *Journal of Biomedical Materials Research*, 1973. 7(2): p. 155-166.
15. Lam, C.X.F., et al., Evaluation of polycaprolactone scaffold degradation for 6 months *in vitro* and *in vivo*. *Journal of Biomedical Materials Research Part A*, 2008. Epub ahead of print: p. NA.
16. Pietrzak, W.S., D.R. Sarver, and M.L. Verstynen, Bioabsorbable polymer science for the practicing surgeon. *J Craniofac Surg*, 1997. 8(2): p. 87-91.
17. Riseborough, E.J., I.R. Barrett, and F. Shapiro, Growth disturbances following distal femoral physal fracture-separations. *J Bone Joint Surg Am*, 1983. 65(7): p. 885-893.
18. Niemeyer, K.H. and R.E. Hoffer, Rush pin repair of distal fractures of long bones in the dog. *J Am Vet Med Assoc*, 1971. 159(11): p. 1433-4.
19. Salter, R.B. and W.R. Harris, Injuries Involving the Epiphyseal Plate. *J Bone Joint Surg Am*, 1963. 45(3): p. 587-622.
20. Degner, D.A. Fractures Involving Growth Plates. 2004 2008 [cited 2008 10/18/2008]; Available from: http://www.vetsurgerycentral.com/growth_plate.htm.
21. Ogden, J.A., The evaluation and treatment of partial physal arrest. *J Bone Joint Surg Am*, 1987. 69(8): p. 1297-1302.
22. Saikku-Bäckström, A., et al., Intramedullary fixation of femoral cortical osteotomies with interlocked biodegradable self-reinforced poly-96/4-lactide (SR-PLA96) nails. *Biomaterials*, 2004. 25(13): p. 2669-2677.
23. Eppley, B.L., et al., Resorbable PLLA-PGA plate and screw fixation in pediatric craniofacial surgery: clinical experience in 1883 patients. *Plast Reconstr Surg*, 2004. 114(4): p. 850-6; discussion 857.

24. Bergsma, E.J., et al., Foreign body reactions to resorbable poly(L-lactide) bone plates and screws used for the fixation of unstable zygomatic fractures. *J Oral Maxillofac Surg*, 1993. 51(6): p. 666-70.
25. Suzuki, T., et al., Resorbable poly-L-lactide plates and screws for the treatment of mandibular condylar process fractures: a clinical and radiologic follow-up study. *J Oral Maxillofac Surg*, 2004. 62(8): p. 919-24.
26. Suuronen, R., Comparison of absorbable self-reinforced poly-L-lactide screws and metallic screws in the fixation of mandibular condyle osteotomies: an experimental study in sheep. *J Oral Maxillofac Surg*, 1991. 49(9): p. 989-95.
27. Suuronen, R., et al., Sagittal split osteotomy fixed with biodegradable, self-reinforced poly-L-lactide screws. A pilot study in sheep. *Int J Oral Maxillofac Surg*, 1992. 21(5): p. 303-8.
28. Suuronen, R., et al., Mandibular osteotomy fixed with biodegradable plates and screws: an animal study. *Br J Oral Maxillofac Surg*, 1997. 35(5): p. 341-8.
29. Suuronen, R., et al., A 5-year *in vitro* and *in vivo* study of the biodegradation of polylactide plates. *J Oral Maxillofac Surg*, 1998. 56(5): p. 604-14; discussion 614-5.
30. Suuronen, R., et al., Comparison of absorbable self-reinforced multilayer poly-l-lactide and metallic plates for the fixation of mandibular body osteotomies: an experimental study in sheep. *J Oral Maxillofac Surg*, 1992. 50(3): p. 255-62.
31. Suuronen, R., et al., New generation biodegradable plate for fracture fixation: comparison of bending strengths of mandibular osteotomies fixed with absorbable self-reinforced multi-layer poly-l-lactide plates and metallic plates--an experimental study in sheep. *Clin Mater*, 1992. 9(2): p. 77-84.
32. Nakamura, T., et al., Biodegradation and tumorigenicity of implanted plates made from a copolymer of epsilon-caprolactone and L-lactide in rat. *J Biomed Mater Res*, 1998. 42(4): p. 475-84.
33. Daniels, A.U., M.K. Chang, and K.P. Andriano, Mechanical properties of biodegradable polymers and composites proposed for internal fixation of bone. *J Appl Biomater*, 1990. 1(1): p. 57-78.
34. Suuronen, R., et al., Bioabsorbable self-reinforced plates and screws in craniomaxillofacial surgery. *Biomed Mater Eng*, 2004. 14(4): p. 517-24.

35. Ashammakhi, N., et al., Successful use of biosorb osteofixation devices in 165 cranial and maxillofacial cases: a multicenter report. *J Craniofac Surg*, 2004. 15(4): p. 692-701; discussion 702.
36. Kurpad, S.N., J.A. Goldstein, and A.R. Cohen, Bioresorbable fixation for congenital pediatric craniofacial surgery: a 2-year follow-up. *Pediatr Neurosurg*, 2000. 33(6): p. 306-10.
37. Gosain, A.K., et al., Biomechanical evaluation of titanium, biodegradable plate and screw, and cyanoacrylate glue fixation systems in craniofacial surgery. *Plast Reconstr Surg*, 1998. 101(3): p. 582-91.
38. Vaananen, P., et al., Biomechanical *In Vitro* Evaluation of the Effect of Cyclic Loading on the Postoperative Fixation Stability and Degradation of a Biodegradable Ankle Plate. *Journal of Orthopaedic Research*, 2008. 26: p. 485-1488.
39. Pitt, C.G. and A. Schnider, Capronor-A biodegradable delivery system for levonorgestrel. , in Long-acting contraceptive systems, G. Zatachini, Editor. 1984, Harpen and Row: Philadelphia, PA. p. 63-84.
40. Corden, T.J., et al., Physical and biocompatibility properties of poly-[var epsilon]-caprolactone produced using in situ polymerisation: a novel manufacturing technique for long-fibre composite materials. *Biomaterials*, 2000. 21(7): p. 713-724.
41. Gurav, N. and S. Downes, A qualitative *in vitro* evaluation of the degradable materials poly(caprolactone), poly(hydroxybutyrate) and a poly(hydroxybutyrate)-(hydroxyvalerate) copolymer. *Journal of Materials Science: Materials in Medicine*, 1994. 5(11): p. 784-787.
42. Fujihara, K., M. Kotaki, and S. Ramakrishna, Guided bone regeneration membrane made of polycaprolactone/calcium carbonate composite nano-fibers. *Biomaterials*, 2005. 26(19): p. 4139-4147.
43. Rohner, D., et al., *In vivo* efficacy of bone-marrow-coated polycaprolactone scaffolds for the reconstruction of orbital defects in the pig. *J Biomed Mater Res B Appl Biomater*, 2003. 66(2): p. 574-80.
44. Sun, H., et al., The *in vivo* degradation, absorption and excretion of PCL-based implant. *Biomaterials*, 2006. 27(9): p. 1735-40.
45. Barrows, T.H., Degradable implant materials: a review of synthetic absorbable polymers and their applications. *Clin Mater*, 1986. 1: p. 233-257.

46. Perrin, D.E. and J.P. English, Polycaprolactone, in Handbook of Biodegradable Polymers, A.J. Domb, J. Kost, and D.M. Wiseman, Editors. 1997, Harwood Academic Publishers: Amsterdam. p. 63-78.
47. Poly(ϵ -Caprolactone) (overview), in Polymeric Materials Encyclopedia, J.C. Salamone, Editor. 1996, CRC Press, Inc.: Boca Raton. p. 5687.
48. Piskin, E., Biodegradable Polymers in Medicine, in Degradable Polymers: Principles and Applications, G. Scott, Editor. 2003, Kluwer Academic Publishers: Norwell, MA. p. 330.
49. Perrin, D.E. and J.P. English, Polyglycolide and Polylactide, in Handbook of Biodegradable Polymers, A.J. Domb, J. Kost, and D.M. Wiseman, Editors. 1997, Harwood Academic Publishers: Amsterdam. p. 3-28.
50. Hutmacher, D.W., Scaffolds in tissue engineering bone and cartilage. *Biomaterials*, 2000. 21(24): p. 2529-2543.
51. Yasin, M. and B.J. Tighe, Polymers for biodegradable medical devices: VIII. Hydroxybutyrate-hydroxyvalerate copolymers: physical and degradative properties of blends with polycaprolactone. *Biomaterials*, 1992. 13(1): p. 9-16.
52. Lewis, D., R.L. Dunn, and R. Casper, Absorbable fixation plates with fiber reinforcement. *Trans. Soc. Biomater*, 1981. 4: p. 61.
53. Casper, R.A., R.L. Dunn, and B.S. Kelly, Totally biodegradable fracture-fixation plates for use in maxillofacial surgery. *Trans. Soc. Biomater*, 1984. 7: p. 728.
54. Petzold R., H.-F. Zeilhofer, and W.A. Kalender, Rapid prototyping technology in medicine - basics and applications. *Computerized Medical Imaging and Graphics*, 1999. 23: p. 277-84.
55. Liska, W.D., et al., Custom Total Knee Replacement in a Dog with Femoral Condylar Bone Loss. *Veterinary Surgery*, 2007. 36(4): p. 293-301.
56. Harrysson, O.L., et al., Rapid prototyping for treatment of canine limb deformities. *Rapid Prototyping Journal*, 2003. 9(1): p. 37-42.
57. Davis, J., Till Death Do Us Part. *Wired*, 2003. 10: p. 110-120.
58. Yaxiong, L., et al., The customized mandible substitute based on rapid prototyping. *Rapid Prototyping Journal*, 2003. 9(3): p. 167-174.

59. Heissler, E., et al., Custom-made cast titanium implants produced with CAD/CAM for the reconstruction of cranium defects. *International Journal of Oral and Maxillofacial Surgery*, 1998. 27(5): p. 334-338.
60. Johnson, E.E., Custom titanium plating for failed nonunion or delayed internal fixation of femoral fractures. *Clin Orthop Relat Res*, 1988(234): p. 195-203.
61. Potamianos, P., et al., Rapid Prototyping for Orthopaedic Surgery. *Proceedings of the I MECH E Part H Journal of Engineering in Medicine*, 1998. 212: p. 383-393.
62. Marcellin-Little, D.J., O.L.A. Harrysson, and O. Cansizoglu, *In vitro* evaluation of a custom cutting jig and custom plate for canine tibial plateau leveling. 2008. p. 961-966.
63. Harrysson, O.L.A. and D.R. Cormier, Direct fabrication of custom orthopedic implants using electron beam melting technology, in *Advanced manufacturing technology for medical applications*, I. Gibson, Editor. 2006, John Wiley & Sons Ltd: Chichester, England. p. 193–208.
64. Kling-Petersen, T. and M. Rydmark, Modeling and modification of medical 3D objects. The benefit of using a haptic modeling tool. *Stud Health Technol Inform.*, 2000. 70: p. 162-167.
65. Karapatis, N.P., J.P.S. Van Griethuysen, and R. Gardon, Direct rapid tooling: A review of current research. *Rapid Prototyping Journal*, 1998. 4(2): p. 77-89.
66. Osswald, T.A., L.-S. Turng, and P. Gramann, *Injection Molding Handbook*. 2nd ed. 2008, Munich: Carl Hanser Publishers. 764.
67. Bagley, E.B., End Corrections in the Capillary Flow of Polyethylene. *Journal of Applied Physics*, 1957. 28(5): p. 624-627.
68. Cracknell, P.S. and R.W. Dyson, *Handbook of Thermoplastics Injection Mould Design*. 1993, London: Blackie Academic and Professional. 132.
69. Tay, F.E.H., et al., Manufacture of RP tools with high quality surface finish using high temperature epoxy resin and electroless nickel plating. *Surface Engineering*, 2000. 16(3): p. 250-252.
70. Pistner, H., et al., Poly(L-lactide): a long-term degradation study *in vivo* I. Biological results. *Biomaterials*, 1993. 14(9): p. 671-677.

71. Altpeter, H., et al., Non-conventional injection molding of poly(lactide) and poly(epsilon-caprolactone) intended for orthopedic applications. *J Mater Sci Mater Med*, 2004. 15(2): p. 175-84.
72. Hildreth, B.E., et al., *In vitro* evaluation of five canine tibial plateau leveling methods. 2006. p. 693-700.
73. Smith, G.K., Biomechanics pertinent to fracture etiology, reduction and fixation, in *Textbook of Small Animal Orthopedics*, C.D. Newton and D.M. Nunamaker, Editors. 1985, Lippincott: Philadelphia, PA. p. 195-230.
74. Nordin, M. and V.H. Frankel, Biomechanics of bone, in *Basic Biomechanics of the Musculoskeletal System*, M. Nordin and V.H. Frankel, Editors. 1989, Lea & Febiger: Philadelphia, PA. p. 3-29.
75. Schwarz, P.D., Biomechanics of fractures and fracture fixation. *Semin. Vet. Med. Surg (Small Anim)*, 1991. 6: p. 3-15.
76. Carter, D.R. and D.M. Spengler, Biomechanics of fracture, in *Bone in Clinical Orthopaedics: A Study in Comparative Osteology*, G. Sumner-Smith, Editor. 1982, Saunders: Philadelphia, PA. p. 305-334.
77. Slater, R.B. and R.W. Harris, Fractures involving the epiphyseal plate. *J Bone Joint Surg Am*, 1963. 45: p. 587-622.
78. Brashear Jr., H.R., Epiphyseal fractures: A microscopic study of the healing process in rats. *J Bone Joint Surg Am*, 1959. 41: p. 1055-1064.
79. Sukhiani, H.R. and D.L. Holmberg, Ex vivo biomechanical comparison of pin fixation techniques for canine distal femoral physal fractures. *Vet Surg*, 1997. 26(5): p. 398-407.
80. Belkoff, S.M., D.L. Millis, and C.W. Probst, Biomechanical comparison of three internal fixations of slipped capital femoral epiphysis in immature dogs. *Am J Vet Res*, 1990. 51: p. 123-127.
81. Snow, M., G. Thompson, and P.G. Turner, A mechanical comparison of the locking compression plate (LCP) and the low contact-dynamic compression plate (DCP) in an osteoporotic bone model. *Journal of Orthopaedic Trauma*, 2008. 22(2): p. 121-125.

82. Schmitt-Thomas, K.G., Z.G. Yang, and T. Hiermer, Development of torsion loading facility used for evaluating shear performance of polymeric composite implant rods. *Polymer Testing*, 1998. 17: p. 117-130.
83. Russias, J., et al., Fabrication and mechanical properties of PLA/HA composites: A study of *in vitro* degradation. *Materials Science & Engineering* 2006. 26: p. 1289-1295.
84. Shapiro, S.S., M.B. Wilk, and H.J. Chen, A comparative study of various tests for normality. *Journal of the American Statistical Association*, 1968. 63(324): p. 1343-1372.
85. Shapiro, S.S. and M.B. Wilk, An analysis of variance test for normality (complete samples). *Biometrika*, 1965. 52, 3 and 4: p. 591-611.
86. Pilliar, R.M., J.M. Lee, and C. Maniopoulos, Observation on the effect of movement on bone ingrowth into porous-surfaced implants. *Clin Orthop Relat Res*, 1986. 208: p. 108-113.
87. Sballe, K., E.S.B. Hansen, and H. Rasmussen, Tissue ingrowth into titanium and hydroxyapatite-coated implants during stable and unstable mechanical conditions. *Journal of Orthopaedic Research*, 1992. 10: p. 285-299.

APPENDICES

Appendix A

Table A.1: Comparison of cycles 1,2, and 3 for the commercial plate specimens during non-destructive cranial, medial and torsional testing. A p-value less than 0.05 is significant.

ANOVA			
Structural Stiffness			
Commercial Plate			
Cycle 1	Cranial Bending (kN/m)	Medial Bending (kN/m)	Torsional Loading (N-m/rad)
Mean	24.58	24.46	60.85
SD	4.71	4.36	7.64
N=8			
Cycle 2	Cranial Bending (kN/m)	Medial Bending (kN/m)	Torsional Loading (N-m/rad)
Mean	24.53	24.84	60.95
SD	4.49	4.60	7.74
N=8			
Cycle 3	Cranial Bending (kN/m)	Medial Bending (kN/m)	Torsional Loading (N-m/rad)
Mean	24.88	24.84	60.76
SD	4.92	4.50	8.04
N=8			
p-value	0.987	0.981	0.999

Table A.2: Comparison of cycles 1,2, and 3 for the titanium plate specimens during non-destructive cranial, medial and torsional testing. A p-value less than 0.05 is significant.

<i>ANOVA</i>			
<i>Structural Stiffness</i>			
<i>Titanium Plate</i>			
Cycle 1	Cranial Bending (kN/m)	Medial Bending (kN/m)	Torsional Loading (N-m/rad)
Mean	23.95	24.64	66.44
SD	4.56	7.48	15.06
N=8			
Cycle 2	Cranial Bending (kN/m)	Medial Bending (kN/m)	Torsional Loading (N-m/rad)
Mean	24.08	25.01	66.09
SD	4.68	7.72	14.40
N=8			
Cycle 3	Cranial Bending (kN/m)	Medial Bending (kN/m)	Torsional Loading (N-m/rad)
Mean	24.20	24.85	65.34
SD	4.77	7.48	14.87
N=8			
p-value	0.994	0.995	0.988

Table A.3: Comparison of cycles 1,2, and 3 for the resorbable (4mm) plate specimens during non-destructive cranial, medial and torsional testing.
A p-value less than 0.05 is significant.

<i>ANOVA</i>			
<i>Structural Stiffness</i>			
<i>Resorbable (4mm) Plate</i>			
Cycle 1	Cranial Bending (kN/m)	Medial Bending (kN/m)	Torsional Loading (N-m/rad)
Mean	14.32	31.39	63.54
SD	3.74	4.48	13.54
N=8			
Cycle 2	Cranial Bending (kN/m)	Medial Bending (kN/m)	Torsional Loading (N-m/rad)
Mean	14.44	31.51	62.90
SD	3.68	4.85	13.51
N=8			
Cycle 3	Cranial Bending (kN/m)	Medial Bending (kN/m)	Torsional Loading (N-m/rad)
Mean	14.48	31.62	63.05
SD	3.76	4.83	12.99
N=8			
p-value	0.996	0.995	0.995

Table A.4: Comparison of cycles 1,2, and 3 for the resorbable (2mm) plate specimens during non-destructive cranial, medial and torsional testing.
A p-value less than 0.05 is significant.

<i>Structural Stiffness</i> <i>Resorbable (2mm) Plate</i>			
Cycle 1	Cranial Bending (kN/m)	Medial Bending (kN/m)	Torsional Loading (N-m/rad)
Mean	12.76	26.01	68.04
SD	3.15	4.31	9.78
N=8			
Cycle 2	Cranial Bending (kN/m)	Medial Bending (kN/m)	Torsional Loading (N-m/rad)
Mean	12.84	25.85	67.79
SD	3.26	4.14	9.64
N=8			
Cycle 3	Cranial Bending (kN/m)	Medial Bending (kN/m)	Torsional Loading (N-m/rad)
Mean	13.00	25.94	67.91
SD	3.28	4.08	9.66
N=8			
p-value	0.986	0.997	0.999

Table A.5: Comparison of cycles 1,2, and 3 for the Kirschner wire specimens during non-destructive cranial, medial and torsional testing. A p-value less than 0.05 is significant.

<i>Structural Stiffness</i>			
<i>Kirschner Wire</i>			
Cycle 1	Cranial Bending (kN/m)	Medial Bending (kN/m)	Torsional Loading (N-m/rad)
Mean	4.66	18.23	54.31
SD	1.45	7.54	8.33
N=8			
Cycle 2	Cranial Bending (kN/m)	Medial Bending (kN/m)	Torsional Loading (N-m/rad)
Mean	4.69	18.27	54.26
SD	1.43	7.47	8.27
N=8			
Cycle 3	Cranial Bending (kN/m)	Medial Bending (kN/m)	Torsional Loading (N-m/rad)
Mean	4.72	18.53	54.20
SD	1.46	7.52	8.00
N=8			
p-value	0.997	0.996	1.000

Appendix B

Table B.1: Structural stiffness mean values of three cycles of cranial bending for all constructs. Overall mean and standard deviation (SD) values also provided for each construct.

<i>Structural Stiffness (kN/m)</i> <i>Cranial Bending</i>										
Trial	Commercial		Titanium		Resorbable 4mm		Resorbable 2mm		Kirschner Wire	
	Mean	SD	Mean	SD	Mean	SD	Mean	SD	Mean	SD
1	33.76	0.60	17.59	0.06	18.83	0.06	18.34	0.34	3.71	0.04
2	23.78	0.16	24.89	0.11	13.59	0.21	11.91	0.15	3.44	0.02
3	23.21	0.28	23.94	0.03	14.34	0.13	8.41	0.04	5.33	0.03
4	19.75	0.20	23.29	0.10	19.06	0.13	16.25	0.12	5.25	0.10
5	22.18	0.13	27.59	0.37	16.19	0.16	13.83	0.17	3.96	0.03
6	28.79	0.50	17.35	0.16	14.60	0.07	10.99	0.17	4.09	0.09
7	20.10	0.13	30.31	0.47	8.72	0.04	12.78	0.10	3.79	0.02
8	25.74	0.08	27.63	0.13	9.97	0.17	10.37	0.12	5.43	0.02
mean	24.66		24.07		14.41		12.86		4.38	
SD	4.71		4.67		3.73		3.23		0.82	

Table B.2: Structural stiffness mean values of three cycles of medial bending for all constructs. Overall mean and standard deviation (SD) values also provided for each construct.

<i>Structural Stiffness (kN/m)</i> <i>Medial Bending</i>										
Trials	Commercial		Titanium		Resorbable 4mm		Resorbable 2mm		Kirschner Wire	
	Mean	SD	Mean	SD	Mean	SD	Mean	SD	Mean	SD
1	28.85	0.29	17.77	0.12	29.93	0.25	29.50	0.17	21.96	0.59
2	21.36	0.35	34.73	0.33	33.92	0.29	31.87	0.56	22.08	0.43
3	29.04	0.26	17.01	0.09	25.71	0.22	20.33	0.14	28.68	0.09
4	26.67	0.41	16.00	0.18	39.03	0.50	20.42	0.12	24.50	0.12
5	22.87	0.27	28.39	0.05	31.13	0.03	29.04	0.26	9.62	0.12
6	18.19	0.09	29.54	0.10	35.63	0.36	24.97	0.10	9.61	0.29
7	20.73	0.12	33.18	0.74	25.17	0.06	26.50	0.24	10.17	0.08
8	29.98	0.71	22.03	0.22	31.54	0.42	24.84	0.20	20.15	0.20
mean	24.71		24.83		31.51		25.93		18.35	
SD	4.48		7.56		4.72		4.17		7.50	

Table B.3: Structural stiffness mean values of three cycles of torsional loading for all constructs. Overall mean and standard deviation (SD) values also provided for each construct.

<i>Structural Stiffness (N-m/rad)</i> <i>Torsional Loading</i>										
Trials	Commercial		Titanium		Resorbable 4mm		Resorbable 2mm		Kirschner Wire	
	Mean	SD	Mean	SD	Mean	SD	Mean	SD	Mean	SD
1	53.32	1.19	57.61	0.53	85.25	0.12	79.90	0.47	---	---
2	72.80	0.13	63.70	0.83	52.71	0.28	62.46	0.11	63.16	0.16
3	58.75	0.47	54.12	0.47	59.64	0.10	63.69	0.23	57.14	0.23
4	58.12	0.86	64.94	0.12	75.92	1.21	62.25	0.49	---	---
5	71.96	0.18	90.09	1.07	42.78	0.91	84.98	0.30	39.33	0.20
6	54.76	0.31	78.39	0.19	65.12	0.37	69.84	0.58	59.02	0.41
7	63.12	1.00	75.04	1.02	56.99	1.63	57.26	0.41	52.56	0.26
8	54.00	0.68	43.77	1.01	66.93	0.13	62.95	0.56	54.32	0.09
mean	60.85		65.96		63.17		67.91		54.25	
SD	7.78		14.77		13.33		9.69		8.20	

Table B.4: Displacement mean values of three cycles of cranial bending for all constructs at a 10N applied force. Overall mean and standard deviation (SD) values also provided for each construct.

<i>Displacement (mm) at 10N Applied Force Cranial Bending</i>										
Trial	Commercial		Titanium		Resorbable 4mm		Resorbable 2mm		Kirschner Wire	
	Mean	SD	Mean	SD	Mean	SD	Mean	SD	Mean	SD
1	0.33	0.01	0.56	0.01	0.60	0.00	0.58	0.01	2.52	0.02
2	0.50	0.01	0.41	0.01	0.78	0.01	0.78	0.01	2.55	0.05
3	0.42	0.00	0.47	0.01	0.73	0.00	1.22	0.02	1.88	0.03
4	0.64	0.01	0.52	0.00	0.57	0.01	0.63	0.00	1.52	0.01
5	0.50	0.01	0.38	0.01	0.74	0.01	0.70	0.02	2.49	0.01
6	0.35	0.00	0.57	0.01	0.73	0.01	0.96	0.01	2.40	0.02
7	0.57	0.01	0.34	0.00	1.14	0.02	0.95	0.02	2.55	0.01
8	0.40	0.00	0.41	0.01	1.02	0.01	1.06	0.03	1.83	0.02
Mean	0.46		0.46		0.79		0.86		2.22	
SD	0.11		0.09		0.20		0.23		0.41	

Table B.5: Displacement mean values of three cycles of medial bending for all constructs at a 10N applied force. Overall mean and standard deviation (SD) values also provided for each construct.

	<i>Displacement (mm) at 10N Applied Force Medial Bending</i>									
Trials	Commercial		Titanium		Resorbable 4mm		Resorbable 2mm		Kirschner Wire	
	Mean	SD	Mean	SD	Mean	SD	Mean	SD	Mean	SD
1	0.43	0.00	0.60	0.00	0.43	0.01	0.41	0.01	0.80	0.00
2	0.48	0.01	0.31	0.01	0.34	0.01	0.36	0.01	0.48	0.00
3	0.38	0.01	0.62	0.01	0.44	0.00	0.49	0.01	0.60	0.00
4	0.40	0.02	0.64	0.01	0.30	0.01	0.54	0.00	0.47	0.01
5	0.44	0.01	0.36	0.01	0.37	0.01	0.38	0.00	1.02	0.01
6	0.60	0.01	0.39	0.01	0.30	0.00	0.41	0.00	1.28	0.01
7	0.50	0.01	0.41	0.01	0.45	0.01	0.45	0.01	0.90	0.01
8	0.41	0.01	0.48	0.01	0.32	0.00	0.39	0.01	0.51	0.01
Mean	0.46		0.48		0.37		0.43		0.76	
SD	0.07		0.13		0.06		0.06		0.30	

Table B.6: Torque mean values of three cycles of torsional loading for all constructs at a 2 degree rotation. Overall mean and standard deviation (SD) values also provided for each construct.

<i>Torque (N-m) at 2 deg Rotation Torsional Loading</i>										
Trials	Commercial		Titanium		Resorbable 4mm		Resorbable 2mm		Kirschner Wire	
	Mean	SD	Mean	SD	Mean	SD	Mean	SD	Mean	SD
1	1.78	0.00	1.92	0.01	2.86	0.00	2.53	0.02	---	---
2	2.39	0.00	2.20	0.01	1.70	0.01	2.08	0.02	2.05	0.02
3	1.84	0.01	2.03	0.01	1.96	0.01	2.10	0.01	1.92	0.02
4	1.59	0.01	2.10	0.01	2.52	0.03	1.08	0.01	---	---
5	2.38	0.03	3.01	0.02	1.52	0.01	2.78	0.03	1.39	0.01
6	1.85	0.02	2.58	0.02	2.16	0.01	2.42	0.03	1.67	0.41
7	1.83	0.03	2.52	0.04	1.91	0.01	1.83	0.02	1.71	0.01
8	1.81	0.01	1.51	0.01	2.22	0.02	2.11	0.01	1.81	0.01
Mean	1.93		2.24		2.11		2.12		1.76	
SD	0.29		0.46		0.43		0.51		0.23	